



**UNIVERSITY  
OF TRENTO - Italy**  
DEPARTMENT OF INDUSTRIAL ENGINEERING

---

---

XXIX cycle

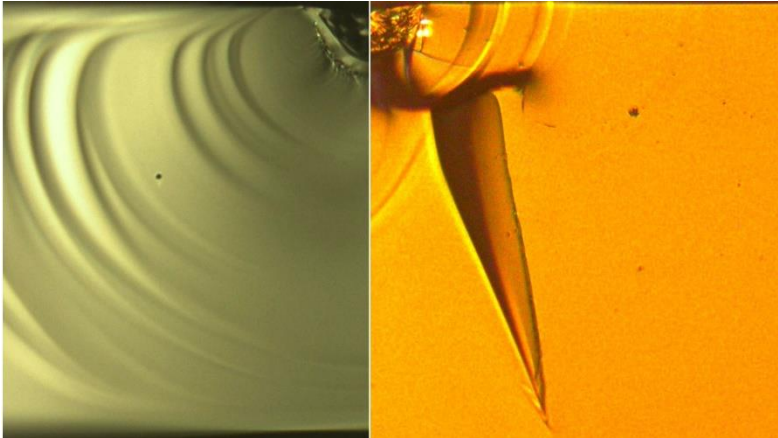
Doctoral School in Materials, Mechatronics  
and Systems Engineering

---

---

## **Strengthening of Soda-Borosilicate Glasses by Ion Exchange Processes**

**Ali Talimian**



---

---

**December 2016**

---

---



# STRENGTHENING OF SODA-BOROSILICATE GLASSES BY ION EXCHANGE PROCESSES

Ali Talimian

E-mail:ali.talimian@unitn.it

Approved by:

Prof. Vincenzo M. Sglavo, Advisor  
Department of Industrial Engineering  
*University of Trento, Italy.*

Ph.D. Commission:

Prof. Gian Domenico Soraru,  
Department of Industrial Engineering,  
*University of Trento, Italy.*

Prof. Rodrigo Moreno,  
Instituto de Ceramica y Vidrio CSIC,  
Madrid, *Spain.*

Prof. Enrico Bernardo,  
Department of Industrial Engineering  
*University of Padova, Italy.*

University of Trento,  
Department of Industrial Engineering

December 2016



**University of Trento - Department of  
Industrial Engineering**

**Doctoral Thesis**

**Ali Talimian 2016  
Published in Trento (Italy) – by University of Trento**

**ISBN: - - - - -**



*To my family*



## Abstract:

Flexible electronics and displays rely on strong thin borosilicate glasses. Furthermore, borosilicate glass play a vital role in pharmaceutical packaging, particularly for the container of liquid medicine in the auto-injectors. Because of the risk of failure due to the fracture of the glass ampule the costumers need to purchase several units of auto-injector; also, the injector price increases dramatically. This renewed the interest in the strengthening of soda-borosilicate glass. Moreover, the applications of strong thin borosilicate glasses in flexible electronics attracted attention. Chemical strengthening is a practical means of improving the mechanical performance of soda borosilicate glasses.

The chemical strengthening process involves the immersion of an alkali-silicate glass in a molten nitrate salt containing potassium ions at temperatures below the glass-transition temperature where the replacement of small alkali ions in the glass with larger potassium ions from the molten salt occurs. The glass composition, salts impurities, temperature and time, are crucial factors of the treatment. Furthermore, applying an electric field can speed up the process and improves the efficiency. This study investigates the impact of potassium for sodium ion exchange and its parameters on the final strength of alkali borosilicate glasses.

Alkali borosilicate tubes, used in pharmaceutical packaging, were subjected to ion exchange in potassium nitrate salts containing different impurities. The initial surface flaws have a significant impact on the final strength due to the limited case depth of surface compression in alkai borosilicate glass subjected to ion exchange. Nonetheless, the results revealed that the sodium poisoning of salt has a limited influence on strengthening; conversely, even a small amount of calcium spoils the strengthening. The replacement of sodium ions with calcium is thermodynamically favoured with respect to Na/K ion-exchange. Calcium can penetrate into the glass surface and prevent the replacement of sodium with potassium and, consequently, the generation of compressive stress.

Interestingly, performing electric field assisted ion exchange, EF-IE, for 10 min produces an ion-exchanged layer as deep as conventional strengthening for 4 hours in soda borosilicate glass. Electric field assisted ion exchange also augments the glass strength and makes the glass more damage resistant; however, the initial defects on the glass surface have an adverse influence on the efficiency, as expected.

Applying an electric field changes the governing mechanism of ion exchange and accelerates the penetration of potassium ions into the glass; furthermore, the glass structure of the layer undergone electric field assisted ion exchange is modified during the process. Although EF-IE generates a strong surface compression in glass, the inhomogeneous distribution of residual stress is a drawback. Performing EF-IE using AC E-fields produces homogenous ion-exchanged layers in glass and is, probably, a practical approach to balancing the residual stress in glass.

Chemical strengthening of a thin alkali-borosilicate glass ,D 263 Teco®, is also investigated in the present work. Na/K ion exchange improves the glass strength three times. Although the surface compression generated by ion-exchange in alkali borosilicate glasses is not as strong as typically used glasses for chemical strengthening ( alkali aluminosilicate), it can be used to improve the mechanical properties of borosilicate glass. Annealing prior to the ion exchange increases the compressive stress generated on the surface; however, its effect on strengthening is trivial.

The compressive stress produced by Na/K ion exchange in thin alkali borosilicate glass improves the damage resistance and the bending strength of glass. Due to the limited thickness of samples, heat treatments with high heating and cooling rates can be conducted. Such heat treatments can be used to carry out surface relaxation and improve the strength of samples by “surface relaxation”. A fast heat treatment after ion exchange improves the final strength samples about 40%.

# Table of Contents

Abstract:	i
Chapter I. Introduction .....	1
1.1 Ion Exchange in Glass .....	4
1.1.1 Glass structure .....	4
1.1.2 Diffusion in glass .....	5
1.2 Thermodynamics and Kinetics of Ion Exchange .....	6
1.3 Electric field assisted ion exchange .....	10
1.4 Stress generation by ion exchange .....	14
1.5 Stress relaxation .....	16
1.6 Chemical Strengthening of Borosilicate Glass .....	19
Chapter II. Experimental Methods .....	23
2.1 Materials .....	23
2.1.1 Glass .....	23
2.1.2 Salt .....	24
2.2 Preparation Technique .....	25
2.2.1 Conventional Ion Exchange .....	25
2.2.2 Electric Field Assisted Ion Exchange .....	27
2.3 Characterization Methods .....	28
2.3.1 Chemical composition .....	28
2.3.2 Mechanical properties .....	29
2.3.3 Thermal Analysis .....	37
2.3.4 Structural evolution .....	38
Chapter III. Results and Discussions .....	39
3.1 Ion-exchange strengthening of borosilicate glass .....	40
3.1.1 Effect of Glass Composition .....	44
3.1.2 Influence of Temperature .....	49

3.1.3 Influence of Salt Composition .....	52
3.1.4 Summary .....	66
3.1.5 Further studies .....	67
3.2 Electric Field Assisted Ion Exchange of Borosilicate Glass .....	69
3.2.1 Current density and E-field intensity .....	69
3.2.2 Diffusion coefficient under an electric field .....	78
3.2.3 Structural Modifications .....	83
3.2.4 Mechanical performance .....	88
3.2.5 Summary and further studies .....	91
3.3 Chemical strengthening of flat borosilicate glass .....	93
3.3.1 Sodium-Potassium Ion Exchange .....	94
3.3.2 Effect of Annealing.....	101
3.3.3 Stress build up and relaxations .....	106
3.3.4 Influence of post-ion exchange heat treatment .....	113
3.3.5 Summary .....	119
Chapter IV. Conclusions.....	121
4.1 Na/K exchange in soda borosilicate glass.....	121
4.2 Electric field assisted ion exchange of borosilicate glass.....	121
4.3 Chemical strengthening of thin alkali borosilicate glass.....	122
4.4 Implications and future research .....	123
Appendix I: Thermodynamics of molten salt .....	125
Appendix II: Electric field assisted ion exchange in soda lime silicate glass .....	127
I Introduction .....	127
II Material and method.....	128
III Results and discussion .....	128
III.a K/Na exchange .....	128
III.b Cs/Na exchange .....	133
III.c Mechanical performance .....	136

IV Conclusions.....	139
References	141
Scientific Production .....	157
Participation to Congresses, Schools and Workshops.....	159
Other activities	160
Acknowledgements	161



# Chapter I.

## Introduction

Glass is the strongest human-made material, but the surface defects introduced during the fabrication decrease the strength by two order of magnitude lower than the pristine glass [1-7]. The glass strength is unreliable since it depends on the measurement method [8, 9]; for example, a set of glass bars can have an average strength around 150 MPa, but the standard deviation is 50 MPa [10]. According to Griffith's theory about the failure of brittle materials, such as glasses and ceramics, the mechanical strength depends on the shape and size of surface flaws [8, 9, 11, 12]. The flaws dramatically deteriorate the theoretical strength of glass. The classic Griffith equation for the fracture of brittle materials can be applied to show the impact of flaws on the fracture stress,  $\sigma_f$ , of glass [13]:

$$\sigma_f = \frac{K_{IC}Y}{\sqrt{c}} \quad (1.1)$$

where  $K_{IC}$  is the fracture toughness,  $c$  the crack length and  $Y$  is a constant relating to the flaw geometry. Generally, this equation shows that  $\sigma_f$  is proportional to the inverse square root of flaw size. By considering  $Y=\pi^{-1/2}$  in Eq. 1.1, Kurkjian, C.R. has presented a comprehensive fracture stress against flaw size diagram, which illustrates typical values of practical glass strength and the flaw size at fracture [14, 15]. Figure I-1 shows the influence of flaws on the strength of borosilicate glass using Kurkjian diagram.

The flaws produced during the handling of glass extend from few microns to about 20 microns and decrease the strength to one tenth of expected values (50-200 MPa vs. 1-2 GPa); moreover, some deep defects can exist in articles, which account for the scattered and unreliable strength [13].

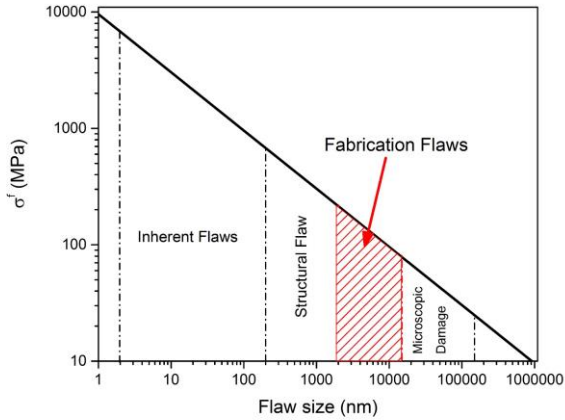


Figure I-1 Glass strength against the size of flaw presented on the glass, Kurkjian diagram.

Glass properties are also a function of chemical composition and thermal history; therefore, the properties such as mechanical strength can be improved by modifying the chemical composition of either bulk or surface [7, 16]. Several techniques can be implemented in order to recover the glass strength; Table 1 summarises the techniques used for improving the glass mechanical performance [2-4, 17]. Among those methods mentioned in Table 1, thermal tempering and chemical strengthening are the most commercialised methods for structural and electronic applications [2]. Both techniques in principle rely upon producing a compressive stress on the glass surface that prevents the formation and propagation of the flaws and cracks.

Thermal tempering is based on cooling rate gradient across the glass thickness and the production of glasses with different fictive temperatures [18]. This technique is conducted by a rapid cooling from a temperature above the glass-transition temperature. Therefore, this treatment procedure is not applicable to the glasses with low thermal expansion or complex shape like hollow shape or thin glasses (thinner than 2 mm) [3, 18]. In fact, thermal tempering is limited to window glass and rarely can be applied for new glass applications like flexible electronics.

Table 1 commercial methods used in modification and post processing of silicate glasses [19]

Removing the surface flaws		Surface coating		Modifying the surface	
Mechanical	Grinding	Plasma	Ion plating	Diffusion	Glass-staining
	Polishing		Ion implanting		Optical waveguide
	Water jet/sand blasting		PE-CVD		Antibacterial
Chemical	Etching	Gas Phase	PVD	Strengthening	DE alkalization
	Forested glass		CVD		
Thermal	Fire polishing	Liquid/Solid Phase	Paint Glazing CVD		Thermal Chemical

Ion exchange strengthening, also known as chemical strengthening, has several advantages over thermal tempering: the most important feature of the chemical strengthening is that the glass can be strengthened almost regardless of its geometry. Furthermore, the surface compression is significantly larger than the other mentioned strengthening methods [1, 4, 20, 21]. This technique is the only method that can be done in order to improve the mechanical properties of borosilicate glasses used in pharmaceutical applications [22, 23].

Ion exchange has been used since centuries ago to modify the optical properties of glass, i.e. colour [24, 25]. However, chemical strengthening was introduced as an avenue towards improving the mechanical properties of alkali-containing glasses in the 1970s [26-30]. Chemical strengthening has been used in different applications such as windshields, governmental buildings and hurricane resistant windows [31]. The thin flexible glasses produced by chemical strengthening have been in the vanguard of strong-glass development since the flexible electronics and portable devices were introduced.

In chemical strengthening a compressive stress is generated in the surface of the glass immersed in a molten salt containing larger alkali ions. The generation of compressive stress in the surface of glass is due to stuffing larger alkali ions into the site of smaller alkalis; therefore, the compression depends directly on the amount of the exchanged ions. The process takes place by the inter-diffusion of ions; consequently, the depth of exchanged layer, as a determining parameter for strengthening, depends on the time and the temperatures of treatments [16, 20, 21].

## 1.1 Ion Exchange in Glass

Chemical strengthening involves the swap of alkali ions between a molten salt and the glass surface followed by the inter-diffusion of ions in the glass. In order to understand the chemical strengthening, we, first, need to review the mechanics of diffusion process in the glass structure [7, 16, 32].

### 1.1.1 Glass structure

The structure of silicate glass can be described by a continuous network of silicon-oxygen tetrahedral units linked together at corners. In multicomponent silicate glasses, some cations can substitute silicon in the silicon-oxygen network; for example, introducing alkali and alkaline earth elements (the modifiers) the continuous network is broken up, which is resulting in a decrease in glass viscosity [7, 16, 33]. Nevertheless, the backbone of the new glass remains similar to the silica glass, which is containing a continuous network of silicon-oxygen tetrahedral units. In such a network, some oxygens are bonded to two silicon ions and some to one. The network modifiers are distributed throughout the glass and, therefore, the glass structure can be considered as a solid fabric of structural units allowing the movement of mobile elements, such as the alkali ions; consequently, the transfer of alkali ions can be described by the similar principals to heat conduction in solids [34, 35]. Glass can be considered as an isotropic medium in which physical and chemical properties are independent of direction; therefore, the movement of alkali ions can also be considered as an isotropic phenomenon.

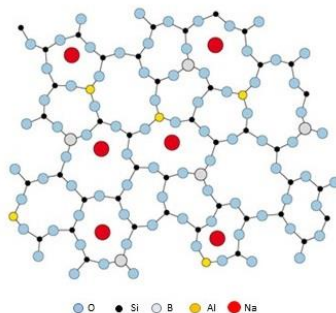


Figure I-2 alkali-glass structure

### 1.1.2 Diffusion in glass

By assuming glass as an isotropic permeable material to alkali ions, it is possible to apply Fick's law, Eq. 1.2, to describe the flux of ions in the glass structure [3, 34]. The flux of diffusing species is against the direction of the chemical potential gradient in the glass as illustrated in Figure I-3.

$$J_x = -D \frac{\partial c}{\partial x} \quad (1.2)$$

where  $J_x$  is the flux of ions and  $c$  being their concentration.  $D$ , the proportionality factor, is the self-diffusion coefficient. The process continues towards establishing an equilibrium in chemical potential gradient, which is usually considered by the chemical concentration gradient. The law can be expanded for three-dimensional systems which lies out of the interest of this report and can be easily found in the textbooks [34-37].

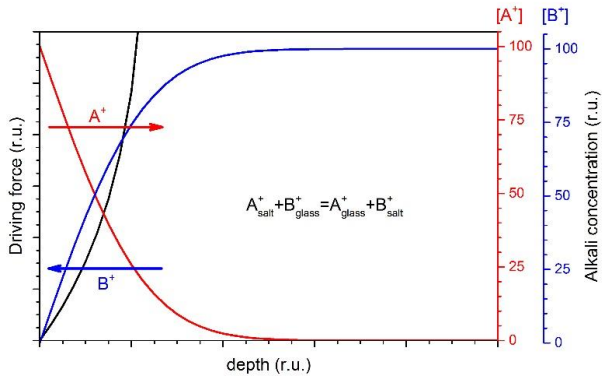


Figure I-3. Relative driving force, chemical potential, and concentration of alkali actions involved in ion exchange (Note: the graph is not to scale)

The concentration variations against time and location are related to each other via Fick's second law as given by Eq. 1.3.  $D$  is usually considered independent of the concentration and constant; however,  $D$  is reported to be also composition dependent in long treatments [32, 38-40]. In practice, in short treatments like what we are

interested in, the diffusion coefficient is assumed constant and, therefore, Eq 1.3.-a can be written in the simple form of Eq 1.3.b [3].

$$\frac{\partial c}{\partial t} = \nabla \cdot (D \nabla c) \quad (1.3-a)$$

$$\frac{\partial c}{\partial t} = D \frac{\partial^2 c}{\partial x^2} \quad (1.3-b)$$

The mobility of ions and diffusion coefficient depend on temperature [41-44]. By increasing the temperature, the diffusion coefficient becomes larger which is discussed later on.

## 1.2 Thermodynamics and Kinetics of Ion Exchange

Ion exchange is typically conducted by using a molten salt bath containing the alkali cations, an oxide layer or a metallic coating on the surface of the glass. The methods using coatings as the source of cations are less popular for the mechanical applications and usually used in optical applications [1, 17].

As mentioned above, the most common technique for ion exchange is conducted by immersing glass in a molten salt containing a significant amount of cations desired to take the place of the glass alkali ions. A schematic draw of the process for replacing sodium in the glass with potassium is shown in Figure I-4. The process can be considered as a series of mass transfer steps including: the convection stirring of salt in the bath, the movement of sodium and potassium in the static layer of salt adjacent the glass surface, swapping sodium with potassium on the glass surface, potassium exchange for sodium and the interdiffusion of alkali ions in the glass.

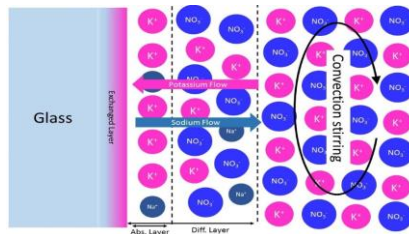
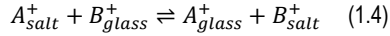


Figure I-4 Schematic draw of potassium-sodium ion exchange conducted in molten salt. Abs. layer represents the layer formed near the surface of immersed glass and the cations absorbed to the surface. Diff. layer is produced because of the local E-Field of Abs. layer. It is worth to

mention that the progress of ion exchange depends on the diffusion of cations through these layers

The whole process can also be considered as a chemical reaction between glass and salt in which the salt cations, i.e.  $K^+$ , are taking the place of the glass alkalis such as lithium and sodium. Eq. 1.4 presents the reaction describing the exchange of monovalent cations between glass and salt [45]. This equation will be referred to estimate salt-glass equilibrium.



- **Glass-Salt Equilibrium**

The ion exchange, Eq. 1.4, proceeds by the transfer of alkali ions through each step presented in Figure 1-4. In industry, the changes in the salt's composition during ion exchange is negligible because of the large volume of salt compared to the glass articles; such an approximation may fail in particular practices [46]. Therefore, how the substituting ions' concentration changes on the surface by the salt composition matters.

It is assumed that if a piece of glass is immersed in the salt, the equilibrium between the glass surface and salt is established immediately. By considering Eq. 1.4, Garfinkel reported a sigmoidal increase of A ions in the glass surface against the same ion concentration in the bath [47]. Araujo explained this behaviour by using the thermodynamic requirements of equilibrium between the surface and the salt as described below [45, 48].

The ion exchange reaction becomes into equilibrium when the chemical potentials difference of the involved ions in either system is the same [48, 49], Eq. 1.6.

$$\mu_A^{glass} - \mu_A^{bath} = \mu_B^{glass} - \mu_B^{bath} \quad (1.5)$$

The chemical potential of an element of interest in a phase at a certain temperature, T, can be calculated by Eq 1.6:

$$\mu_i = \frac{\partial(-kT \ln Q)}{\partial N_i} \quad (1.6)$$

where Q being the partition function, N the number of ions. And, K is the Boltzmann constant:

$$Q = q_A^{N_A} q_B^{N_B} \sum_{N_{AB}} \Omega(N_A, N_B, E(N_{AB})) \exp\left(\frac{-E(N_{AB})}{kT}\right) \quad (1.7)$$

where  $q_i$  is the partition function of the phase of interest (glass or salt) when it contains only ions of  $i$ ; the mixing energy must also be considered in the partition function when the both types of monovalent ions are present. The summation part of Eq. 1.7 represents all possible values of interaction energy.  $\Omega$ , the number of states of a particular interaction, cannot be evaluated in complex systems; however, in a one-dimension system where the ions are only interacting with the neighbour ions, it can be estimated; the detailed calculations are reported in literature [45, 46]. By using the molar concentration of elements  $X_i$  and considering the bond strength varying in either phase, the equilibrium constant,  $K_{eq}$ , is given by:

$$K_{eq} = \left( \frac{X_A^{glass} X_B^{bath}}{X_B^{glass} X_A^{bath}} \right) F(bath) F(glass) = \frac{q_A^{glass} q_B^{bath}}{q_B^{glass} q_A^{bath}} \quad (1.8)$$

Helmholtz free energy,  $F$ , is a function of the interactions between the elements of phases. When the salt composition and temperature are fixed, the system's degree of freedom becomes zero; in other words, there is a unique glass surface composition in equilibrium with the salt at a definite temperature and salt composition. One can expect that the difference of bonding energies in each phase (the difference of chemical potentials) is important rather than the bonding energy itself; besides, the polarizability of cations is weaker than the anions in oxide glasses. Therefore, the polarisation of anions by near alkali ions might determine the interaction energy; such assumption is fairly in agreement with Garfinkel's experimental data [47, 50].

The equilibrium between the glass surface and salt, determined by thermodynamics, contributes to ion exchange progress by two means: first, it defines the surface concentration of stuffed ions. Secondly, the diffusion is driven by the chemical driving force dependent on the equilibrium.

- **Alkali ions diffusion in glass**

As mentioned above, the diffusion of alkali ions is one of the fundamental steps in ion exchange. Swapping of ions occurs by the penetration of the salt cation inward the glass and diffusion of the glass cations outward the glass; it is worth to have a closer look on the formulation of the diffusion of ions in glass. The electric charge and mass balance and, hence, the flux of ions are the first requirements of ion exchange process; the equal flux gradient satisfies the charge neutrality requirement:

$$\nabla \cdot J_A + \nabla \cdot J_B = 0 \quad (1.9)$$

Jost employed the flux gradient balance and described the mutual-diffusivity as a function of the ions number in a small volume, N, and the diffusivity of every individual ion [51]. The mutual diffusivity,  $\tilde{D}$ , for a binary exchange can be written as following:

$$\tilde{D} = \frac{D_A D_B}{N_A D_A + N_B D_B} \quad (1.10)$$

where  $D_A$  and  $D_B$  being the self-diffusion coefficients. The mutual-diffusivity is a function of the ratio of mobile ions engaged in ion-exchange. Therefore, in a typical concentration profile produced by ion exchange, the mutual diffusivity is also a function of distance from the surface [45, 48].

Usually, sodium is replaced with potassium in chemical strengthening; larger and heavier potassium ions are less mobile in the glass structure; consequently, the self-diffusions diverge; this changing the diffusion equation from the typical form, presented by Eq. 1.3, to the mentioned below:

$$\frac{\partial c}{\partial x} = \frac{D_K}{1-\alpha c} \left[ \frac{\partial^2 c}{\partial x^2} + \frac{\alpha}{1-\alpha c} \left( \frac{\partial c}{\partial x} \right)^2 \right] \quad (1.11)$$

where  $\alpha$  depends on the ration between the diffusion coefficient of ions;  $\alpha=1-(D_K/D_{Na})$ . It is mentioned before that the self-diffusion also depends on temperature, and the temperature increase makes the difference of the coefficients larger. Also, long time treatments produce complex concentration profiles in the glass.

Varshneya et al. have reported the concentration-dependent inter-diffusion coefficients in potassium-sodium exchange of borosilicate glass [22]. The dependency is known to be related to the mixed alkali effect in silicate glass reported by Doremus and by Lachame [52]; however, Ingram et al. have reported that a series of structural modifications account for the coefficient variations [53, 54], which will be discussed later.

Nevertheless, in short time treatments at low temperatures, the concentration profiles generated by ion exchange are fitted well by using a complimentary error function:

$$\frac{C(x,t)-C_i}{C_s-C_i} = \operatorname{erfc}\left(\frac{x}{2\sqrt{Dt}}\right) \quad (1.12)$$

where  $C_i$  and  $C_s$  are the initial concentration of potassium in glass and the surface concentration respectively, and  $t$  being time. Ion exchanges with the aim of

strengthening are conducted at temperatures below the glass-transition temperature for a short time to avoid stress relaxation as discussed in 1.5 .

Ion mobility and, consequently, the diffusion coefficient,  $D$ , are dependent on temperature and following Arrhenius' law:

$$D = D_0 \exp\left(\frac{-Q}{RT}\right) \quad (1.13)$$

where  $Q$  is the activation energy. The activation energy can be easily estimated through investigating the variations of either diffusion depth or diffusion coefficient by changing temperature.

The approximated chemical profiles are in good agreement with the practical results if the diffusion coefficient is composition independent. However, as pointed before in conditions including high temperature or long process time, the mentioned approach overestimates the depth of ion-exchanged layer, and a sophisticated technique should be used to identify diffusion coefficients; i.e. using Boltzmann-Matano method based on microprobe chemical analysis besides employing complex models available for inter-diffusion [55]. There is a general agreement between the concentration profiles estimated through a complimentary error function and stress profiles; however, there are some discrepancies, which are related to stress relaxation on the surface and will be reviewed later.

### **1.3 Electric field assisted ion exchange**

Using an external source of energy such as ultrasonic agitation, microwave heating, and electric fields affects the diffusion of ions and increases the ion exchange and , consequently, the chemical strengthening [1, 2, 25]. Applying an electric field pushes the ions in one direction that decreases not only the time and temperature of treatment but also produces concentration profiles resembling different shape, which can improve the chemical strengthening efficiency. The formation of the concentration profiles in glasses subjected to E-field assisted ion exchange from a molten salt, or a solid state coating has been studied in the past [41-44, 56]. In following, the equations describing the generation of the concentration profiles, based on the formulation proposed by Abou-El-Leil M. and Cooper A. are presented [56, 57].

Here, the equations are derived again by considering the required corrections and modifications regarding the samples preparations in this study and reported corrections and modifications in literature [25, 58-60]; furthermore, only sodium-

potassium ion exchange has been considered. To describe the formation of a potassium concentration profile in a sodium-containing silicate glass during electric field assisted ion exchange, some assumptions are made, which are summarised as follows:

- Applied E-field is a DC field with a constant intensity across the glass
- The raw glass has only one mobile monovalent cation, Na<sup>+</sup>
- Sodium ions are ahead of potassium in the direction of Electric field.
- Ions mobility and, therefore, the self-diffusion coefficients of cations are constant and composition independent. Self-diffusion coefficient is related to the mobility of ions by Einstein's relation:
- 

$$D_i = \mu_i k_B T \quad (1.14)$$

where D is the self-diffusion coefficient,  $\mu$  is the ion mobility and  $k_B$  and T being Boltzmann constant and absolute temperature, respectively. A schematic draw of the glass subjected to electric field and ions is shown in Figure I-5.

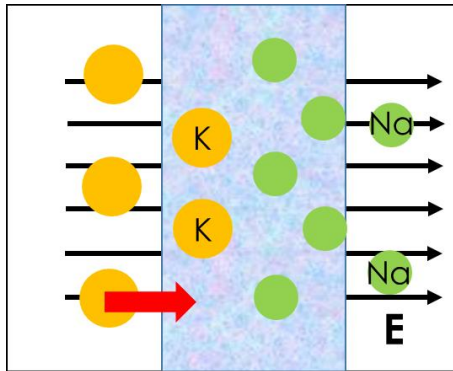


Figure I-5 Cations accelerated in the direction of applied E-field during Electric field assisted ion exchange

The flux of cations, J, can be written as:

$$J_A = \frac{D_i E C_i}{k_B T} - D_i \frac{\partial C_i}{\partial x} \quad (1.15)$$

The diffusion part, the second term of Eq. 1.15, describes the diffusion of cations in the opposite direction of the electric field due to the chemical potential. The molar density of alkali ions, or the alkali sites, is constant. Hence, the concentration of alkali ions,  $C_{\text{alkali}}=C_{\text{Na}}+C_{\text{K}}$  is constant. By applying the continuity conditions, the concentration gradient of potassium, K, can be derived as:

$$\frac{\partial C_K}{\partial x} = D_K \left[ \frac{\partial^2 C_K}{\partial x^2} - \frac{1}{k_B T} \left( E \frac{\partial C_K}{\partial x} + C_A \frac{\partial E}{\partial x} \right) \right] \quad (1.16)$$

When a glass is subjected to a constant E-field, the last term on the right side of Eq. 1.16 is eliminated. By considering the electric charge balance, the total flux of ions should be constant. If the alkali ions are the only charge carriers in glass, the flux of ions is related to the current density, J, as following:

$$\frac{\bar{I}}{F} = J_0 = J_{Na} + J_K = D_{Na} \frac{E C_{Na}}{k_B T} - D_{Na} \frac{\partial C_{Na}}{\partial x} + D_K \frac{E C_K}{k_B T} - D_K \frac{\partial C_K}{\partial x} \quad (1.17)$$

where F is Faraday's constant. By using the mobility ratio of potassium to sodium,  $M=J_{Na}/J_K$ , Eq. 1.17 is written as:

$$E = \frac{k_B T \left[ M J_0 + D_K (M-1) \frac{\partial C_A}{\partial x} \right]}{D_K [C_{\text{alkali}} + (M-1) C_K]} \quad (1.18)$$

The local electric field intensity is a function of both the concentration profile and the ion flux. The following equation describes the variation of E-field by time:

$$\frac{\partial E}{\partial t} = k_B T \left\{ \frac{(M-1) \left( \frac{\partial^2 C}{\partial x^2} \right)}{C_K + (M-1) C_K} - \frac{[\mu J_0 + D_K (M-1) \frac{\partial C_K}{\partial x}]}{D_K [C_0 + (M-1) C_K]^2} (M-1) \frac{\partial C_K}{\partial x} \right\} \quad (1.19)$$

Combining Eq. 1.16 and Eq. 1.19 gives the characteristic differential equation of E-field assisted ion exchange process:

$$\frac{\partial C^*}{\partial t^*} + \frac{M}{1+(M-1)C^*} \frac{\partial C^*}{\partial x^*} = \frac{\partial}{\partial x^*} \left[ \frac{1}{1+(M-1)C^*} \frac{\partial C^*}{\partial x^*} \right] \quad (1.20)$$

where

$$x^* \equiv \frac{J_0 x}{C_0 D_K}, t^* \equiv \frac{J_0^2 t}{C_0^2 D_K}, C^* \equiv \frac{C_K}{C_0}$$

The boundary conditions of Eq. 1.20 can be specified by considering the treatment conditions; the parameters used for samples' preparation are deemed to apply the

boundary conditions and derive the characteristic equation of electric field ion exchange. The nominal composition of the glass subjected to electric field assisted ion exchange has only one alkali element( section 2.1.1 ); furthermore, considering the concentration of the elements in the glass the diffusion coefficient can be considered equal to the self-diffusion coefficient of alkalis [38, 39, 61]. Moreover, applying a strong enough electric field causes that conventional diffusion makes no significant contribution in the process and, therefore, the analytical solution for Eq. 1.20 is obtained as follows [25]:

$$C_K(x, t) = \frac{C_K^{surface}}{2} \operatorname{erfc}\left(\frac{x - \mu_K E t}{2\sqrt{Dt}}\right) \quad (1.21)$$

The concentration profiles in the glass produced by the conditions mentioned above are presented in Figure I-6. Potassium variation across the glass resemble a step-like profile and when the E-field intensity increases, the depth of exchanged layer increases considerably.

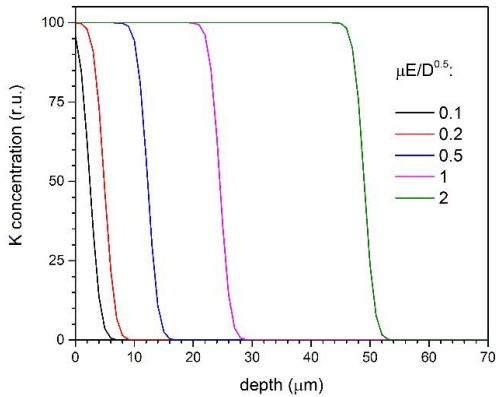


Figure I-6 Typical concentration profiles, calculated, produced in alkali-silicate glass by subjecting to EF-IE. The profiles were drawn by considering the applied E-field variable which was normalised to the square root of diffusion coefficient, D,

## 1.4 Stress generation by ion exchange

Stuffing larger potassium ions into the glass and the formation of concentration profiles yield the glass network strain and, consequently, compressive stress build up. The first perception about the compression profiles is that the compressive profile is following concentration profiles produced by ion exchange [62]. The formation of compressive stress is understood to be similar to the stress built up in metals using the nitridation technique and the stress generation on the surface is formulated by considering the analogy with thermal stress [1, 7, 17, 63].

By using the analogy to thermo-elasticity, the stress-strain relationship for a cubic element located in the ion exchange layer (as presented in Figure I-7) in which all alkali ions are replaced with the larger invading ions can be written as:

$$\begin{aligned}\varepsilon_{xx} &= \left(\frac{1}{E}\right) [\sigma_{xx} - \nu(\sigma_{yy} + \sigma_{zz})] + BC \\ \varepsilon_{yy} &= \left(\frac{1}{E}\right) [\sigma_{yy} - \nu(\sigma_{xx} + \sigma_{zz})] + BC \\ \varepsilon_{zz} &= \left(\frac{1}{E}\right) [\sigma_{zz} - \nu(\sigma_{yy} + \sigma_{xx})] + BC \\ \varepsilon_{xy} &= \frac{\sigma_{xy}}{G}; \quad \varepsilon_{yz} = \frac{\sigma_{yz}}{G}; \quad \varepsilon_{xz} = \frac{\sigma_{xz}}{G} \quad (1.22)\end{aligned}$$

where E= Elastic modulus, G= shear modulus and  $\nu$  is the Poisson's ratio. B is the linear strain of glass per unit concentration change of alkali oxide:

$$B = \frac{1}{3\Delta C} \frac{\Delta V}{V_0} \quad (1.23)$$

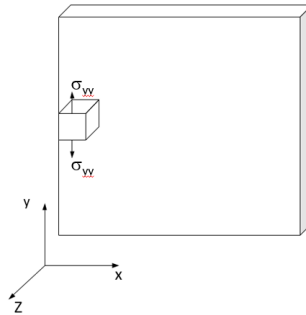


Figure I-7 Schematic unit of a semi-infinite glass sheet subjected to ion exchange along x-axis  
Only the generated stress in one direction is shown

In a semi-infinite plate which has been completely exchanged in x-direction, one can assume that the stress generated along x-axis,  $\sigma_{xx}$ , is zero because the plate is allowed to expand in that direction freely. By considering the specimen is constrained at the edges and confined by the substrate glass, it can be expected that  $\varepsilon_{yy}=\varepsilon_{zz}=0$ . By applying these boundary conditions to the Eq. 1.22; the generated stress is estimated as

$$\sigma_{yy} = \sigma_{zz} = -\frac{BEC}{1-\nu} \quad (1.24)$$

Eq. 1.24 corresponds to the compression produced by the stuffing of ions into the glass. Cooper A. et. al have adopted the formulations to describe the formation of stress in glasses subjected to ion exchange [64, 65]: The generated stress in an alkali containing glass subjected to ion exchange with a semi-infinite plate geometry follows the concentration of stuffed ions, C, by:

$$[\sigma_{yy}]_x = [\sigma_{zz}]_x = -\frac{BEC}{1-\nu} + \left(\frac{BE}{\delta(1-\nu)}\right) \int_0^\delta C(x)dx \quad (1.25)$$

where B= network dilation coefficient, E= Elastic modulus, and  $\nu$  is the Poisson's ratio.  $\delta$  is being the thickness of the glass. The second term represents the balancing tension generated because of the compatibility of exchanged layer to the uninfluenced bulk glass. According to Eq. 1.25, the effect of stress relaxation is negligible; on the contrary, stress relaxation has a significant influence. Cooper et al. have investigated the stress relaxation at elevated temperatures; by taking into account the stress loss because of the relaxation. The compressive stress produced by ion exchange after time t is estimated from:

$$\sigma_{yy}(x, t) = \frac{-BE}{1-\nu} \left(\frac{1}{\delta} \int_0^{t_1} R(t_1 - t) \left(\frac{\partial}{\partial t} \int_0^\delta C(x)dx\right) dt\right) \quad (1.26)$$

where R and  $t_1$  being the normalised relaxation function and the ion exchange time respectively. According to Eq. 1.26 the maximum compressive stress is located at the surface of glass; whereas, the maximum of compressive stress is measured below the surface in practice [3]. The mismatch between the stress profiles and the concentration profiles is attributed to the dependence of stress relaxation on time and the concentration of the invading ions [66]. The theoretical compressive stress is far larger than the experimental values, which is related to the theoretical dilation coefficient [67, 68]. The network dilation coefficient, also known as linear network dilation coefficient, LNDC, can be expressed as:

$$B = \frac{1}{3} \left[ \frac{\partial \ln V}{\partial C} \right] \quad (1.27)$$

By assuming that the glass produced by ion-exchange has a similar molar volume to the compositionally equivalent to melt glass, CEAM, glass the LNDC is given by:

$$B = \left( \frac{1}{3C_0} \right) \ln \left( \frac{V_{CEAM}}{V_{Raw}} \right) \cong \frac{V_{CEAM} - V_{Raw}}{3V_{Raw}C_0} \quad (1.28)$$

where  $C_0$  is the mole fraction of alkali glass in exchanged layer and  $V_{Raw}$  being the molar volume of the raw glass. The volume change is divided to 3 in order to calculate the linear dilation [63]. The estimated LNDC is usually about three to five times larger than the measured values from the stress profiles measured in practice, which is known as “dilation anomaly” [63, 69]. The plastic deformation can occur during stuffing of larger ions into the glass instead of the elastic strain and it is probably responsible for the difference between the values calculated by theory and the practical measurements [17]. Many efforts have been made to improve the understanding of network dilation anomaly, i.e. considering the stress relaxation; however, it has remained controversial [1].

## 1.5 Stress relaxation

Subjecting to elevated temperatures, at which ion-exchange is practised, accelerates the glass transitions, such as stress and structural relaxations, and causes compressive stress reduction [63, 70, 71]. The stress relaxation role is of crucial importance in chemical strengthening [66, 71, 72]. Since stress relaxation also accounts for the stress profiles anomalies, such as the stress intensity and the maximum stress beneath the surface, it has been extensively studied [21, 63, 71]. The glass viscous flow is considered to be responsible for the compressive stress degradation at typical ion-exchange temperatures [1, 4]. Conversely, the compressive stress at zero time after ion exchange is far less than the predicted by the theoretical approach even after considering the relaxation because of viscous flow [63, 73].

Varshneya et. al have proposed a model in which a series of structural modifications cause stress loss in very few seconds after ion exchange [73]. The model predicts that a strong compressive stress is produced by stuffing large potassium ions into glass in picoseconds after potassium exchange for sodium. Then, some structural modifications, like changing the distances between bridging / non-bridging oxygens and potassium, decrease the built-up stress. The further stress loss happens because

of the ions jump from one cage to the other and penetration of ions while there are no topological changes of structure in these steps [53, 63, 73].

Further stress loss may occur by structural modifications that might take place by breaking and reforming of bridging oxygens. Cation-induced relaxation of network, CIRON, has been proposed to describe the stress loss by short-range structural evolutions. CIRON is known to be the best representative of this kind of relaxation [53, 74]. In this model, the diffusion of cations into the glass occurs by breaking the bridging oxygens corresponding to  $Q_2$  and  $Q_4$  species and the formation of new  $Q_3$  species. These changes modify the orientation of alkali sites and the new sites can host larger potassium ions. Figure I-8 shows a schematic draw of structural variations in the diffusion path of ions in the glass [53, 54]. The structural modifications are probably responsible also for the shrink of glass free volume. Such processes and the stress relaxation because of viscous flow perhaps account for the stress decline or in extreme cases producing a stress-free ion-exchanged glass. Although the glass is more stable after all the relaxation processes during the ion exchange, the glass structure and, therefore, its volume is different from the chemically equivalent as melt glass [75]. It is worth mentioning that the structural evolution and stress relaxation of glass during ion exchange and chemical strengthening are open questions and need to be answered.

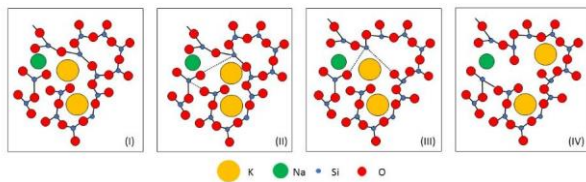


Figure I-8 Schematic draw of structural modification of glass by breaking and reforming of bridging oxygens during ion exchange. The bridging oxygen of a  $Q_4$  group is stretched, weakened, broken and recombined with a  $Q_2$  to accommodate larger potassium cation. The process produces 2  $Q_3$  species.

The stress-free ion-exchanged glass is known as a “forbidden glass” due to the different structure from the as-melt [76]. In this step, the glass undergoes long-range structure relaxations to take a similar structure to the as-melt glass towards decreasing the free energy; the process here may last several years at low temperatures [70, 77, 78].

The stress loss in the first steps is too fast, few picoseconds, to be controlled and considered as a process parameter. On the other hands, the last step is so slow, decades, that is not essential for chemical strengthening in practice. Therefore, what matters is the stress relaxation due to the relaxations processes occurring at an intermediate slot.

The glass viscous flow has been considered responsible for stress relaxation, which is represented by mechanical models which are essentially consisting Burger elements, a Maxwell and a Voigt-Kelvin element in series, attached to a rigid support [21, 66, 71, 73]. The relaxation transitions in glass can also be estimated by a sophisticated model: the stretched exponential model.

The stretched exponential model, which is proposed empirically by Kohlrausch in 1847, fits well the stress relaxation behaviour of disordered and quenched molecular systems [77-79]. The property subjected to relaxation, which is the surface stress in this case, is a function of time as follows:

$$\sigma_t^R = \sigma_0^R e^{-\left(\frac{t}{\tau}\right)^\gamma} \quad (1.29)$$

where  $\sigma_t^R$  and  $\sigma_0^R$  are the residual stress and the zero-time residual stress;  $t$  is time.  $\tau$  being the relaxation time,  $\gamma$  the exponent factor which accounts for the non-Maxwellian behaviour of the glass [63]. This function can also be used for structural relaxations in frequency domain [78, 79]; however, in this study, the time-dependent relaxations were investigated (section 3.3.3).

Eq. 1.29 has only two free parameters: the relaxation time and the stretched exponent, where  $\gamma$  satisfies  $0 < \gamma \leq 1$ , and  $\gamma=1$  presents Burger's model as a simple exponential model. Lower values of  $\gamma$  are corresponding to more complex relaxation mechanisms [70, 79]. Two particular values for  $\gamma$  are expected in homogeneous glassy systems:  $\gamma=0.6$  for short range transitions such as stress relaxations and  $\gamma=0.43$  corresponding to the long range structural relaxations [77]. These numbers are known as "magic" values of glass relaxations; these numbers were deduced from the axiomatic diffusion trap model and had been validated using commercial glass specimens [77, 79].

Typically, the relaxation time lies between  $10^5$  to  $10^7$  s for the temperatures at which ion exchange is carried out. Moreover, the relaxation temperature is well fitted with the Vogel-Fulcher expression [7, 32, 70]:

$$\tau(T) = \tau_0 e^{-Q \frac{T-T_0}{T_0}} \quad (1.30)$$

where  $T$  is the relaxation temperature, and  $T_0$  and  $Q$  being Vogel-Fulcher parameters which are obtained by fitting the experimental data with Eq. 1.30.

For successful chemical strengthening, a strong compressive stress with an enough depth is a must to reinforce the surface flaws and, consequently, increase the mechanical strength. Because of the diffusional nature of the process, producing the desired exchanged layer requires subjecting to elevated temperatures for several hours. Therefore, finding the critical parameters and their influences are the very first requirements of chemical strengthening of glass.

## 1.6 Chemical Strengthening of Borosilicate Glass

The glass strength is affected by the surface defects, and the idea of glass strengthening is to “reinforce” the surface cracks. Although the mean flaw size of glass changes from few nanometers to millimetres, as-received glass usually contains flaws with a size between 1-15  $\mu\text{m}$  (Kurkjian diagram- Figure I-1). The compression layer and, consequently, the exchanged layer must be thicker than the critical flaw size to improve the glass strength. Producing such layer in a glass is simple to say but often hard to do.

As mentioned above (section 1.4 ), the surface compression has a pivotal role in chemical strengthening; intense surface compression is required to “reinforce” the surface flaws and improve the strength of glass. The surface compressive stress is also responsible for increasing the damage resistance of glass by preventing the formation of cracks in impacts and sharp contacts. Therefore, chemical strengthening has been practiced, fundamentally, on alkali-aluminosilicate glasses that yield intense compressive stress [31]. However, even a strong compressive stress on the surface has no use for improving the strength of glass if it contains large surface defects.

Figure I-9 shows typical characteristic depths of the ion-exchanged layer produced in lithium-aluminosilicate (LAS), soda borosilicate (SBS) and soda lime silicate glasses (SLS) by subjecting to ion exchange [80-84]. The graph is plotted in linearized coordination by using and the correlation between the characteristic depth,  $x$ , and ion exchange time,  $t$ , and  $D$  the estimated diffusion coefficient:  $x = 2(D^*t)^{1/2}$ .

The thickness of exchanged layer depends on the diffusion coefficient of ions into the glass and the time of treatment regarding Eq. 1.12. Although a thick compressive layer can be produced by carrying out long time treatment, the production of a thick layer is

at the cost of surface compressive stress degradation due to relaxation; moreover, long treatments increase the cost of treatment besides rising environmental concerns. Therefore, the exchanged layer produced by a typical chemical strengthening, i.e. 4 h, must cover most of the surface flaws generated during the fabrication processes. Lithium-aluminosilicate and soda-borosilicate glasses provide the required exchanged layer.

Recently, the demand for strong borosilicate glass renewed the interested in the strengthening methods of this glass; soda borosilicate glass is one of the less practiced materials in chemical strengthening [1, 17, 22]. In contrast, the thick exchanged layer makes it possible to improve the strength of borosilicate glass by chemical strengthening. However, there are limited reported about chemical strengthening of borosilicate glasses [1].

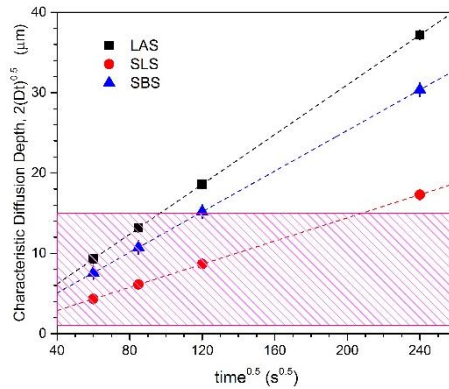


Figure I-9 Characteristic diffusion depth (DOL) produced by ion exchange in different glass families; the shaded area represents the typical size of surface defects of glass before subjecting to the strengthening treatments.

The knowledge about the strengthening of alkali-aluminosilicate and soda lime silicate can be employed to modify and re-design the conventional ion-exchange methods for the chemical strengthening of alkali-borosilicate glasses, especially the glasses used in pharmaceutical packaging, solar cells, micro electro mechanical systems (MEMS), and electronics.

It is, therefore, a major task to understand the influences of processing parameters including temperature, salt bath impurities and glass composition on the efficiency of chemical strengthening. Conventional treatments needs to be practised in order to

acquire the understanding. By using a different family of glass new avenues are possibly opened towards conducting less practiced methods of ion exchange, such as electric field assisted ion exchange, as mentioned in section 1.3 , aimed to improve the mechanical performance of glass. Indeed, this introduced new parameters yet to be investigated. Furthermore, the effects of limited thickness and thermal shock resistance of thin borosilicate glass on stress build up and relaxation in chemical strengthening are required to be studied.

Impacts of processing parameters on the final strength of soda-borosilicate glasses are investigated in this thesis. Conventional ion exchange as well as electric field assisted ion exchange are conducted for the treatment of glass tubes used in pharmaceutical packaging. Furthermore, thin alkali-borosilicate glass sheets are subjected to potassium for sodium ion exchange in order to investigate chemical strengthening of borosilicate glass, annealing and post-ion exchange heat treatment on the final strength of glass.



# Chapter II.

## Experimental Methods

This chapter presents an overview of the raw materials, preparation methods and characterisation techniques used in this work; some techniques used for a specific characterisation are excluded and will be discussed besides the corresponding results.

Commercial soda borosilicate glasses were used as the raw glass in the ion exchange processes. The sample preparation process is modified depending on the geometry of the sample and the applied E-field. Mechanical tests and microstructural characterizations were conducted to assess the performance of ion exchange strengthening.

### 2.1 Materials

#### 2.1.1 Glass

Two different geometries of alkali borosilicate glasses, tubes and flat, were used in this study. The influences of salt impurities on the chemical strengthening of glass used in pharmaceutical packaging were investigated by using the tubes. Electric field assisted ion exchange was also performed by using test tubes made from soda-borosilicate glass. Thin alkali borosilicate glass produced by the down-drawing process was subjected to chemical strengthening and the stress build up, and relaxation of glass were investigated.

- **Tube**

Soda-borosilicate canes, Type I- Class B, provided by Nipro-Glass, France, and Schott AG, were used in this study. The dimensions of glass canes are summarised in Table 2, and the chemical composition of the glasses will be discussed later in Table 7 in detail.

Sane, A.Y et al. have reported that the generated stress by chemical strengthening may change 90° corners of glass and such edges will become dog-ear shape after ion exchange [85]. Varshneya, A. has reproduced the results and confirmed such a change in the glass subjected to chemical strengthening [1]. The deformation of corners produces weaker edges in the strengthened glass and it is suggested to round sharp edges before chemical strengthening. Accordingly, both ends of tubes, cut from

glass canes by using the scribe and bend method, were polished with SiC paper, Grit 320.

Table 2 Dimensions of the BS glass canes used for producing tubes, the glass tubes used in studying the conventional ion exchange

	<b>Commercial name</b>	<b>OD(mm)</b>	<b>ID(mm)</b>	<b>Length (mm)</b>
<b>Nipro Glass</b>	<b>Nipro</b>	6.85	4.65	1500
<b>Schott AG</b>	<b>Fiolax-Clear</b>	6.85	4.65	1500
	<b>Fiolax-Clear</b>	10.85	8.65	1500

Test tubes with rimmed cap made from Fiolax-Clear, Schott AG, were used as the raw glass in the electric field assisted ion exchanges. Table 3 shows the final dimensions of tubes produced for mechanical tests.

Table 3 Dimension of samples cut from the canes and subjected to ion exchange

	<b>OD(mm)</b>	<b>ID(mm)</b>	<b>Length (mm)</b>
<b>Tube</b>	10.85	8.65	100
<b>Tube</b>	6.85	4.65	60
<b>Test tubes (Fiolax-clear)</b>	9.65	7.45	100

- ***Flat glass***

Square samples with the dimension of  $45 \times 45 \text{ mm}^2$  were cut from the flat glass, D 263 Teco® supplied by Schott AG, with the nominal dimensions of  $360 \times 440 \times 0.21 \text{ mm}^3$  by the scribe and bend technique using a glass cutter, M18 MicroPenett diamond wheel, GCD-MP-M18S, MDI, Japan.

### **2.1.2 Salt**

The ion exchange of glass tubes were conducted in three salt baths already used in the chemical strengthening of soda lime silicate glasses in the lab with different amounts of impurities, mainly sodium and calcium, named as Low-Na, High-Na and High-Ca to ease pointing the characteristic contaminant. The ion exchanges of thin glass and electric field assisted ion exchanged were conducted by using pure potassium nitrate Sigma-Aldrich (ACS grade,  $\geq 99.0\%$ ).

The chemical composition of the salts was initially checked by ICP-OES (Spectro-Ciros, Kleve, Germany) and the melting point was measured by Differential Scanning Calorimetry (DSC) (DSC2010, TA Instruments, USA). The composition of salts was monitored by ICP-OES to keep the concentration of impurities constant. Table 4 shows

the fundamental impurities of salts, the melting temperature and the commercial source of them. The calcium contamination was introduced to the salts using calcium nitrate tetrahydrate (Sigma-Aldrich, nominal purity  $\geq 99.0\%$ ) calcined at  $350\text{ }^{\circ}\text{C}$  for 24 h prior mixing with the  $\text{KNO}_3$  salt.

Table 4 Fundamental impurities and melting temperature ( $T_m$ ) of the  $\text{KNO}_3$  baths (ND = not detected).

	[Na] (ppm)	[Ca] (ppm)	[Mg] (ppm)	$T_m(^{\circ}\text{C})$	Source
Pure $\text{KNO}_3$	10	8	<1	334	Sigma-Aldrich (ACS grade, $\geq 99.0\%$ )
Low-Na	1039	ND	5	330	Sigma-Aldrich (ACS grade, $\geq 99.0\%$ ) used for chemical strengthening of SLS
High-Na	2431	ND	5	322	provided by unknown source, already used for at least 1000 h in Na-K
High-Ca	769	68	5	327	Haifa – Eurochemicals (technical grade, $\geq 99.4\%$ ) contaminated by Calcium

## 2.2 Preparation Technique

### 2.2.1 Conventional Ion Exchange

Tubes cut from canes were, first, ultrasonically washed in distilled water, cleaned in acetone and air dried. Then, the treatments were carried out using a semi-automatic oven designed for chemical strengthening, TC 20A, Lema, Italy. Samples were placed in a stainless steel sample holder, which contains up to 30 samples at the same time. The tubes were kept over the salt bath 20 minutes before and after ion exchange according to the standard procedure of the furnace. The glass tubes were subjected to ion exchange at  $450$  and  $465^{\circ}\text{C}$  for 4h. Also, the glass to salt weight ratio was kept below 1:35.

The thin glass samples, cut into  $45 \times 45\text{ mm}^2$  squares, were ultrasonically washed in acetone and air dried; then, the samples were immersed in molten salt straight after drying by using a stainless steel sample holder. After the treatment, samples were

removed immediately from the molten salt and the sample holder to avoid sticking of the samples to the metallic frame due to the salt solidification. The glass to salt weight ratio was kept below 1:50. Ion exchanges were carried out at a temperature between 350-500°C for 1-16 h. A schematic illustration of the conventional ion exchange procedure is shown in Figure II-1.

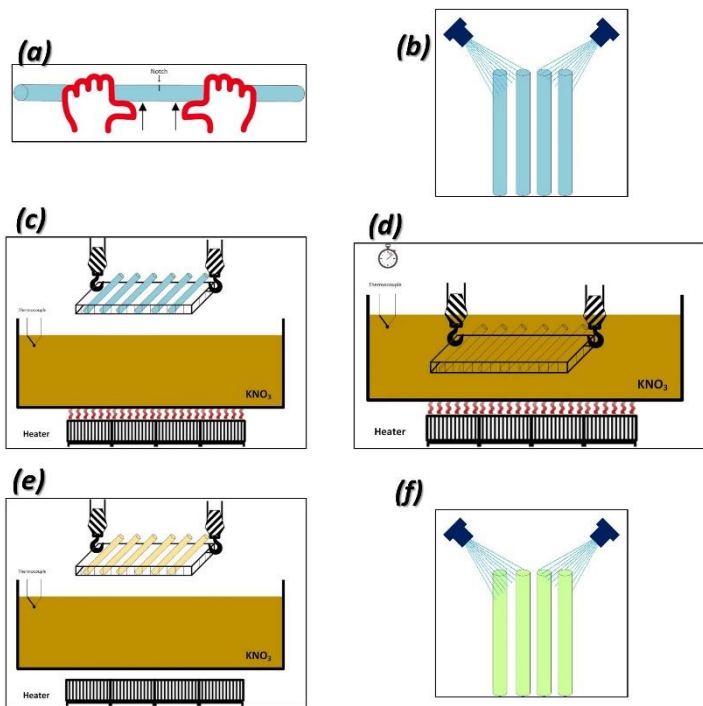


Figure II-1 Schematic of the conventional ion exchange procedure ( used for borosilicate glass tubes). (a) cutting the canes, (b) washing the tubes with water, (c) pre-heating of tubes in the within the furnace; (d) Ion-exchange process through immersing the tubes in the molten salt bath, (e) post-cooling and (f) removing the salt residue by washing

## 2.2.2 Electric Field Assisted Ion Exchange

Electric field assisted ion exchange, EF-IE, treatments were conducted using a modified oven for this type of chemical strengthening, TC 20S, Lema, Parma, Italy. The salt bath was insulated from the metallic frame of the oven by placing mica insulating sheets between the furnace wall, heating modules and the salt vessel.

The electric fields were applied using a power supply, DLM 600, Sorensen. The applied voltage and passing current were monitored using digital Multimeters, DMM 2000 and DMM 2100, Keighley. The applied E-field was controlled via a feedback control scheme, and current density limits were applied to prevent the spark formation surrounding the titanium electrodes, made of commercial Ti rods-grade 2. Figure II-2 shows a schematic draw of the setup used to produce the EF-IE samples. The salt bath temperature was stabilised before treatments; in each treatment, three glass tubes were processed. The electric field was varied between  $100 \text{ V cm}^{-1}$  and  $3000 \text{ V cm}^{-1}$  in constant power mode of the power supply; the current density limit was fixed at 4, 8 and  $16 \text{ mA cm}^{-2}$  to prevent spark formation because of the salt electrolysis near the electrodes. The electric field was applied for up to 10 min.

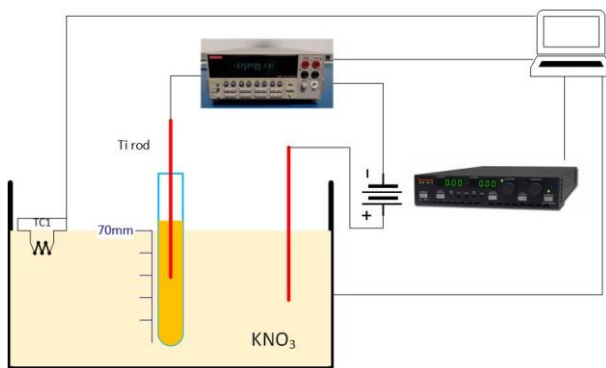


Figure II-2 Schematic of the experimental setup and the instrumentation for monitoring and controlling the electric field [81].

## 2.3 Characterization Methods

### 2.3.1 Chemical composition

Energy-dispersive X-ray spectroscopy was used to measure the chemical composition of samples; in this method, some considerations are required for measuring Na/K exchange. An electron beam with high energy can remove sodium from the glass surface and makes difficulties in the evaluation of sodium concentration; this becomes significant when the sample is subjected to a condensed beam with a diameter less than 1  $\mu\text{m}$  for several seconds, such as the required conditions for line scans [86-88]. We tried to avoid this effect by measuring the chemical concentration profiles across the glass fragment and the chemical composition on the glass surface. The spectrum corresponding to the surface composition was collected on a spot with the area of  $320 \times 240 \mu\text{m}^2$  with a dwelling time of 30 s; these conditions no significant changes in Na-K $\alpha$  have been observed. The background of collected spectra was fitted by a polynomial function and removed. The characteristic X-ray energy attributed to each element K $\alpha$  was used to regenerate the spectrum by fitting the collected spectra, and afterwards the mass concentration of present elements in the glass was determined by using the ZAF correction method [89]. The measurements were conducted at least ten times for each treatment condition. The X-ray spectrum was calibrated using the raw glass composition measured by XRF-WDS as the reference.

The concentration profiles were measured on the cross-section of the fragments of samples undergone to mechanical tests. The fragments were ultrasonically washed in acetone; then, fixed on an aluminium disk using a conductive tape, and afterwards the samples were slightly coated with a Pt-Pd alloy. A scanning electron microscope (JEOL, JSM 5500) equipped with an energy dispersion X-ray spectrometer (EDS 2000, IXRF system, USA) was used in the measurement of the chemical concentration of glass and the concentration profiles near the surface of treated samples. All known elements from the XRF analysis, except boron, were collected simultaneously. The profiles were measured from the surface up to 50  $\mu\text{m}$  into the glass; the scans were conducted through 512 points along the measurement line ( sampling frequency) with a dwelling time of 1 s. Line scans were performed at least five times for each condition.

The glass composition in the depth of 200  $\mu\text{m}$  of the surface was considered as the baseline for the measurement corresponding to the untreated glass<sup>1</sup>. The intensities of the characteristic X-ray energy of elements,  $K\alpha$  were recorded simultaneously; afterwards, the ratio between the intensities to Si- $K\alpha$  was used to generate the concentration profiles. The high-frequency noise of the collected data from the EDS interface was removed using a low pass filter. Then, the profiles of samples treated were fitted by common complementary error function, Eq. 1.12; the concentration profiles corresponding to EF-IE samples were fitted by a modified complementary error function, Eq. 1.21. The characteristic depth of ion-exchanged layer was measured by using Eq. 3.5 and the fitting curves and the estimated diffusion coefficients.

### 2.3.2 Mechanical properties

The mechanical characterizations were conducted to ascertain, first, the residual stress in samples and, then, the strength improvement of samples. The residual stress generated by ion exchange were estimated by using Vickers' indentations or visible light refractometry. Bending tests were performed to check the failure resistance of samples and assess the efficiency of chemical strengthening.

- ***Vickers' Indentations***

Several techniques have been developed for measuring the residual stresses in materials. Among those methods some can be used for transparent materials: X-ray and neutron diffraction, optical retardation, strain-curvature measurements, hole drilling, chemical etching and indentation techniques [90-94].

The fracture mechanics-based methods using a sharp invading indenter are well-known procedures developed to measure the mechanical properties of materials such as the fracture toughness and residual stresses near the surface [90, 95]. Figure II-3 shows a schematic draw of the formed cracks near the indentation imprints. Usually, during the loading step, radial and median cracks nucleated and developed perpendicular to the surface, and lateral cracks form during unloading of the invading indenter. Such behaviour is observed in normal glasses like soda lime silicate. Radial

---

<sup>1</sup> In the case of thin flat glass, the depth of 100  $\mu\text{m}$  was considered as the untreated glass composition because of the limited thickness of glass sheets (200  $\mu\text{m}$ )

cracks can be initiated from the corners of the impression, which is called “primary cracks”, or initiate from the edges of the Vickers’ impression, which is called “secondary cracks” [96]. In particular cases such as the presence of a deep compression layer beneath the surface, the lateral cracks might develop to the surface and cause chipping. Figure II-4 shows typical radial and lateral cracks produced by Vickers’ indenter, load of 9.81 N and dwelling time 15 s, on the surface of soda lime silicate glass treated by Na-K ion exchange at 475°C for 4 h ( compressive stress: 420 MPa, case depth: 20 μm). The image intends to demonstrate the difference between the cracks generated by indentation in a normal glass (soda lime silicate) and an anomalous one (borosilicate).

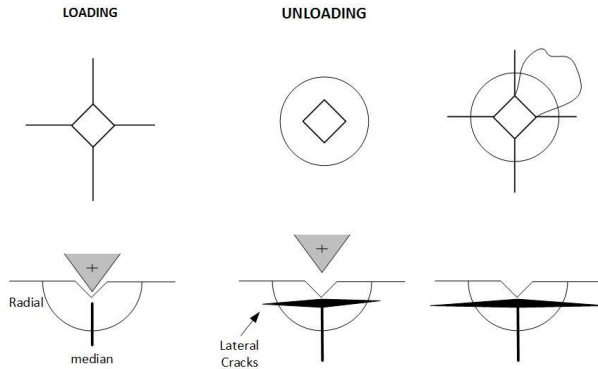


Figure II-3 Typical cracks produced by Vickers indentation in the borosilicate glass during loading and unloading phases;

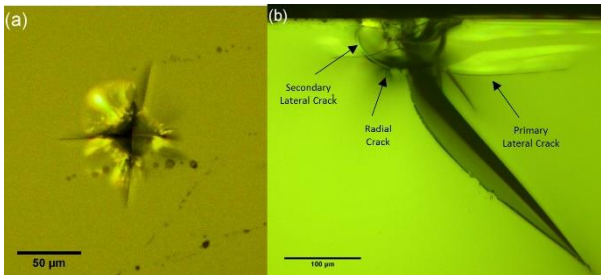


Figure II-4 Typical radial/median cracks generated by Vickers diamond on SLS glass subjected to Sodium-Potassium ion exchange at 475°C for 4 h ( surface compressive stress: 420 MPa, case depth: 20 μm; the indentation was conducted using load of 19.6 N and dwelling time of 15 s)

Cone cracks are usually the first cracks initiated during loading of borosilicate glasses; these cracks, if initiated, grew during loading and when the load is removed they become closed. Primary radial cracks are nucleated and developed a little during the loading step. Secondary cracks are formed during loading and grow along with primary cracks; moreover, lateral cracks are possibly initiated and grow depending on the load and the indentation conditions like humidity [97]. Borosilicate glass is an anomalous glass from the indentation point of view, which means the cracks surrounding the indentation are produced during loading. Consequently, in order to estimate the surface compression, the indentation load has been considered as the parameter. The indentations were carried out at different loads varying between 0.98N to 49 N.

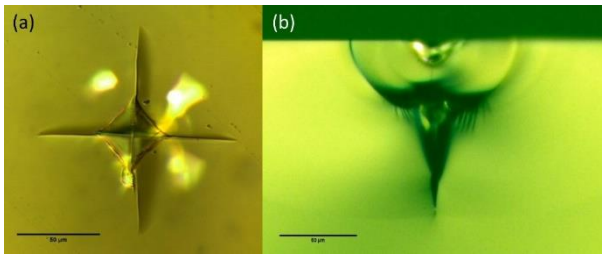


Figure II-5 Typical Vickers indentation cracks formed beneath the surface of stress-free borosilicate glass; the indentation was made by a 5 N load ( 15 s). The cracking system involves median and half-penny cracks: (a) top view of indentations, (b) cross section

If a radial crack is generated by a Vickers' diamond in a stressed surface, the stress intensity,  $K$ , is related to the length of crack,  $c$ , and the compressive residual stress in the surface layer,  $\sigma^R$ , is given by [8, 91]:

$$K = K^{Residual} + K^{Indentation} = -\sigma^R \psi \sqrt{c} + \frac{\chi P^*}{\sqrt{c^3}} \quad (2.1)$$

where  $P^*$  is the maximum applied load during Vickers' indentation,  $\psi$  is the crack shape factor which can be calculated for a given geometry. The shape factor in this study is considered equal to 0.41 for the radial cracks produced in borosilicate glasses [98, 99].  $\chi$  being a semi-empirical stress-field amplitude that can be calculated by:

$$\chi = \xi \sqrt{\frac{E}{H}} \quad (2.2)$$

where  $E$  and  $H$  are the elastic modulus and the hardness of glass ( $E \approx 73$  GPa and  $H \approx 5.5$  GPa [100]), respectively.  $\xi$  is a materials invariant constant equal to

0.016±0.004. The equilibrium length of cracks can be calculated by considering the stress intensity equal to the fracture toughness of glass.

Figure II-6 shows a schematic sketch of the compressive layer and a radial crack generated by Vickers' indentation. The depth of compressive stress can be assumed equal to the characteristic depth of diffusion to ease the calculations [83].

The stress intensity factor of a semi-circular crack at the surface of glass containing a uniformly distributed residual stress, is derived by Lawn et al. [101]:

$$K^{Residual} = \frac{\psi}{\sqrt{c}} \int_0^d \sigma(x) \left( \sqrt{\frac{c}{x}} - 1 \right) dx \quad (2.3)$$

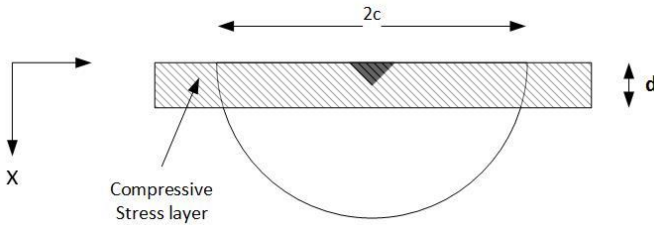


Figure II-6 Schematic draw of the fracture system considered to estimate the surface stress using the indentation approach; the compressive stress on the surface is assumed to be distributed over a strip located on the surface of the glass and in the mouth of radial cracks.

Despite the discrepancy in the location of maximum compressive stress in chemically strengthened glasses, the compressive stress distribution can be considered fairly similar to the concentration profiles; Eq 1.13 [84]. Even for more simplification, it is often considered as a linear function of the distance from the surface of glass:

$$\sigma(x) = \sigma^{surface} \left( 1 - \frac{x}{d} \right) \quad (2.4)$$

by substituting Eq. 2.4 in Eq 2.3, the compressive stress intensity can be derived as:

$$K^{Residual} = \frac{4}{3} \psi \sigma^R \sqrt{d} \quad (2.5)$$

Finally, by combining Eq 2.5 and Eq 2.1, and using the fracture toughness of material,  $K_{Ic}$ , the compressive stress on the surface can be calculated using:

$$\sigma^R = \frac{3}{4\psi\sqrt{a}} \left( \frac{\chi P^*}{\sqrt{c^3}} - K_{IC} \right) \quad (2.6)$$

Although the fracture mechanics is convenient for measuring the compressive stress on the surface, it is limited to the indentations that produce visible cracks. Damage resistance is one of the chemical strengthening goals, and the formation of radial/median cracks in an ion-exchanged glass is not desired in practice; therefore, in a well-treated glass by chemical strengthening, observing the radial cracks produced by indentation must be difficult. One approach to measure the residual stress near the surface of materials is through the indentation load-displacement curves [102]. Figure II-7 illustrates the typical variations in load-displacement curve measured by the method proposed by Oliver and Pharr when a residual stress is present [103]. The presence of residual stress on the surface of glass causes deviations from the original curve attributed to the stress-free surface materials. The compressive stress acts as a force resisting against the invading indenter, while the tensile stress acts as a hydrostatic pressure that helps the compaction of plastic materials during the indentation. It should be noted that the impact of residual stress on the LOAD-DISPLACEMENT curve is much more significant than the change in the fracture behaviour.

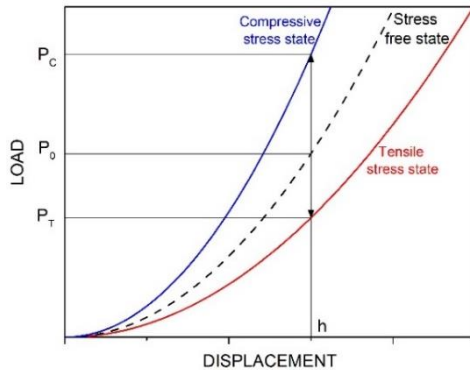


Figure II-7 Typical load-displacement curve during the loading phase measured by a load and depth sensing indentation; the influence of residual stress on changing the LOAD-DISPLACEMENT curve is also shown [102]

It is readable to check the formulation for measuring the residual stress in the surface region of materials that can be considered as pressure on the lateral faces of an

invading indenter penetrating into the surface. Figure II-8 shows a schematic draw of compressive stress state. The pressure is resolved to perpendicular and parallel stresses to the faces of the indenter where the projected stress parallel to the penetration direction acts as the preventing force; therefore, the required load for the penetration is larger.

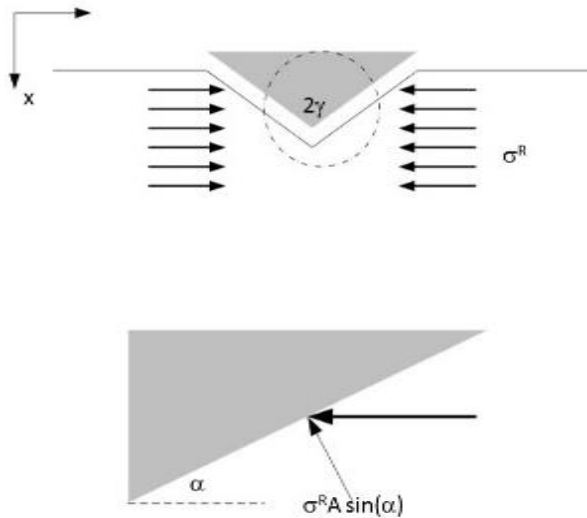


Figure II-8 Schematic of residual stress in the glass surface and the stress resolve on the Vickers diamond faces acting as a force resisting against the Vickers' diamond invasion

The extra load required for producing the same penetration, Figure II-7, is given by:

$$\Delta P = P_C - P_0 = \sigma^R A \sin \alpha \quad (2.7)$$

where  $\alpha$  depends on the geometry of the indenter, for example, the angle of standard Vickers' diamond:  $\alpha=22^\circ$ .

- **Refractometry [104, 105]**

Flat glasses subjected to ion exchange have a variant reflective index beneath the glass surface, and the exchanged layer becomes stratified; therefore, when a light ray enters the glass, it is guided within the stratified medium. The guided rays in the

exchanged layer undergo the mirage effect and gain a concave path faced to the surface

The light can be collected by using a prism with a reflective index larger than the glass. The curvature of the path depends on the reflective index of the layer in which the mirage effect occurs. After collecting the rays, it is possible to obtain the reflective indexes of different layers. If a polarised light source is used, the polarisation state of the collected rays depends on the stress and the distance between the mirage points. Consequently, the compressive stress on the surface of the flat sample can be measured. The instrument used for measuring the stress using this method is called Epidiascope. Stratorefractometer, which is basically an Epidiascope with the light source at infinity, can also be used for measuring the residual stress in flat glasses, its profile and case depth. Figure II-9 shows a schematics draw of a Stratorefractometer.

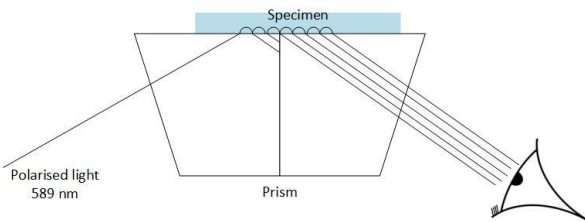


Figure II-9 Schematic draw of the formation of TE and TM fields in optical measurements of residual stress on the surface of a flat glass treated by ion-exchange

In this study, a surface stress meter, FSM 60 LE, (Lucoo Co Ltd., Tokyo, Japan), was used to measure the residual stress produced in the flat glass by ion exchange. The measurements were carried out according to ASTM C1279-13 [106]. The surface compressive stress and the case depth were calculated using the instruction mentioned in the instrument user manual. The stress optical coefficient of borosilicate glass was considered as 3.4 Brewster<sup>2</sup>.

---

<sup>2</sup> 1 Brewster= TPa<sup>-1</sup>

The compressive stress of each surface of flat glass samples was measured along two perpendicular directions: the samples that show a difference between directions more than 5 % were removed from the data series. The measurements were repeated at least 20 times for each treatment conditions.

- ***Flexural Bending***

The strength of samples was assessed using four-point bending, and ring-on-ring biaxial flexural configurations: the first configuration was used to measure the strength of glass tubes and the latter was used for thin flat glass. The tests were carried out with a hydraulic uniaxial test frame, MTS 810.

#### **4-point bending**

The closed end of test tubes was removed using SiC abrasive paper, Grite 320; then, the tubes were taped and placed between the supports carefully to put the polished ends and untreated end of EF-IE out of the support span; the loading span of 18 mm and the support span of 40 mm were used. All measurements were conducted at room temperature and air atmosphere.

The load cell used in measurements had the capacity of 100 kN: the data recorded with a sampling frequency of 100 Hz. The loading rate was kept for all the samples equal to  $1.1 \text{ MPa s}^{-1}$ . The samples were cleaned carefully by rubbing with an acetone wet tissue and taped on the exterior the surface.

#### **Ring on Ring biaxial bending**

The flexural strength of glass was measured using ring-on-ring biaxial bending configuration with the support diameter of 35 mm and loading ring diameter of 10 mm. The loading rate was kept constant at  $5 \text{ N s}^{-1}$ . Because of the significant deformation of samples, the application of linear elastic theory was not possible [107, 108]. The failure loads were recorded and used as the representative of the samples strength; moreover, to ease the data analysis by Weibull statistics, the failure loads were normalised to the minimum failure load of the raw glass<sup>3</sup>.

---

<sup>3</sup> The relative strength has been used in order to make comparison between experimental data and technical reports provided by SCHOTT AG possible.

For a better comparison of the strength results, Weibull distribution of strength was considered. The probability of failure,  $F$ , assigned to the  $i$ th sample in an ascending ordered strength is calculated using:

$$F = \frac{i-0.5}{N} \quad (2.8)$$

The probability of failure is typically related to the strength through a two-parameter Weibull distribution as:

$$F = 1 - e^{\left(-V\left(\frac{\sigma}{\sigma_0}\right)^m\right)} \quad (2.9)$$

where  $V$  is the specimen volume;  $m$  is the Weibull modulus ;  $\sigma$  and  $\sigma_0$  are the failure stress and the normalised stress, respectively. By taking natural logarithm twice of Eq. (2.9):

$$\ln(-\ln(1 - F)) = m \ln \sigma - m \ln \sigma_0 \quad (2.10)$$

Weibull statics was used to analysis the mechanical strength of samples. 16 samples were tested at least for each treatment condition.

### 2.3.3 Thermal Analysis

Differential scanning calorimetry, DSC, was employed to measure the glass transformations including the glass-transition temperature,  $T_g$ , and the structural relaxations. The measurements were performed by using a differential scanning calorimeter, TA 2010, Thermal Instruments. DSC samples were prepared by grinding the glass in an agate mortar and collecting the powder with a particle size below 45  $\mu\text{m}$ . The glass powder was ultrasonically cleaned in acetone for 10 min and dried at 105 °C overnight.

The baseline of aluminium pans used for the measurements and the reference, an empty pan, was recorded by heating to 600 °C with the heating rate of 10 °C  $\text{min}^{-1}$  and dwelling time of 15 min and afterwards cooling down to room temperature. The cycle was repeated twice to remove the aluminium oxide formation noise.

The glass powder was placed into the aluminium pan and situated on the sample holder of DSC at room temperature. The sample, first, was heated to 120°C and equilibrated for 10 min to remove the humidity on the surface; then, it was heated to 610 °C, and afterwards held at the temperature for 5 min, and cooled to 200 °C; both

heating and cooling rate were kept  $10^{\circ}\text{C min}^{-1}$ . The samples were subjected to two runs of upscans.

#### **2.3.4 Structural evolution**

The structural variations of glass after subjecting to EF-IE was investigated by using Raman spectroscopy. The micro-Raman spectra were taken across the borosilicate tubes samples subjected to EF-IE and fixed in the metallographic mount. The glass cross section was polished down to  $2.5\ \mu\text{m}$  using silicon carbide paper to get a cross-section of the tube wall. The exposed surface was carefully polished down to  $0.5\ \mu\text{m}$  using cerium oxide suspension.

Micro-Raman spectrum was collected using a backscattered geometry via a triple-axis monochromator (Horiba-Jobin Yovn, Model 64000). The spectra were excited using  $514.5\ \text{nm}$  Ar-Kr laser; the beam was focused to a spot size of less than  $5\ \mu\text{m}$  through the lens of a  $100\times$  microscope; the scattered radiation from the excited region was collected via the same objective. The configuration and parameters of the measurements are reported elsewhere in detail [109].

The first point for collecting the spectra was chosen in the exchanged layer  $5\ \mu\text{m}$  below the glass and resin interface and the second point was taken at  $200\ \mu\text{m}$  from the glass surface. The background of collected spectra was removed, and the noise was removed using a modified algorithm based on the correction technique reported by Zhang et al. [110].

# Chapter III.

## Results and Discussions

**Part of this chapter has been published in:**

Ali Talimian, Vincenzo M. Sglavo

Can Annealing Improve the Chemical Strengthening of Thin Borosilicate Glass?

J. Non-Cryst. Solids, DOI: 10.1016/j.jnoncrsol.2017.03.038.

Ali Talimian, Vincenzo M. Sglavo

Ion-exchange strengthening of borosilicate glass: Influence of salt impurities and treatment temperature

J. Non-Cryst. Solids, 456 (2017) 12-21.

Ali Talimian, Gino Mariotto, Vincenzo M. Sglavo,

Electric Field Assisted Ion Exchange Strengthening of Borosilicate and Soda Lime Silicate Glass,

Int. J. App. Glass Sci. (2017) 00:1-10.

Vincenzo M. Sglavo, Ali Talimian, Norbert Oskco,

Chemical Strengthening of Soda Lime Silicate Glass in Calcium Contaminated Salt

J. Non-Cryst. Solids, 458 (2017) 121-128

Ali Talimian and Vincenzo M. Sglavo.

Electric Field-Assisted Ion Exchange of Borosilicate Glass Tubes, in Ion Exchange - Studies and Applications

ISBN: 978-953-51-2164-0, InTech, DOI: 10.5772/60805.

This chapter investigates the influences of ion exchange parameters on the final mechanical strength of borosilicate glass, such as bending strength. It demonstrates the feasibility of ion exchange in order to improve the strength and, afterwards discusses the effects of glass chemical composition, treatment temperature and salt impurities. It also presents the impact of applying an electric field on ion exchange and strengthening of borosilicate glass. Finally, it explores the influence of ion exchange and heat treatments on bending resistance of thin alkali borosilicate glass.

### 3.1 Ion-exchange strengthening of borosilicate glass

Table 5 provides the surface chemical composition of borosilicate glass, Fiolax Clear-Schott AG, with the diameter of 10 mm before and after immersion in  $\text{KNO}_3$  ([Na]:1000 ppm) at  $450^\circ\text{C}$  for 4 h. Because of the limits of measurement technique, the concentration of boron cannot be estimated. We, nevertheless, can see that the concentration of silicon oxide is considerably decreased after ion exchange. It should be noted that Table 5 presents the weight concentration of components and by replacing lighter sodium ions with heavier potassium ions, the weight portion of the other elements is reduced [3].

Since silicon oxide is the main network former of the glass, its concentration remains constant as long as the glass surface is not corroded. We observed no evident degradation of the glass surface; consequently, the concentration of silicon oxide is considered constant and the glass molar composition is calculated; Table 6 gives the measured values.

Table 5 The surface composition of glass, in weight percent, measured by EDS before and after ion exchange, the numbers between brackets present calculations error

	$\text{Na}_2\text{O}$ (wt%)	$\text{K}_2\text{O}$ (wt%)	$\text{CaO}$ (wt%)	$\text{Al}_2\text{O}_3$ (wt%)	$\text{SiO}_2$ (wt%)
<b>Raw Glass</b>	5.95 (0.05)	0.09 (0.09)	1.69 (0.03)	9.16 (0.36)	83.11 (0.29)
<b>IE (<math>450^\circ\text{C}</math>, 4 h)</b>	0.27 (0.12)	19.98 (0.71)	1.68 (0.13)	8.63 (0.30)	69.43 (0.61)

Sodium is replaced with potassium in the ion-exchanged samples and the molar content of potassium oxide on the ion-exchanged glass surface is significantly larger than the raw glass; the concentration of calcium oxide is substantially constant. Figure I-5-a shows X-ray spectra collected from the surface of glasses. The intensity of the peak attributed to sodium (1.04 keV, X-ray fluorescence) is clearly depressed after ion exchange. The aluminium peak remains unchanged, and the spectrum in the window

of 3 to 4 keV becomes completely different. The peak associated with the metallic coating, Au, is not discussed here.

Table 6 Surface composition of glass presented by the molar ratio to silicon oxide

	<b>Na<sub>2</sub>O</b>	<b>K<sub>2</sub>O</b>	<b>CaO</b>	<b>Al<sub>2</sub>O<sub>3</sub></b>	<b>SiO<sub>2</sub></b>
<b>Raw Glass</b>	0.0693	0.0007	0.0217	0.0649	1
<b>IE (450°C, 4 h)</b>	0.0038	0.1833	0.0259	0.0732	1

According to the limits of measurement technique, the estimation of sodium concentration involves a large uncertainty [86, 89]. The other inaccuracy is related to the overlap between the characteristic X-ray energies of potassium and calcium that can cause the overestimation of the concentration of calcium on the glass surface. Although some of these error sources are considered in the quantification method, standard-less technique (ZAF), quantitative measurements should be carried out with meticulous care. Despite the error, the chemical analysis on the surface, particularly the variations of concentrations, can be used to appraise the ion exchange.

Nevertheless, we see that potassium is clearly exchanged for sodium on the surface after immersing the glass in the molten potassium nitrate at 450°C for 4 h. Figure III-2 shows the bending strength of glass tubes measured by 4 point bending configurations. The mean bending strength of samples increases from 149 MPa to 326 MPa by ion exchange; the standard deviation of strength is also increased by subjecting to chemical strengthening; such behaviour is a typical feature of chemical strengthening [31].

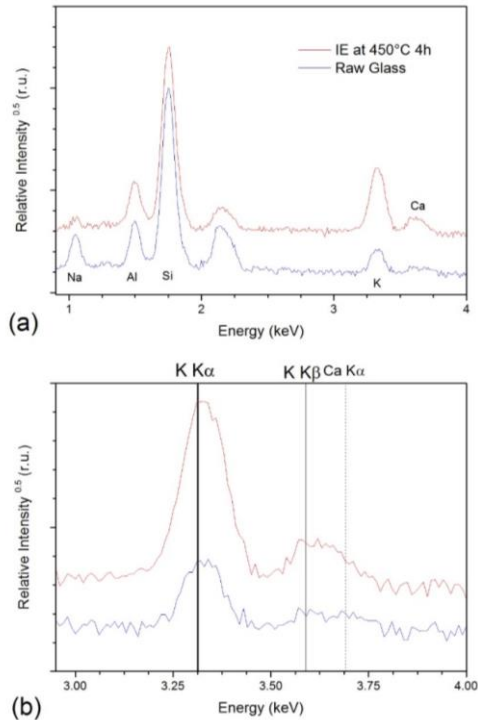


Figure III-1 EDS spectrum collected from the surface of Raw glass and subjected to ion exchange at 450°C, (a) the spectra between 1 to 4 Kev, (b) the region between 3 to 4 keV corresponding the characteristic peaks of potassium and calcium

Stuffing potassium into sodium positions in the glass surface generates a compressive stress that can reinforce the surface flaws and improve the mechanical strength [4]. Figure III-3 shows a typical concentration profile of sodium and potassium near the surface of the fracture surface of ion-exchanged samples. If we consider the depth of exchanged layer as the representative of the depth of compression layer on the surface, we can conclude that the surface compression reinforces most of surface cracks. However, a portion of surface flaws is not “reinforced”. Consequently, the strength of samples containing large flaws is not influenced by potassium for sodium ion exchange. This is responsible for observing samples with similar strength to the “Raw glass” after being subjected to ion exchange.

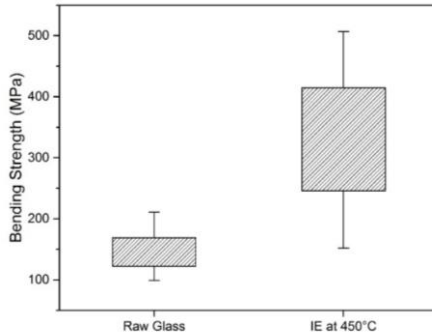


Figure III-2 Bending strength of raw borosilicate glass tubes, OD=10 mm, and ion-exchanged ones (treated at 450°C for 4); 25<sup>th</sup> and 75<sup>th</sup> percentiles as well as minimum and maximum values are shown.

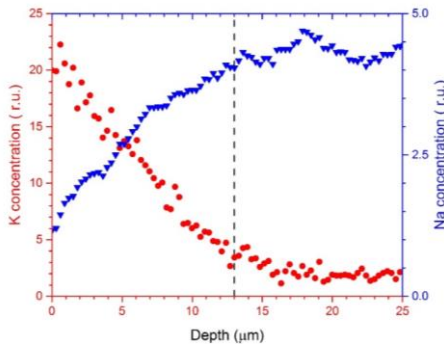


Figure III-3 Potassium and sodium concentration against depth, measured near the glass surface by EDS; the concentration of elements is estimated by considering the relative intensity of X-Ray characteristic peak; the segmented line indicates the depth of layer (the characteristic depth of exchanged layer)

The strength of samples is shown by using Weibull distribution in Figure III-4. The data was fitted by using linear regression to find the statistical parameters ( $\sigma_0$  and Weibull modulus). The strength of glass is clearly increased after subjected to ion exchange: the characteristic strength, where the failure probability is 63 %, increases from 162 MPa to 388 MPa.

Weibull modulus, which presents the scattering of data, does not change significantly after ion exchange. It seems that the generated stress uniformly influences the surface flaws and, hence, the scattering of the strength is not changed significantly. As mentioned above, some large surface flaws cannot be completely reinforced by ion exchange which is responsible for the lower part of the strength distribution of the ion-exchanged glass.

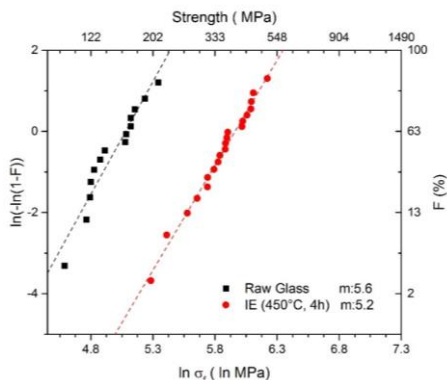


Figure III-4 Weibull distribution of the strength of Raw glass tubes and ion exchanged ones; the dashed line ins representative of fitting line of experimental data used for estimating Weibull modulus.

### 3.1.1 Effect of Glass Composition

The chemical composition of the borosilicate glass used in this study is summarised in Table 7. The composition of both glasses is almost the same; however, Fiolax-HC is characterised by containing more calcium oxide. The slightly different chemical composition of glasses accounts for the different glass-transition temperatures. It is worth to augment the point that the glasses are bought from different companies and, therefore, the thermal history could be different. However, the findings in this study, section 3.3.2, revealed that the thermal history is not a crucial parameter in chemical strengthening. The different concentration of modifiers also influences the hydrolytic resistance of glass, which is lying out of the interest of this study.

Table 7 Chemical composition (in wt %) and the glass transition temperatur measured by DSC of borosilicate glass tubes

	Chemical Composition (wt%)							T <sub>g</sub> (°C)
	Na <sub>2</sub> O	K <sub>2</sub> O	CaO	Al <sub>2</sub> O <sub>3</sub>	B <sub>2</sub> O <sub>3</sub>	SiO <sub>2</sub>	other	
<b>Fiolax - HC</b>	7.0	<0.1	1.5	5.2	10.5	75.5	<0.3	565°C
<b>Nipro - LC</b>	7.0	0.8	0.5	5.8	10.5	74.9	<0.5	540°C

We measured the fracture toughness of tubes by using Vickers indentations. The length of median/radial cracks,  $c$ , produced by a Vickers diamond against the indentation load,  $P$ , are given by Figure III-5. The length of median/radial cracks is a function of applied load as given by [111, 112]:

$$\sqrt{c} = a\sqrt[3]{P} \quad (3.1)$$

where  $a$  is a function of the fracture toughness of glass:

$$a = 0.252 \left(\frac{E}{H}\right)^{1/6} \times \frac{1}{\sqrt[3]{K_c}} \quad (3.2)$$

where  $E$  is the elastic modulus,  $K_c$  the fracture toughness, and  $H$  being the hardness. The experimental data is fitted by Eq 3.1. Both fitting curves are identical and, hence, the fracture toughness of glasses is the same.

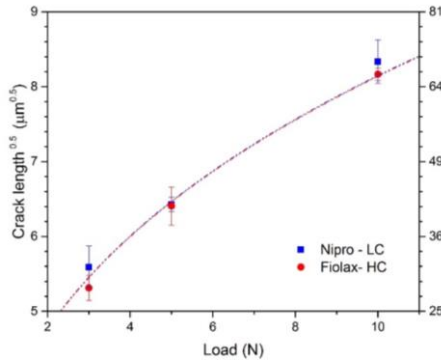


Figure III-5 Length of cracks produced by Vickers indentation against the maximum load: the experimental data is fitted by using Eq. 3.1

Table 8 summarises the bending strength, its maximum, minimum and deviation of LC and HC glass tubes. The bending strength of LC glass is clearly lower than HC; the size of surface flaws defines the strength of a brittle material [111]; therefore, the limited strength of LC is accounted for by the presence of large surface defects. The size of critical flaw can be estimated by using solid mechanics and assuming that the shape factor,  $Y = 1.24$ , for surface flaws [9, 113] ( $c = (0.79 \times K_d / \sigma)^2$ ).

Table 8 Mean bending strength and corresponding standard deviation of each glass reported in Table 7; the minimum and maximum strength of each group are also reported

	Nipro - LC	Fiolax - HC
Number of samples	29	27
Mean Strength (MPa)	194	340
Standard Deviation (MPa)	40	44
Minimum (MPa)	116	264
Maximum (MPa)	284	451

The critical crack size was estimated for each samples; then the flaw size was assumed to be randomly distributed. Afterwards the populations were fitted by a normal distribution as presented in Figure III-6. LC glass contains a wide distribution of flaws with an average crack length of around 17  $\mu\text{m}$ ; the other glass, HC, is characterised by small cracks with the size of 6  $\mu\text{m}$ . Figure III-7 shows the measured bending strength using Weibull distribution. As expected from the size of critical flaw, HC has larger and less scattered strength compared to LC.

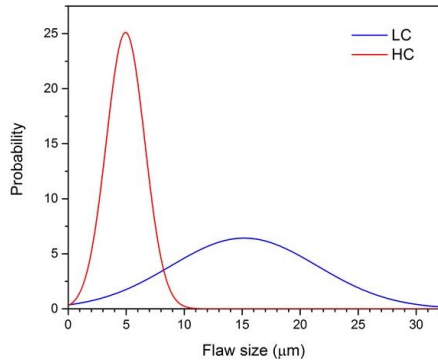


Figure III-6 The distribution of critical flaw size related calculated from the failure strength of samples and fitted by a gaussian function

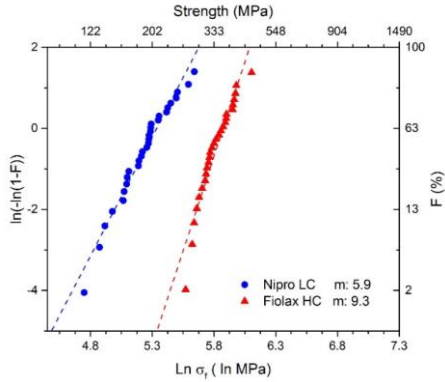


Figure III-7 Weibull distribution of the strength of as-cut glass tubes: LC (Nipro) and HC (Fiolax)

Figure III-8 presents the typical fracture origin of raw glasses; we see different fracture regions such as classic mirror, mist and hackle regions particular in the LC glass. The images show that the LC glass contains larger surface flaws compared to the HC glass. We can obviously see the difference between the defect sizes on the surface; furthermore, the radius of fracture regions also clearly presents the lower load of failure of LC compared to HC. One can conclude that the main difference of these two glasses is the defect size rather than chemical composition.

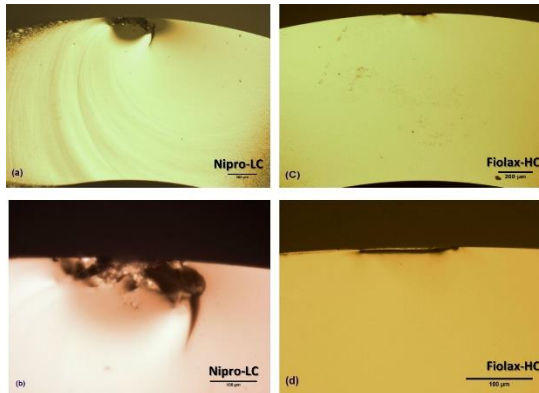


Figure III-8 Micrographs of the typical points from which the failure started in LC glass: (a)-(b) and HC glass: (c)- (d)

The bending strength of tubes treated by chemical strengthening in the molten potassium nitrate containing 1000 ppm of Na at 450°C for 4 h is shown by Figure III-9. Subjecting to ion exchange improves the strength of glasses; the strength increase of HC is more significant than the increase of LC. HC after ion exchange shows more scattered strength which is the typical behaviour of samples showing the strength augmentation after ion exchange [31].

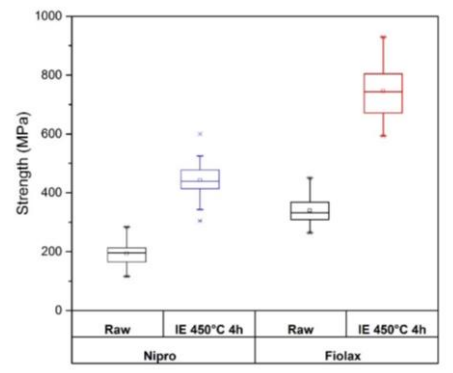


Figure III-9 Bending strength of glass tubes treated by ion exchange at 450°C for 4h; 25<sup>th</sup> and 75<sup>th</sup> percentiles as well as minimum and maximum values are shown.

Figure III-10 shows typical potassium concentration profiles produced by ion exchange in tubes. Both glasses show the same depth of layer which is around 13-14  $\mu\text{m}$ . This depth is thick enough to cover the surface flaws of HC glass; conversely, the ion-exchanged layer cannot cover and reinforce all the surface flaws of LC glass and the strength of LC glass is, consequently, not as large as the strength HC. The size of initial flaws play a major role in the failure of glass and, consequently, the influence of ion exchange. It can easily obscure the impacts of glass composition, particularly CaO, on the chemical strengthening. Sinton, C.W. et. al. have reported that small changes in the chemical composition of glass affects the diffusion of alkali ions and, as a result, the depth of exchange layer. By containing more alkaline earth ion, the depth of exchange layer decreases; conversely, when the glass initially contains both sodium and potassium the depth of layer increases [114]. Using Vickers indentations, the compressive stress on the surface of LC and HC glass was estimated equal  $304 \pm 43$  MPa and  $213 \pm 26$  MPa, respectively. The surface compression is larger in the sample containing less CaO.

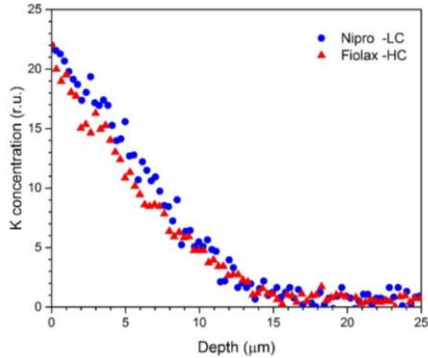


Figure III-10 Typical potassium concentration profiles measured near the surface of glass tubes, Fiolax and Nipro, subjected to ion exchange at 450°C for 4h

It is interesting to ascertain the effectiveness of chemical strengthening by considering the glass strength increase. It can be estimated by:

$$\text{Strength incerse} = \frac{\sigma_{IE} - \sigma_R}{\sigma_R} \quad (3.3)$$

where  $\sigma_R$  and  $\sigma_{IE}$  are the strength of raw (untreated) and ion-exchanged glass, respectively. Using the mean strength of samples, the strength increase is estimated about 1.2 for both samples. Although the samples show different failure stresses, potassium for sodium ion exchange improved the strength in the same way. Therefore, small changes of glass composition does not influence the strengthening directly.

### 3.1.2 Influence of Temperature

Figure III-11 shows the strength of glass tubes subjected to ion exchange in potassium nitrate at 450°C and 465°C. The strength of LC increases with increasing the temperature; conversely, the strength of HC declines by increasing the treatment temperature. The chemical strengthening of glass depends on the generation of compressive stress on the surface which is strong and deep enough to reinforce the surface flaws.

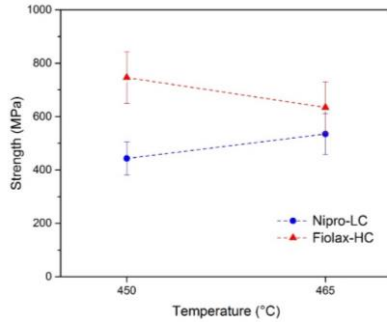


Figure III-11 Bending strength of glass tubes subjected to ion exchange at 450 and 465°C for 4h. Note the lines are drawn as the eye-guide.

The generated compressive stress on the surface is estimated from the length of cracks generated by an invading indenter on the surface [91, 95, 102]. Figure III-12 shows the crack length produced by a Vickers' diamond indenter and the maximum load of 19.6 N and dwelling time of 15 s. The length of radial/median cracks is curtailed by increasing the treatment temperature; it revealing that the compressive stress generation because of stuffing potassium becomes more effective. The influence of temperature on the length of cracks produced by indentation and, therefore, the produced stress on the surface is more prominent in LC glass than HC.

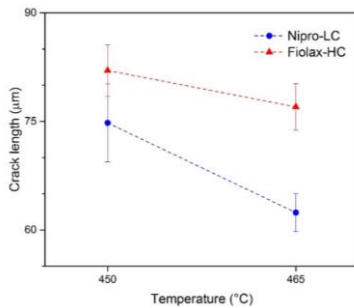


Figure III-12 the length of radial/median cracks produced by Vickers' indentation on the glass tubes subjected to ion exchange at 450 and 465°C for 4h. Note the lines are drawn as the eye-guide.

By considering the crack length produced by Vickers' indentation and the characteristic depth, the compressive stress on the glass surface can be estimated by

using Eq. 2.6. The potassium concentration profiles produced by ion exchange at different temperatures are shown in Figure III-13. The depth of exchanged layer is increased by increasing the treatment temperature in LC glass; whereas, the depth of the layer is almost the same in HC samples treated at either temperature. The diffusion coefficients are estimated via fitting potassium concentration profiles using a complimentary error function as mentioned in Eq 1.12; the potassium content of raw glasses is considered as the baseline of concentration profiles, and afterwards the characteristic depth of exchanged layer was calculated by:

$$d = 2\sqrt{Dt} \quad (3.4)$$

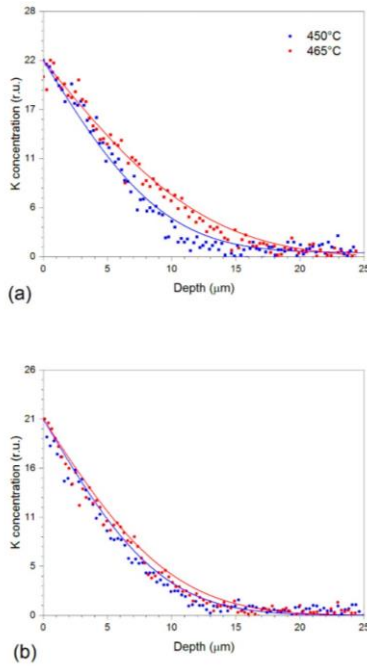


Figure III-13 Potassium concentration profiles recorded by EDS near the surface of (a) LC and (b) HC glass treated at 450°C and 465°C.

Table 9 gives the estimated residual stress and the characteristic depth of ion exchange in the glass tubes after being subjected to Na-K ion exchange in the

potassium nitrate salt bath containing 1000 ppm of Na at 450°C and 465°C for 4h. LC shows larger characteristic depths compared to HC; moreover, the calculated compressive stress on the surface of LC is slightly larger than HC; consequently, more surface defects can be reinforced by the compression layer, which improves the mechanical strength of glass. One can conclude that, by increasing the characteristic depth and compressive stress, more flaws are reinforced in LC and, consequently, the strength improves. On the other hand, the characteristic depth of HC is not significantly changing by temperature; therefore, the strength does not improve significantly. The slight decline in the strength of HC is probably related to the possible reactions between the salts species, such as hydroxyl groups, and the glass surface; this can cause stress relaxation at very first few microns below the surface [72, 115].

Table 9 Estimated characteristic depth and residual compressive stress on the surface of LC and HC glass subjected to ion exchange in potassium nitrate containing 1000 ppm of Na

	Characteristic Depth		Residual Stress (MPa)	
	450°C	465°C	450°C	465°C
<b>Nipro-LC</b>	15.6 (0.4)	21.5(0.5)	304(43)	435(60)
<b>Fiolax-HC</b>	14.4 (0.3)	14.7(0.2)	213(26)	271(44)

The strength improvement defines the efficiency of chemical strengthening; from this perspective, the efficiency of chemical strengthening increases by increasing the treatment temperature in LC glass; conversely, HC glass does not show such improvement.

Performing ion exchange at a higher temperature increases the depth of exchanged layer and compressive stress in LC glass; as a result, the treatment improves the strength. Conversely, the depth of exchanged layer is substantially the same for both treatment temperatures; therefore, the strength is the same for HC glass. In summary, increasing the temperature, which can increase the depth of exchange layer, can improve the strengthening of samples contains large defects. It is worth to mention that treatment at elevated temperatures can cause stress relaxation [21, 71].

### 3.1.3 Influence of Salt Composition

Chemical strengthening is carried out by the replacement of sodium ions in glass with larger potassium ions from a molten salt through an inter-diffusion process driven by the difference in the chemical potential of ions [45, 116]. The variation of the salt's composition affects the driving force of ion exchange and, in turn, the chemical strengthening of glass. Therefore, the salt's impurities have a vital role in the ion-

exchange strengthening process and can impair the ion exchange process [46, 80, 81, 117].

Sodium and calcium are two main contaminants of potassium nitrate baths [46, 118]. The former is introduced into the salt bath as result of the substitution of ions between the bath and glass according to Eq. 1.4. This lowers the thermodynamic driving force for ion exchange and consequently the salt bath is required to be replaced [46], which also increases the cost of chemical strengthening significantly [1]. Calcium can be present in the original nitrate salt or the industrial environmental dust can introduce it; the residue of washing process can also generate such an impurity in the glass. Calcium is known to be responsible for “blocking” of the alkali ions exchange and the inefficient chemical strengthening.

This section investigates the influence of the salt bath impurities on the chemical strengthening of the soda-borosilicate glasses: impacts of sodium and calcium impurities are studied and, afterwards the role of contaminants is looked at by using a thermodynamic paradigm.

- ***Effect of sodium impurity***

Figure III-14 shows the Weibull distributions of the bending strength of LC glass treated in the molten potassium nitrate baths containing about 1000 and 2500 ppm of sodium. Samples were subjected to ion exchange at 450 and 465°C for 4 h. Although the strength of LC is slightly affected by the sodium content in the salt, the variation is negligible if it is compared with the strength increase by ion exchange. In the case of salt containing 2500 ppm of sodium, the distributions corresponding to samples treated at either temperature are almost the same. It seems that the influence of temperature on strengthening is disguised when the salt containing a relatively high concentration of sodium is used.

The strength of HC glass is almost constant, if not decreasing, with the increase of Na content in the salt. The failure resistance slightly decreases when the samples are treated at 465°C in the salt containing 1000 ppm of sodium, as pointed out in Figure III-11. HC glass also shows similar behaviour to the LC if it is treated in the salt containing the higher concentration of sodium ([Na]=2500 ppm).

Sodium impurity decreases the thermodynamic driving force of ion exchange and affects stress build-up because of stuffing of ions [45]; this will be discussed in detail later on.

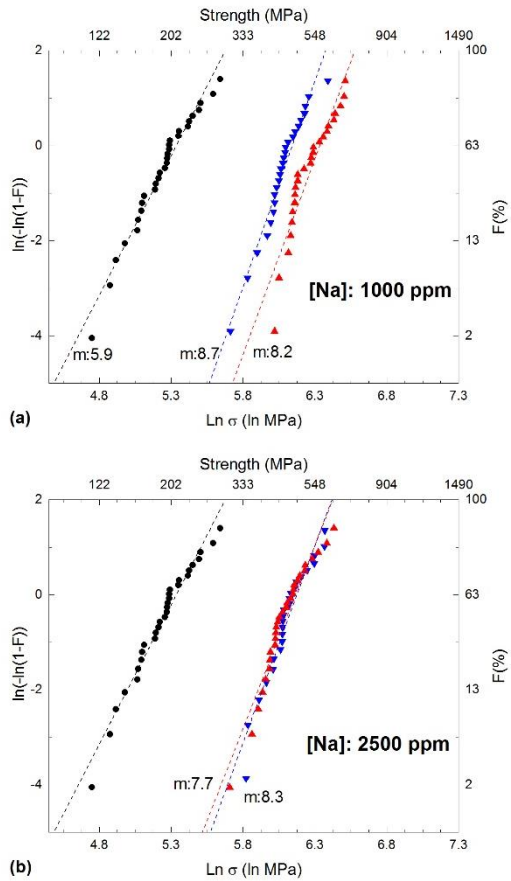


Figure III-14 Weibull distribution of the strength of LC glass tubes treated by ion exchange in potassium nitrate salt containing (a) 1000 ppm and (b) 2500 ppm of Na; Raw glass (●), treated at 450°C (▼) and 465°C (▲)

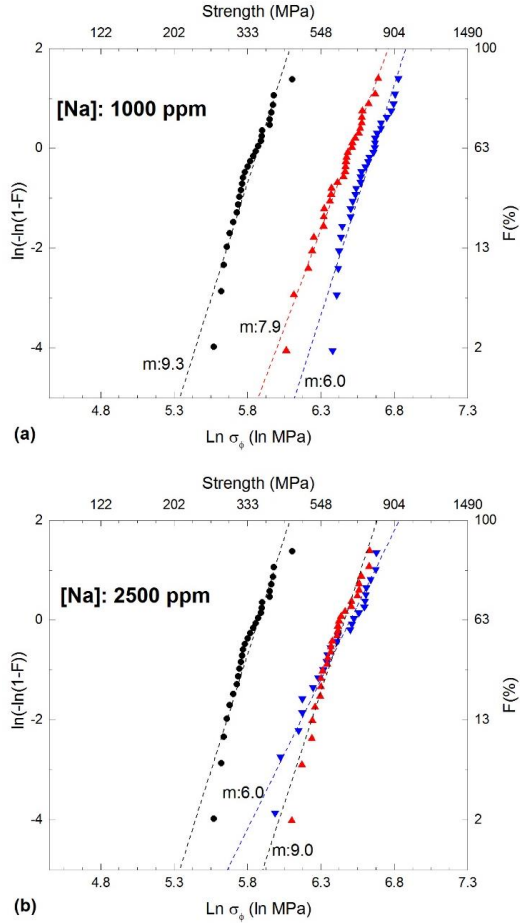


Figure III-15 Weibull distribution of the strength of HC glass tubes treated by ion exchange in potassium nitrate salt containing (a) 1000 ppm and (b) 2500 ppm of Na; Raw glass(●), treated at 450°C (▼) and 465°C (▲)

- **Effect of calcium contamination**

Calcium is a frequent contaminant of salt baths used in chemical strengthening which can be introduced by the dust in the environment, or the residue of washing by water; it is also reported that even a limited amount of calcium has a significant impact on the

efficiency of chemical strengthening [80, 81, 117]. Figure III-16 compares the strength of LC glass when it is treated in the salt bath containing calcium using the Weibull distribution; the strength of samples treated in potassium nitrate bath is also presented for comparison.

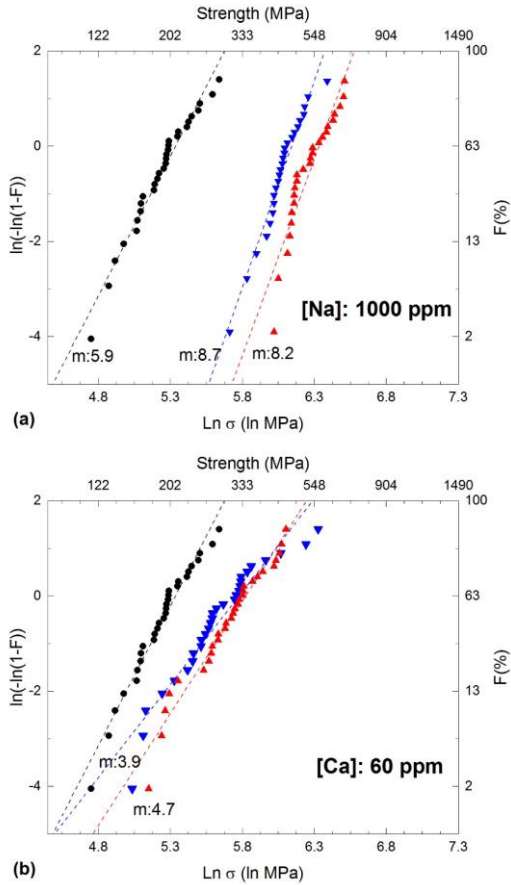


Figure III-16 Weibull distribution of the strength of LC glass tubes treated by ion exchange in potassium nitrate salt containing (a) 1000 ppm of Na and (b) 600 ppm of Na and 60 ppm of Ca; Raw glass(●), treated at 450°C (▼) and 465°C (▲)

Although the failure stress of treated samples in the bath contaminated with calcium improves after ion exchange, it is clearly lower than the samples treated in the calcium-

free salt. The distributions of treated samples and raw glass overlap to some extent; however, the strength of some samples is comparable to the sample treated in calcium free salt.

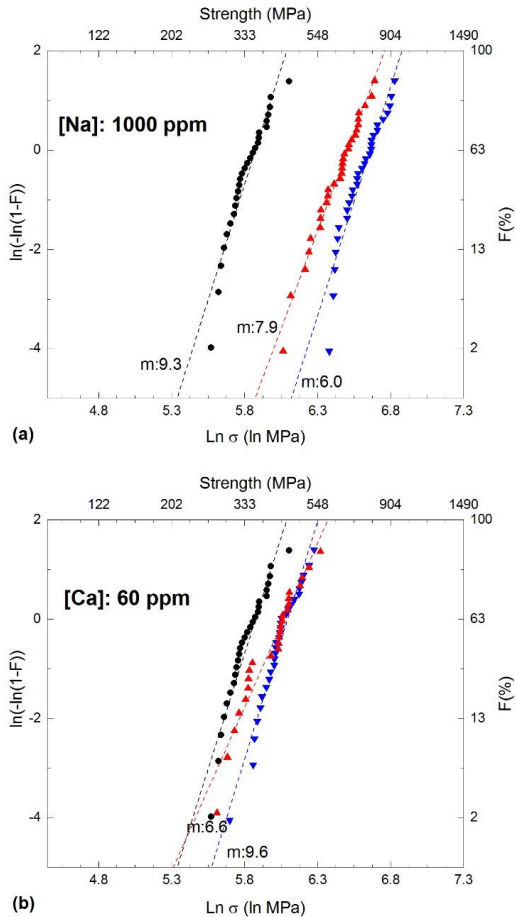


Figure III-17 Weibull distribution of the strength of HC glass tubes treated by ion exchange in potassium nitrate salt containing (a) 1000 ppm of Na and (b) 600 ppm of Na and 60 ppm of Ca; Raw glass(●), treated at 450°C (▼) and 465°C (▲)

The strength of HC glass subjected to ion exchange in the calcium-containing salt is shown in Figure III-17; the behaviour of this glass is similar to the other one. HC glass is characterised by small flaws on the surface; this is making the strength distributed in a narrow window and the strength of samples is not as scattered as the LC tubes. Nevertheless, it is clear that the limited improvement of strength is due to the presence of calcium in the salt bath and calcium plays a critical role in the chemical strengthening of borosilicate glass.

Figure III-18 shows typical indentation impressions produced by applying a load of 19.62 N for 15 s using a Vickers' diamond on the tubes subjected to ion exchange in sodium and calcium contaminated salts; the impression on the raw glass is also shown. The indentation on the raw glass produced primary radial/median cracks; moreover, some lateral cracks are generated beneath the surface that can be distinguished by the birefringence of light surrounding the impression. On the samples treated in the calcium-free salt bath, which contains 1000 ppm of Na in this case, the length of cracks in both systems, radial/median or lateral, are limited because of the surface compression produced by ion exchange, as discussed before. Conversely, the samples treated in calcium containing salt exhibit cracks similar to the raw glass.

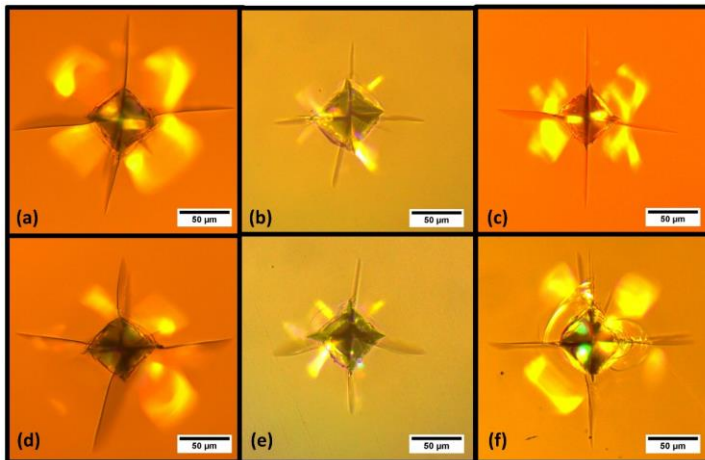


Figure III-18 indentation crack length produced by 19.62 N on the surface Raw glass ( a, LC –d HC); tubes ion exchange at 450°C for 4h in potassium nitrate containing [Na]=1000 ppm ( b, LC-e, HC) and (c, LC-f, HC)

The length of radial cracks generated on the glass surface by Vickers' indentation is shown in Figure III-19. The cracks generated on the surface of samples treated in the calcium-containing salt is rather similar to the crack length of raw glass; this revealing that the compressive stress generated on the surface by potassium for sodium ion-exchange is not intense enough to inhibit the extension of cracks.

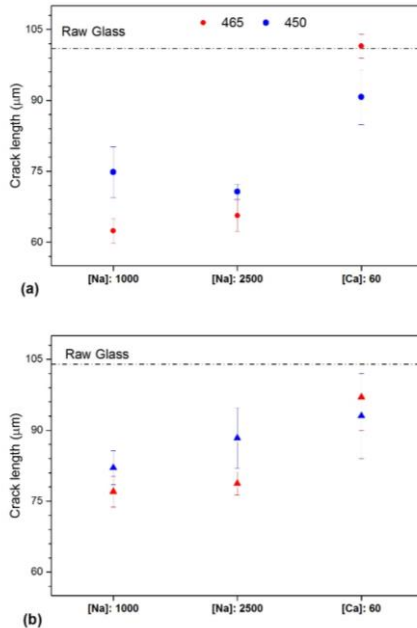


Figure III-19 The length of cracks produced by Vickers' indentation using load of 19.62 N against the concentration of main impurity in potassium nitrate on (a) LC and (b) HC glass; the ion exchanges are carried out at 450 and 465°C.

Table 10 provides the characteristic depth of exchanged layer and the estimated residual compressive stress on the surface of samples treated in the potassium nitrate salt containing 2500 ppm of sodium. Both the characteristic depth and the stress decrease are smaller when the samples is treated in the salt contaminated by 2500 ppm of sodium (Table 9 vs. Table 10). The decrease explains the slight strength decrease of samples. The characteristic depth and residual stress of exchanged layer generated by performing ion exchange in calcium containing salt are also summarised

in Table 10. One should note that the measured stress is too low to be measured by indentation means; therefore, some stress values reported in Table 10 cannot be referred [84, 119, 120].

The characteristic depth is clearly lower than the exchanged layer depth of samples treated in sodium-containing salts (Table 9 and Table 10). The limited ion exchange depth in LC glass is responsible for the scattered strength. HC glass is characterised by small surface flaws and the exchanged layer produced by calcium containing salt covers the surface flaws and reinforces them.

Table 10 Estimated characteristic depth and residual compressive stress on the surface of LC and HC glass subjected to ion exchange in potassium nitrate containing impurities: 2500 ppm of Na and 60 ppm of Ca ([Na]= 1000 ppm)

Slat Impurities	Glass Tube	characteristic Depth		Residual Stress (MPa)	
		450°C	465°C	450°C	465°C
[Na]: 2500 ppm	Nipro-LC	16.3	19.4	364	423
	Fiolax-HC	11.1	12.7	162	269
[Ca]: 60 ppm	Nipro-LC	13.0	17.1	105	62
[Na]: 770 ppm	Fiolax-HC	11.2	12.1	121	20

- **Role of impurities**

In order to corroborate the idea of the major impact of calcium impurity on chemical strengthening, we investigate the variation of the chemical driving force of ion exchange in detail by estimating the variations of the driving force of swapping ions using the ion exchange thermodynamic approach [45]. This part intends only to show how much the Na contamination alters the driving force. An ion exchange treatment using glass powder with a particle size between 0.7 to 1.4 mm, produced in an agate ball mill, was performed at 450°C for 72 h. The glass-to-salt ratio was increased to 1:1 to amplify sodium release in the salt as well as the other possible elements, if there is any. Table 11 shows sodium and calcium concentrations in a potassium nitrate salt before and after the treatment.

Table 11 Chemical composition potassium nitrate (nominally pure) mixed with the glass fragments before and after a heat treatment at 450°C for 72; the concentrations were measured in ppm; numbers between parentheses show the standard deviation.

	Pure salt	After the treatment with LC glass	After the treatment with HC glass
Na (ppm)	13 (1)	21839 (69)	21214 (335)
Ca (ppm)	3 (1)	2 (1)	5 (2)

The exchange of alkaline earth elements is very limited at temperatures below the glass-transition temperature; hence, one can conclude that only sodium is released from the glass to the salt and ion exchange only occurs between sodium and potassium [7]. Sodium concentration increases from a few ppm to about 20000 ppm, which is significantly larger than the sodium concentration of the salts used for chemical strengthening.

The ion exchange between the glass and the salt can be considered as the reaction described by Eq. 1.4, and the chemical potential of exchange reaction can be calculated using Eq. 1.5. Because of the low concentration of sodium, the sodium behaviour in the salt and glass is considered as an ideal solution, and the elements are assumed to obey Raoult's law. Therefore, the chemical potential,  $\mu_i$ , of each element is determined by:

$$\mu_i = \mu_i^* + RT \ln x_i \quad (3.5)$$

where  $\mu_i^*$  is the chemical potential of the pure element; R and T being the gas constant and absolute temperature, respectively.  $x_i$  is the concentration of the element in the solution. Sodium concentrations in the potassium nitrate salt after 72 h can be considered as a standard state; therefore, the chemical potential of ion exchange for each salt can be considered as:

$$\Delta\mu_{Na} = \mu_{Na}^{salt} - \mu_{Na}^{72h} = \{\mu_{Na}^* - RT \ln x_{Na}^{salt}\} - \{\mu_{Na}^* - RT \ln x_{Na}^{72h}\} \quad (3.6)$$

$$\Delta\mu_{Na} = RT \ln \frac{x_{Na}^{72h}}{x_{Na}^{salt}} \quad (3.6)$$

The concentration of sodium in the middle of tubes wall (or particles) is constant; therefore, the chemical potential of sodium in each salt can be measured using Eq 3.6; Table 12 provides the chemical potential of ion exchange of each glass in sodium poisoned salts at 450°C. It should be noted that although such numbers are abstract, we can use them for the assessment of the ion exchange affinity.

Table 12 Estimated driving force of ion exchange for each glass immersed in salts containing different sodium load

	[Na]: 1000 ppm	[Na]: 2500 ppm
<b>Nipro-LC</b>	18.5 kJ mol <sup>-1</sup>	13.0 kJ mol <sup>-1</sup>
<b>Fiolax-HC</b>	18.4 kJ mol <sup>-1</sup>	12.9 kJ mol <sup>-1</sup>

The chemical potential of ion exchange is almost the same for both glasses. It is likely that the variation of chemical strengthening efficiency depends on glass composition but not on salt poisoning. Such a variation agrees well the reported correlation between the activation energy and salt poisoning in soda lime silicate and aluminosilicate glasses reported by Fu. A. et. al. [45, 46].

Though the calcium-containing salt has lesser sodium than the other salts used for ion exchange of borosilicate tubes, the strengthening is inefficient (Table 4). The influence of calcium on chemical strengthening of silicate glasses is known as “blocking effect” [118, 121, 122]. Ion exchange can be forestalled by calcium and, consequently, the generated stress at the surface declines.

The influence of calcium on chemical strengthening was investigated by performing a series of ion exchanges in pure potassium nitrate salt contaminated with different amounts of calcium ( 12, 25 and 70 ppm) at 425, 450 and 475°C for 4 h. The surface chemical composition was checked by EDS analysis, and afterwards the ratio of the molar concentration of potassium and calcium on the surface to the total amount of sodium, calcium and potassium was considered as the relative concentration of elements. It should be noted that no magnesium has been detected in either glass by WDS-XRF analysis; therefore, it was not checked by the EDS microprobe analysis.

Figure III-20 shows the relative concentration of potassium and calcium on the surface of samples subjected to ion exchange in different conditions; the lines are for eye guide. The presence of calcium is clearly responsible for the decrease of potassium concentration and, therefore, an incomplete ion-exchange. The relative concentration of potassium on either glass decreases continuously with increasing the calcium concentration to 14 ppm; then, the concentration variations become moderate compared to the first regime of the plots. By increasing either the treatment temperature or the concentration of calcium, the sodium-potassium exchange becomes more limited, and the concentration of calcium increases slightly at the surface.

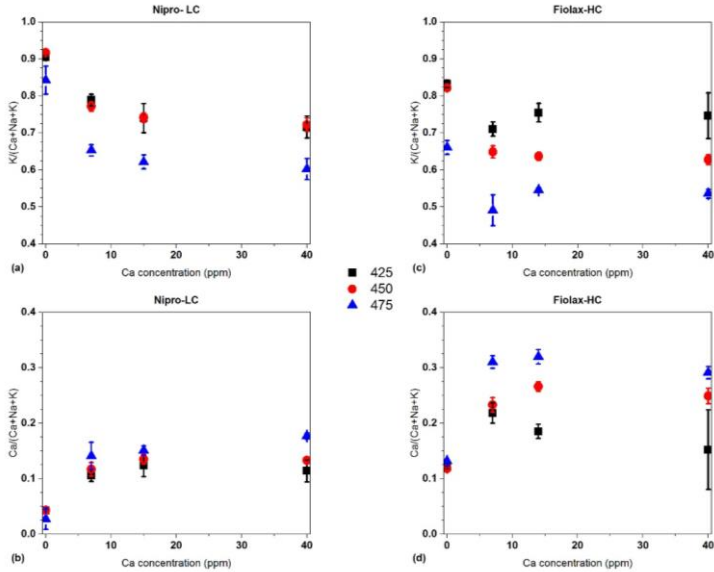


Figure III-20 Relative concentration of potassium and calcium on the surface of tubes immersed in potassium nitrate at 425, 450 and 475°C for 4h against the concentration of calcium in the salt: (a) potassium and (b) Ca concentration on LC glass; (c) potassium and (d) Ca concentration on HC glass

The role of calcium in the potassium exchange for sodium in a molten potassium nitrate can be looked at by using the thermodynamic paradigm of the decomposition of nitrate salts; in this model, the tendency of cations to form oxides instead of nitride is assessed by Gibbs free energy [123]. Figure III-21 presents the Gibbs free energy of possible reaction in which calcium can take the place of alkali ions on the surface of glass. We can see that calcium can be substituted for either sodium or potassium. Interestingly, the calcium exchange for potassium is more favoured than sodium from the thermodynamic point of view. In other words, if calcium is exchanged for potassium (of sodium), it is not possible to turn calcium back to the salt form the oxide state. In contrast, we have not seen a significant increase in the Ca concentration on the surface of the glasses subjected to ion exchange in calcium contaminated salts.

It is interesting to have a glimpse at the kinetics of calcium penetration into a silicate glass. Kirchheim R. has studied the role of alkaline earth in the structure of alkali

alkaline earth silicate glasses and investigated the influence of the replacement on the mobility of ions [124]. Potassium diffuses into the glass by taking sodium sites and the bonds between the sodium sites and non-bridging oxygens stretch to host the larger potassium ions into the position. Sodium can be replaced with calcium in a silicate glass because of the similar ionic radius ( $r_{Na} = 0.102$  nm and  $r_{Ca} = 0.100$  nm); indeed, two sodium sites should be taken by one calcium to keep the charge neutrality. The exchange energy can be assessed using Coulomb interaction of ions in the system and in order to ease the estimation, only the first two non-bridging oxygen close to the replaced site is considered.

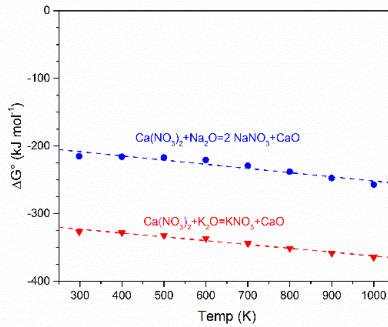


Figure III-21 Gibbs' energy of cation exchange molten nitrate salts from the nitrate to the corresponding oxide; the graph is plotted using the thermodynamic data summarised in Appendix I.

In a hypothetical configuration of atoms as illustrated in Figure III-22, when potassium ions diffused into the glass through the sodium sites occupied by calcium, the exchange energy,  $\Delta E$ , is given by:

$$\Delta E = E^K - E^{Ca} \quad (3.7)$$

where  $E^K$  and  $E^{Na}$  are the interaction energies of ions after ion exchange and in sodium silicate glass, respectively. The energy of each state can be estimated by :

$$E^K = \frac{1}{4\pi\epsilon_0\epsilon} \left[ \sum_{i=1}^2 \frac{2e^2}{r_{Ca} + r_{NBO} + \delta^K r_i} + \sum_{j=1}^4 \frac{e^2}{r_K + r_{NBO} + \delta^K r_j} \right] \quad (3.8)$$

$$E^{Ca} = \frac{1}{4\pi\epsilon_0\epsilon} \left[ \sum_{i=1}^2 \frac{2e^2}{r_{Ca} + r_{NBO} + \delta^{Ca} r_i} + \sum_{j=1}^4 \frac{e^2}{r_K + r_{NBO} + \delta^{Ca} r_j} \right] \quad (3.9)$$

where  $\varepsilon$  and  $\varepsilon_0$  are the relative permittivity and the permittivity of free space, respectively. The radius of calcium, potassium and non-bridging oxygens are  $r_{Ca}$ ,  $r_K$  and  $r_{NBO}$ . The parameter  $\delta$  takes care of the changes in the distances between the charge centres, or the ions, during the ion exchange. By replacing Eq 3.8 and Eq 3.7 into Eq 3.6:

$$\Delta E = \frac{1}{4\pi\varepsilon_0\varepsilon} \left[ \sum_{i=1}^2 \left( \frac{2e^2}{r_{Ca}+r_{NBO}+\delta^K r_i} - \frac{2e^2}{r_{Ca}+r_{NBO}+\delta^K r_i} \right) - \sum_{j=1}^4 \left( \frac{e^2}{r_K+r_{NBO}+\delta^{Ca} r_j} - \frac{e^2}{r_{Ca}+r_{NBO}+\delta^K r_j} \right) \right] \quad (3.10)$$

the variation of the charge centres distance can be neglected compared to the radius of the ions and Eq 3.9 can be simplified as:

$$\Delta E = \frac{1}{4\pi\varepsilon_0\varepsilon} \left[ \sum_{i=1}^2 \frac{2e^2(\delta^K r_i - \delta^{Ca} r_i)}{(r_K+r_{Ca})^2} + \sum_{j=1}^4 \frac{e^2(\delta^K r_j - \delta^{Ca} r_j)}{(r_K+r_{Ca})^2} \right] \quad (3.11)$$

For any given configuration, the distance of nonbridging oxygens and the cations increases when an alkaline earth ion is replaced with a larger alkali cation; therefore, there is a positive exchange energy that increases the required activation energy of exchange. This prevents further potassium exchange for calcium and precludes the replacement of ions. From this point of view, magnesium might have a stronger influence; the influence of salts's contamination by magnesium is an open questions deserves to be answered.

The required amount of calcium needed to hinder completely the penetration of potassium into the glass can be estimated by calculating the number of sodium ions, alkali sites, on the surface of the glass and finding the corresponding concentration in the salt. In order to ease the estimation, the article can be considered as a cube with the length of 1 cm and the surface area is equal to 6 cm<sup>2</sup>. The available sodium sites in the first 10 nm of surface are about 1.6 nmol ( when the glass density= 2.34 g cm<sup>-3</sup> and the sodium oxide concentration is assumed to be 7 %). If all of sodium in this layer is replaced by calcium, 64 ng of calcium is requires. The glass-to-salt ratio in this study is smaller than 1:30; therefore, the required calcium in the salt must be larger than 64 ppb.

Although such estimation clearly presents the vital role of calcium in ion-exchange of alkali borosilicate glasses, it should be noted that because of several simplifications some crucial steps in ion exchange like absorption of calcium to the surface is not

considered and more studies considering the role of different mass transfer steps are required.

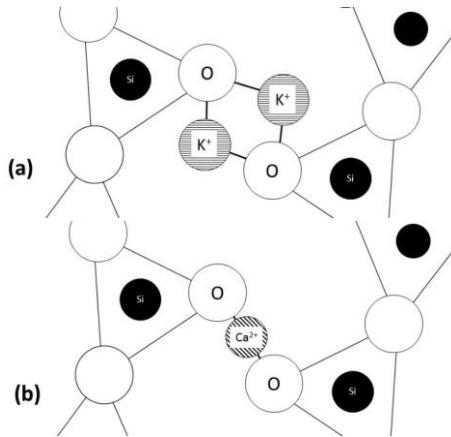


Figure III-22 Schematic draw of non-bridging oxygens surrounding sodium sites: (a) sodium is replaced by potassium; (b) calcium took the site

An extra point about the influence of calcium on the potassium exchange for sodium in borosilicate glasses is the role of temperature. The adsorption of calcium to the glass surface requires an activation energy that can be provided by temperature, this appearing as the fall in the relative concentration of potassium on the surface of glass after the treatment at 475°C, as we see in Figure III-20.

### 3.1.4 Summary

Potassium exchange for sodium, ion exchange, improves the mechanical performance of borosilicate glass used in pharmaceutical packaging; it is a proper technique for strengthening of samples. The glass becomes twice as strong as the raw glass after ion exchange in potassium nitrate salts.

The glass composition, particularly CaO, plays a major role in the formation of surface compressive stress. The glass containing a larger amount of CaO shows smaller surface compression on the surface. However, the effect of such a difference on final strength and, therefore, the strengthening efficiency is not significant; the glass tubes

containing different amounts of CaO showed almost the similar relative strength increase.

Slat's impurities affect the efficiency of chemical strengthening; the sodium contamination decreases the thermodynamic driving force of ion exchange and, consequently, influences the generation of compressive stress in the glass surface. However, the final strength of glass is not influenced significantly when soda borosilicate glass undergoes Na/K ion exchanged in salt containing 2500 ppm of Na. In contrast, even a limited amount of calcium, of the order of a few ppm, has a significant impact on chemical strengthening. By using a thermodynamic paradigm, it was found that sodium is replaced with calcium in the calcium-contaminated salts. This inhibits the potassium for sodium ion exchange and, consequently, the generation of compressive stress.

### **3.1.5 Further studies**

Understanding the governing mechanism of the chemical strengthening of borosilicate glasses in calcium contaminated potassium nitrate salts is a must in improving the efficiency of the process. However, the diffusion of calcium into the glass and the affected layer by calcium is limited. This makes studying the influence of calcium on the surface properties of glass difficult.

One possible approach to investigate the role of calcium is to consider the ion exchange process as a series of inter-diffusion steps and applying the conditions for the mass balance as presented before. Since the diffusion behaviour of the bulk glass remains unchanged in principle, the variations are due to the modifications of the glass by diffusion of calcium into the surface. Another benefit of such approach is to employ the modelling methods, like molecular dynamics, to guess the reactions in the interface layer [125].

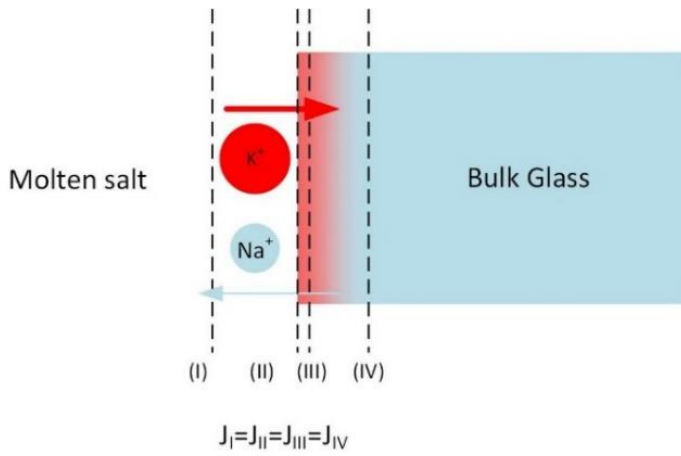


Figure III-23 Schematic draw of the involved mass transport steps between different parts of glass during chemical strengthening

## 3.2 Electric Field Assisted Ion Exchange of Borosilicate Glass

Electric field assisted ion exchange produces thick exchanged layers in glass and can improve the efficiency of chemical strengthening; however, the inhomogeneous stress distribution is the main drawback of this technique. Several pharmaceutical products, such as vials and ampules, have a shape, i.e. cylinders, in which the stress distribution in the glass thickness is less important [82, 126]. This section reports on the E-field assisted ion exchange of borosilicate glass used in pharmaceutical packaging.

### 3.2.1 Current density and E-field intensity

Figure III-24 shows the current density as a function of time for borosilicate tubes immersed in the molten potassium nitrate bath and subjected to E-field with intensities between  $100 \text{ V cm}^{-1}$  to  $3000 \text{ V cm}^{-1}$ . The current density declines with time with a decreasing rate. The current density depends clearly on the E-field intensity and by applying an intense E-field the current density increases. During ion exchange, larger potassium ions, which are also less mobile, take the place of sodium ions. This replacement produces a layer with a higher resistivity; therefore, we expect that the resistivity of the sample also increases as the depth of exchanged layer continuously increases with time and, in turn, the current density decreases [56, 127]. By applying more intense E-fields, the mobile ions in glass are subjected to stronger forces; this producing higher current densities.

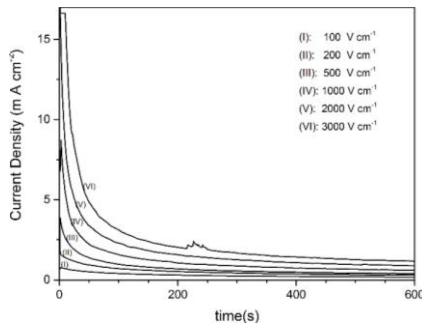


Figure III-24 Current density against time in samples (test tubes) immersed in molten potassium nitrate and subjected to E-Field varying between 100 to  $3000 \text{ V cm}^{-1}$ . A current density limit equal to  $16 \text{ mA cm}^{-2}$  is applied.

The variations of current density as a function of time during EF-IE sample (current density limit =  $8 \text{ mA cm}^{-2}$ ) are shown in Figure III-25. The samples show quite the same behaviour to ones prepared by applying the current limit of  $16 \text{ mA cm}^{-2}$ ; there is a span of time where the current density is equal to the applied limit for E-fields of 2000 and  $3000 \text{ V cm}^{-1}$ . In such cases, after a certain time, the current density decreases and resembles a curve similar to the presented ones in Figure III-24.

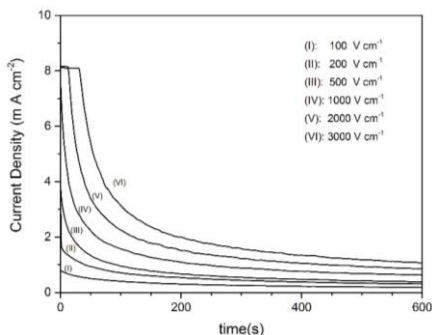


Figure III-25 Current density against time in samples ( test tubes) immersed in molten potassium nitrate and subjected to E-Field varying between 100 to  $3000 \text{ V cm}^{-1}$ . A current density limit equal to  $16 \text{ mA cm}^{-2}$  is applied.

The current density variations against time for subjected samples to an E-field with the intensity of  $3000 \text{ V cm}^{-1}$  and different current density limits are presented in Figure III-26. The length of the constant current span is increasing by decreasing the current density limit; however, the area under the current density curve representing the amount of ions transferred through the glass is substantially constant. It is supposed that potassium takes only the place of sodium; therefore, this area is the representative of the amount of exchanged ions in samples.

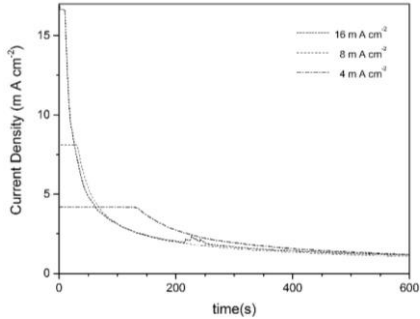


Figure III-26 Current density against time in samples ( test tubes) subjected to a  $3000 \text{ V cm}^{-1}$  E-field with a current and current density limits of 4,8 and  $16 \text{ mA cm}^{-2}$

The current density response of samples is slightly different from the reported behaviour for solid state electric field assisted ion exchange [109, 128-131], and thermal poling [132-134]. In such processes, there are one or two peaks in current density against time curves; those peaks are attributed to the migration of alkali ions towards the anode side. As the charge carriers are not replaced in the glass, the alkali ions (e.g. sodium ions) accumulate near one side of the glass, this generating a strong local E-field on the anode side and a highly electrical resistive glass on the cathode side of glass. In the case of solid state electric field assisted ion exchange, the mentioned process is followed by the oxidation of electrodes coated layer on the glass surfaces.

On the contrary, in an electric field assisted ion exchange treatment by using a molten salt, e.g. potassium nitrate, the electric field accelerates ions in both the glass and salt. No peaks are observed in current density vs. time curves because no reactions like oxidation-reduction occur to yield required ions for ion conduction. As mentioned above the glass resistance increases as a result of the formation of exchanged layer where only potassium occupies the alkali sites. One can conclude that the resistance of glasses with equivalent exchanged layers are the same, this explaining the very similar behaviour of all samples subjected to the E-field with the intensity of  $3000 \text{ V cm}^{-1}$  after a certain time ( Figure III-26).

The potassium concentration profiles were measured across the tubes subjected to the EF-IE for 10 min at  $400 \text{ }^\circ\text{C}$ . The noise of measurement was removed by applying a low pass filter; then, the experimental data was fitted using Eq. 1.21 and illustrated in Figure III-27; a typical concentration profile of a tube subjected to ion exchange for

4 h is also presented for comparison. The concentration profiles contain a constant potassium concentration region followed by a rapid decrease of concentration. The depth of potassium rich layers increases by the intensity of applied electric field.

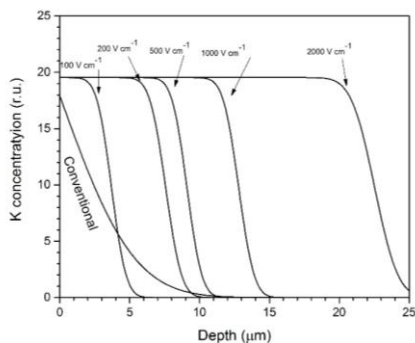


Figure III-27 Relative potassium concentration profiles for the test tubes subjected to electric field-assisted ion exchange (EF-IE) at 400°C (Figure III-25), and conventional ion exchange at 450°C for 4h

Figure III-28 presents the chemical composition across the thickness of the sample treated by 2000 V cm<sup>-1</sup> ; the oxide concentration of boron oxide is not presented because of the limitations of measurement technique. Sodium is replaced by potassium completely in the exchanged layer, 1 and 5 μm. At the border of constant potassium concentration region, some sodium is detected which is confirmed by the decreasing part of the concentration profile of potassium, shown in Figure III-27. In the internal surface of glass, the depth of 600 μm, both sodium and potassium are detected. The presence of potassium on the surface can be explained by the diffusion of cations in opposite direction of the electric field due to the chemical potential [7, 45, 56, 57]. The silicon oxide concentration increases on the inner surface of the glass; a similar increase has been reported in the literature due to the structural modifications of glass to accommodate larger ions during ion exchange [75, 135]; however, such variations are likely not responsible for the observed increase in silicon oxide content. One can explain that by the accumulation of measurement error due to the measurement technique, EDS.

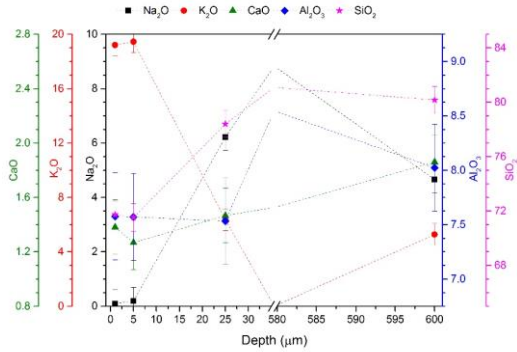


Figure III-28 Chemical composition, in wt%, of glass tubes subjected to EF-IE with an E-field of  $2000 \text{ V cm}^{-1}$  and a current limit equal to  $8 \text{ mA cm}^{-2}$  across the wall

The amount of potassium ions stuffed into the glass surface can be estimated by using either the concentration profiles or the current density vs. time curves. Figure III-29 shows the depth of exchanged layer estimated by the current density vs. time curves and the depth directly measured from the concentration profiles. The depth of layer is chosen as the point where the concentration drops to 0.005 of the surface concentration of potassium.

Considering the concentration of potassium related to the case depth, E 1.21 can be rewrite as:

$$0.005 C_k \text{ surface} = \frac{C_k \text{ surface}}{2} \operatorname{erfc}\left(\frac{x - \mu_K E t}{2\sqrt{Dt}}\right) \quad (3.11)$$

By considering the inverse of the complementary error function about 1.8, the depth of layer as function of the applied E-field is given by:

$$x = (3.6\sqrt{Dt}) + (\mu_K t)E \quad (3.12)$$

Eq. 3.12 shows a linear relation between the applied E-field and the case depth if the mobility ions and time of treatment is not influenced by the electric field. The measured data is close to the experimental results, and follow Eq. 3.12. Although there is a general deviation from the lines especially in higher fields.

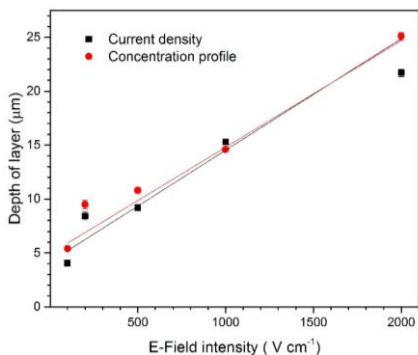


Figure III-29 Depth of exchange layer as a function of the applied field; the depth is estimated from the current density-time curves and the concentration profiles.

Changing the E-field polarisation is suggested as an approach to improve the performance of EF-IE through producing potassium for sodium ion-exchanged layers on both sides of glass [56, 126]. Figure III-30 shows current density variations of a test tube subjected to EF-IE when the polarisation of E-fields is reversed. The sample was prepared by applying an electric field with the intensity of  $1000 \text{ V cm}^{-1}$  in the direction from the exterior surface to the inside of the tube, and afterwards the field direction was inverted by keeping the E-field intensity constant. The current density attributed to the invert E-field is very similar to the current density of direct field before switching the field direction; then, it increases slightly and reaches a maximum following by a slight decreasing regime.

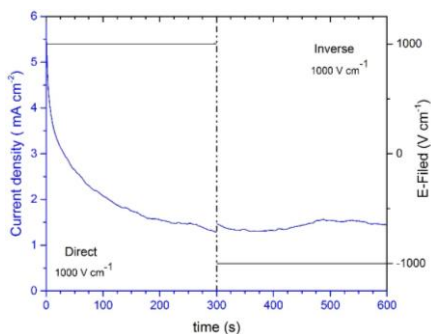


Figure III-30 Current density as a function of time in the samples treated by inverting the E-field polarisation: initially an E-field ( $1000 \text{ V cm}^{-1}$ ) was applied for 300 s and afterwards an E-field with the inverted polarisation was applied

When the E-field has inverted the movement direction of alkali ions in the glass is reversed as well. Potassium ions in the exchanged layer must be pushed back and replaced with sodium ions from the glass bulk while a new exchanged layer is being produced on another side of glass. Therefore, the net thickness of layers undergone the ion exchange is eventually constant and, consequently, the resistance of glass is not changing; the sample shows a similar current density to the forward field after reversing the polarisation when the E-field intensity is not changed ( Figure III-30).

Figure III-31 shows the current density variations versus time of samples subjected to two-step ion exchange in which the intensity of inverse electric field is  $2000 \text{ V cm}^{-1}$ . The current density increases until it reaches a peak after reversing the polarisation. The alkali ions are accelerated in the E-field direction depending on the ion mobility; therefore, sodium moves faster than potassium ions in glass. Applying a stronger E-field causes that sodium penetrates into the exchanged layer, this producing a layer containing two alkali ions. In the exchanged layer, the conductivity of glass is larger than the parent glass; this phenomenon is in contrast with the expected behaviour from the mixed alkali effect (an increase in resistance) [32, 52, 136, 137]. As a consequence, the current density increases.

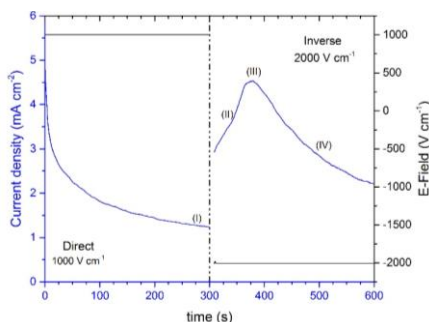


Figure III-31 Current density as a function of time in the samples treated by inverting the E-field polarisation: initially an E-field ( $1000 \text{ V cm}^{-1}$ ) was applied for 300 s and, then, an E-field with the intensity of  $2000 \text{ V cm}^{-1}$  and inverted polarisation was applied

Figure III-32 shows sodium and potassium concentration profiles of samples subjected to EF-IE shown in Figure III-31. The concentration profiles are collected near the samples surface according to the following order: the profile (I) is related to the sample

subjected to the direct E-field of  $1000 \text{ V cm}^{-1}$  for 300 s. The next profile corresponds to the sample prepared by reversing the E-field and increasing the field intensity to  $2000 \text{ V cm}^{-1}$ ; this sample was subjected to the E-field for 50 s which is located before the peak centre of current density curve, point (II). The invert E-field pushes backwards the exchanged layer; besides, sodium advances into the potassium exchanged layer faster than potassium, as expected from the ion mobility. The decreasing part of concentration profiles depends on the applied electric field intensity and the diffusion coefficient of the glass according to Eq. 1.21.

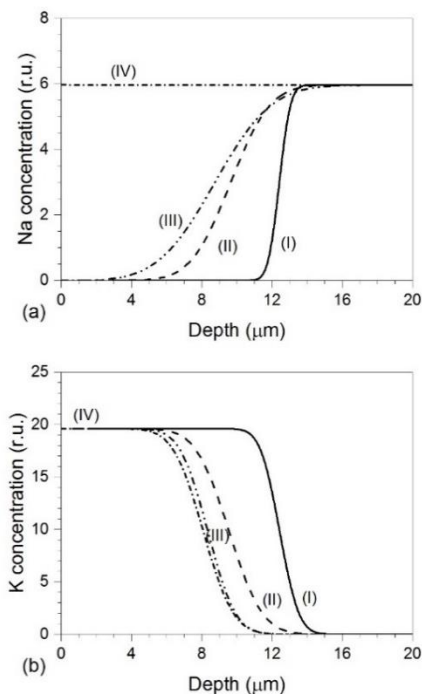


Figure III-32 Potassium concentration profiles in samples subjected initially to a  $1000 \text{ V cm}^{-1}$  E-field and afterwards treated by applying a reverse field with the intensity of  $2000 \text{ V cm}^{-1}$ . The concentration profiles were measured on the samples at the points marked in Figure III-31. (a) shows sodium concentration profiles and (b) illustrates K concentration profiles.

The slope of concentration profiles becomes steeper, perhaps, because of the increase of the diffusion coefficient of ions in the layer subjected to potassium exchange for sodium. The sodium containing layer extends to the surface of the

samples subjected to the reverse E-field until the point (III), and potassium steps back a little. Subjecting to the reverse field for longer causes the concentration of sodium becomes constant within the layer (IV). It seems that potassium rich layer moves back until a certain point after reversing the E-field. It should be noted that the potassium concentration on the surface decreases slightly after point (III); this has been not presented in Figure III-32 to ease the profiles comparison.

During the reverse regime of EF-IE, when there is a layer containing both Na and K, the transfer of cations can be conducted through the alkali sites occupied by the similar ions because ionic jumps in the direction of the applied E-field is energetically favoured. Such phenomenon can be anticipated from Eq. 3.9 when the ionic size and charge of potassium and sodium are used; hence, the glass can be assumed to contain two split paths for mass transfer. This glass can be modelled by two resistors in a parallel configuration in which most of the current passing through the part with the preferential path for charge carriers (alkali ions); consequently, the thickness of the produced layer in the initial step remains eventually constant (Figure III-33).

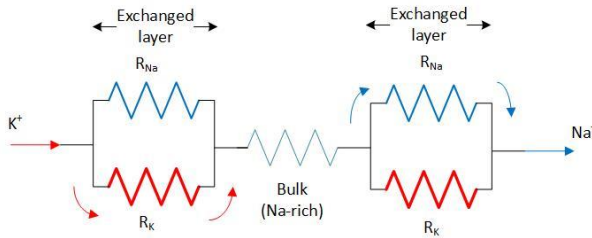


Figure III-33 Equivalent circuit for modelling the current path when the polarisation is reversed

The concentration profiles produced in samples by applying an AC field with the sine waveform (frequency of 100 Hz) and the intensity of  $1000 \text{ V cm}^{-1}$  is shown in Figure III-34; the E-field were kept on for 10 min and 60 min. An exchanged layer with the thickness of  $5 \mu\text{m}$  is produced in the samples treated for 60 min. One may note that when an AC field with sine waveform is applied, the maximum field intensity is applied for a short time and, therefore, the exposure time in these treatments is different from the DC field. It seems applying an AC field can be used to produce concentration profiles which have the characteristics of the EF-IE (depth and shape) on both sides of glass. However, implementing this method requires more investigations.

Subjecting to the electric field, stuffing and movement of larger potassium ions in the glass structure are probably responsible for structural changes and the formation of a new glass which has a structure more similar to the raw glass than an as-melted glass with the same chemical composition. The modified structure allows the alkali ions to move faster in the structure, and advance rapidly into the exchanged layer near the surface [53, 54]. The applied electric field probably provides the required energy for changing the glass structure. The following part investigates the influence of applied E-field on the ion mobility and the diffusion coefficient of potassium.

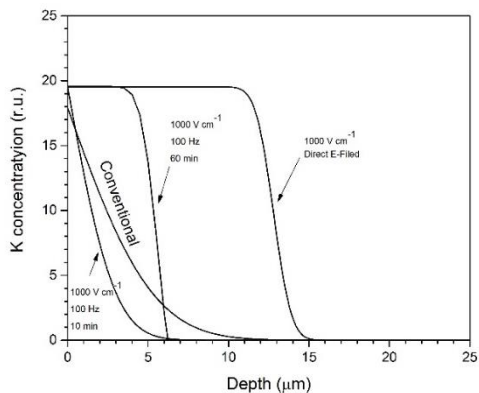


Figure III-34 potassium concentration profiles produced in glass tubes by subjecting the samples to an AC E-field with a square waveform with the frequency of 100 Hz and intensity of  $1000 \text{ V cm}^{-1}$ ; the E-field was applied for 10 and 60 min.

### 3.2.2 Diffusion coefficient under an electric field

The variations of diffusion coefficient against temperature were initially checked by immersing the glass tubes in the molten potassium nitrate salt for 4 h at temperatures varying between  $400$  to  $500^\circ\text{C}$ . Then, the concentration profiles were measured near the glass surface using EDS measurements, and afterwards the profiles were fitted by Eq. 1.12 in order to estimate the diffusion (inter-diffusion) coefficient. By considering the diffusion coefficient as a function of temperature, Eq. 1.13, it is possible to find the required activation energy for diffusion,  $Q$ .

Figure III-35 shows the measured inter-diffusion coefficient against the treatment temperature using linearized coordination from Eq. 1.13. The activation energy of diffusion is  $94 \text{ kJ mol}^{-1}$ , which agrees fairly with the other measurements on sodium-potassium inter-diffusion in soda-borosilicate glass [39, 40, 138]. As expected,

temperature provides the activation energy for mobility of ions and, as a result, the inter-diffusion coefficient increases.

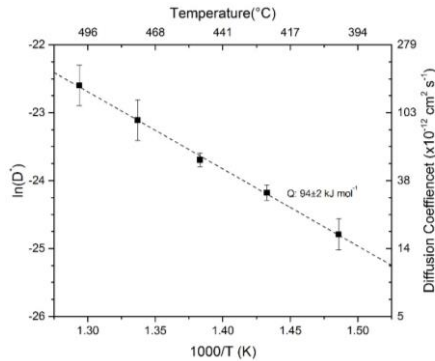


Figure III-35 Logarithm of the measured diffusion coefficient,  $D$ , against the reciprocal temperature; the samples were kept in the molten potassium nitrate for 4 h.

We can also estimate the diffusion coefficient from the concentration profiles produced by EF-IE. The concentration profiles presented in Figure III-28 were fitted using Eq. 1.21. The experiment conditions influence the diffusion coefficient measurement; therefore, a reference sample was immersed in pure potassium nitrate for 1h and the diffusion coefficient was measured as the reference point. The measured diffusion coefficients are different from the measured values using the thermal activation process which is probably due to the influence of applied E-field on the mobility of ions. Nonetheless, here the variations of the coefficients are of interest, not the absolute values; therefore, the estimated values are referred as “apparent diffusion coefficient”.

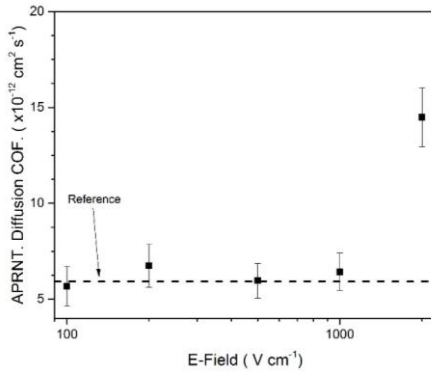


Figure III-36 Apparent diffusion coefficient of potassium in the glass against the applied E-field

The apparent diffusion coefficient goes up and down around the measured value for the reference sample. The sample subjected to an E-field with the intensity of 2000 V cm<sup>-1</sup> shows a clear increase in the relative diffusion coefficient; such behaviour has also been observed in electric field assisted ion exchange of soda lime silicate glass, which is reported in Appendix II.

Figure III-37 shows the glass tube resistivity, which is calculated from the ratio of applied E-field to the current density, against the applied field. It should be noted that titanium electrodes were used in sample preparation and an oxide layer is produced on the electrodes during the process because of the corrosion of metal which increases the resistance of the cell in the first seconds of applying the E-field [139-141]. Then, after a certain E-field and current density, the oxide layer is destroyed [142]. The interference of the oxide layer was removed from the measured values, and the real electric field was considered in measurements.

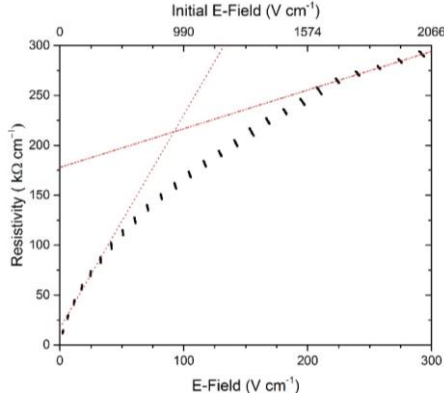


Figure III-37 Evolution of resistivity as a function of applied electric field for glasses immersed in potassium nitrate at 400°C; The second x-axis presents the applied E-field regarding the power supply output voltage

The resistivity of glass increases continuously with increasing the applied E-field. The initial and final regimes of experimental data were fitted by linear functions; the fitting lines are only to point out the change of the increase rate. The increase rate of resistivity decreases by applying stronger fields.

The ion-exchanged layer and bulk glass can be considered as two resistors in a series configuration, as illustrated in Figure III-38. The resistance of glass against time can be estimated by using the equation describing the concentration profiles as a function of time. If we consider the glass resistance in the exchange layer constant, the resistance of glass can be calculated by:

$$R_{total} = xR_{exch} + (1 - x)R_{bulk} \quad (3.13)$$

where  $R_{exch}$  and  $R_{bulk}$  are the resistivities of the exchanged layer and the bulk, respectively.  $x$  is the ratio between the exchanged layer and the glass thickness. If we consider that the thickness of the exchanged is negligible compared to sample thickness ( in this case, 20  $\mu\text{m}$  vs. 600  $\mu\text{m}$ ), the current density,  $J$ , is a function of resistivity under the constant applied voltage as:

$$J = \frac{V/A}{xR_{exch} + R_{bulk}} \quad (3.14)$$

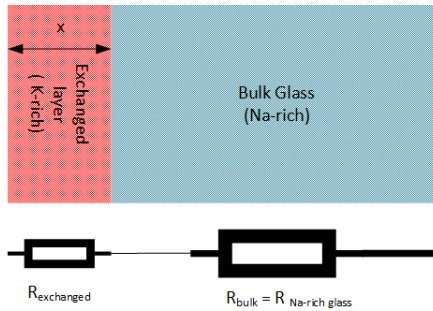


Figure III-38 Equivalent circuit model of a glass subjected to electric field assisted ion exchange [126]

By replacing the thickness of layer from Eq. 3.12, and using  $R=\rho/l/A$ , Eq. 3.14 can be re-written as:

$$J = \frac{v}{(3.6\sqrt{Dt} + \mu_0 Et)\rho_{exch} + \rho_{Na}} \quad (3.15)$$

If we assume that the mobility of ions and, consequently, the resistivity and conductivity of glass are constant with time, the current density curves versus time can be fitted by Eq. 3.15. Figure III-39 shows the fitted curve using the data given in Figure III-25 in the slot between 20 s and 550 s in order to avoid the current density limit influence. The estimated constants of the fitting curves are summarised in Table 13. It should be noted the physical meaning of each constant lies out of the interest of this text and the experience of author. Nevertheless, it is interesting to consider the variations of the parameters of the applied field. We see that the resistivity of the bulk glass, which contains sodium, decreases continuously by increasing the applies E-field; conversely, the parameter corresponding the mobility of the ions in the exchanges layer is practically constant. Both of these are perhaps related to the evolution of the glass structure because of the influence of the applied E-field [68, 75, 109, 131, 143]. In the following section, we investigate the glass structure in the ion-exchanged layer and the bulk glass by Raman spectroscopy.

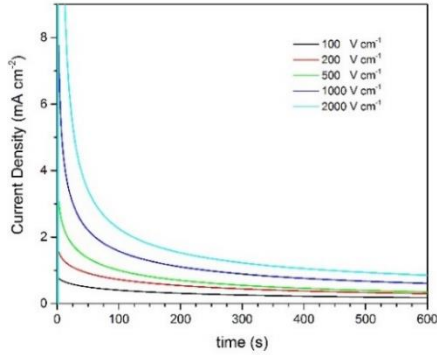


Figure III-39 Current density as a function of time; the curves are drawn by using Eq. 3.15 and fitting the points shown in Figure III-25.

Table 13 Constants estimated by fitting the current density versus time curves shown in Figure III-25; the numbers between parentheses are representative of the generated error in calculations

E-field(V cm <sup>-1</sup> )	C1: $3 \cdot 6\rho_K\sqrt{D}$	C2: $\mu E\rho_K$	C3: $\rho_{Na}$
100	625(10)	25(0)	7727(40)
200	1029(8)	22(0)	6214(35)
500	2000(14)	29(1)	3966(47)
1000	2998(11)	24(0)	1666(43)
2000	4703(45)	25(2)	-4324(155)

### 3.2.3 Structural Modifications

The glass structure was studied by collecting micro-Raman spectra on the raw glass; and across the samples undergone EF-IE using an E-field with the intensity of 2000 V cm<sup>-1</sup>. The collected spectra on the raw glass is shown in Figure III-40.

The spectrum can be split into four main regions. The first frequency region, between 200 and 650 cm<sup>-1</sup>, is attributed to the mix stretching and bending of Si-O-Si units [75, 144-146]. The maximum of the regions is at about 500 cm<sup>-1</sup>; this frequency is assigned to the Si-O-Si bending [145, 147]. The Raman intensity at the low-frequency region is

related to Si-O-Si vibrations and changing in bond angle causes the asymmetric band in this frequency.

The 650-850  $\text{cm}^{-1}$  region involves two significant peaks centred at 650 and 800  $\text{cm}^{-1}$ . The latter is related to the asymmetric Si motion in Si-O cages [75, 147, 148]. The first peak locates in a region known to be attributed to the metaborate rings, and other borate and borosilicate-ring units [147]. The characteristic peak of tetraborate groups, 670  $\text{cm}^{-1}$ , matches well to the appeared peak. However, the peak can be also attributed to the breathing mode of borosilicate ring at 630  $\text{cm}^{-1}$ . It should be noted that the glass composition contains about 10 wt. % of  $\text{B}_2\text{O}_3$ ; therefore, some peaks may be hindered by the effect of Si-O bonds, which is fairly in agreement with the reported spectra related to the alkali alkaline earth borosilicate glasses [147, 149].

The peaks in the region between 850 to 1250  $\text{cm}^{-1}$  are due to the stretching of Si-O bond within silicate tetrahedra [144, 145, 148, 150]. The Raman shift is related to the Si-O bond length, which is making the higher wavenumber peaks attributed to the shorter bond length. Consequently, the peaks located in this region are related to  $Q_1$ ,  $Q_2$ ,  $Q_3$  and  $Q_4$  respectively. By the deconvolution of this region, the glass structure can be studied and the relative concentration of the  $Q_n$  species can be found. It should be noted that such quantifications intend to show the possible variations of the glass structure; in fact, an accurate quantification needs to be considered all the activities located in peak pockets.

The last region between 1250 to 1800  $\text{cm}^{-1}$  can be assigned to B-O stretching in chains of metaborate groups [151-153]. The peak centred at 1410  $\text{cm}^{-1}$  is attributed to  $\text{BO}_3$  units connecting  $\text{BO}_4$ ; whereas, the component at about 1480  $\text{cm}^{-1}$  corresponds to  $\text{BO}_3$  units bonding  $\text{BO}_3$  units [149]. Though this region can be used to study the evolution of glass structure during electric field assisted ion exchange, using deconvolution of peaks and quantitative methods is not accurate due to the low intensity of boron oxide units in the spectra.

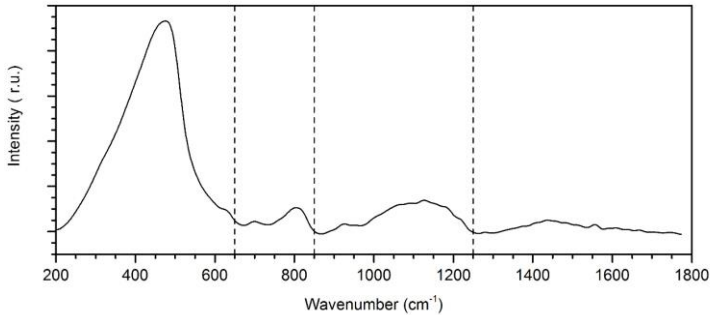


Figure III-40 Micro-Raman spectrum collected from the raw borosilicate glass before EF-IE

Raman spectra collected from the layer beneath the tube surface where underwent the ion exchange by EF-IE and the middle of the tube wall which is not affected by replacing of ions are shown in Figure III-41; the wavenumber is limited to the region related to the  $Q_n$  species. The spectra shape is clearly changed in the region between 1000 to 1300  $\text{cm}^{-1}$ . Furthermore, the maximum intensity of the region is shifted to the lower wavenumbers. The change of the spectrum is due to the modifications of glass structure by changing the population of  $Q_n$  species during electric field assisted ion exchange.

The region was fitted by four gaussian peaks; the initial peak centres were chosen at around the reported values in literature[144, 148]; then the constraint was removed and the peak centres were considered flexible to achieve the best fitting. The final peaks were located at 930, 1040, 1125 and 1188  $\text{cm}^{-1}$  that are attributed to  $Q_1$ ,  $Q_2$ ,  $Q_3$  and  $Q_4$  respectively; the corresponding  $Q_n$  species were selected by considering the length of Si-O bond in  $Q_n$  units. The location of the  $Q_n$  species is slightly different from the Raman shifts reported in the literature for silicate glasses; this is probably related to the presence of boron in the glass composition and changes in silicon-oxygen bonding. The mismatch of the fitting spectrum and the experimental data is probably related to the splifications have been taken about  $Q_n$  units as well as  $\text{BO}_4$  and  $\text{BO}_3$  species.

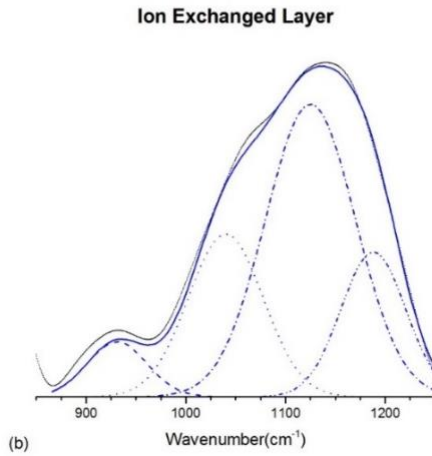
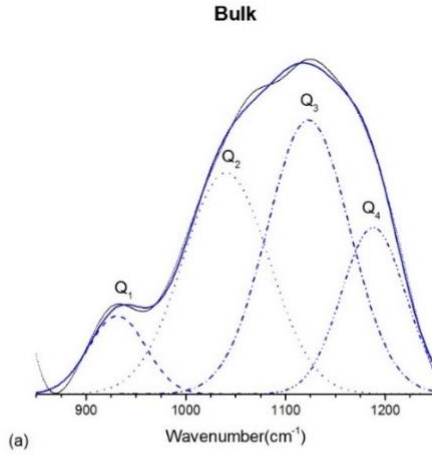


Figure III-41 Micro-Raman spectra in the region of 850 to 1250 cm<sup>-1</sup> taken from the glass bulk and edge (EF-IE): Borosilicate glass: (a) bulk, (b) Ion-exchanged layer

The intensity of Raman shift is given by:

$$I_R \propto \nu^4 I_0 N \left( \frac{\partial \alpha}{\partial A} \right)^2 \quad (3.16)$$

where  $I_0$  and  $\nu$  are the incident laser intensity and frequency respectively,  $N$  being the number of scattering molecules in a given state,  $\alpha$  is the polarizability of the molecules, and  $A$  is the vibrational amplitude;  $(\partial\alpha/\partial A)$  is the Raman cross section. During the collection of Raman spectrum of  $Q_n$  species in samples, all the parameters of Eq. 3.16 are constant but  $I_R$  and  $N$  [154]. In practice, the intensity of peaks is the function of only the concentration of each species; nonetheless, it can be considered directly related to the intensity of Raman shift associated with the species. The intensities of fitted peaks to the collected spectra were used to check the variations of the  $Q_n$  species by subjecting to electric field assisted ion exchange.

Figure III-42 shows the relative concentration of  $Q_n$  series calculated from the spectra presented in Figure III-41. The concentration of  $Q_2$  decreases clearly and the amount of  $Q_3$  increases. Ingram, M.D. et al. have reported that the silicate glass structure changes during the diffusion of larger potassium ions and the bonds of  $Q_n$  species break and reform to make a path for ion movement, CIRON [53]. The corresponding reaction of the proposed structural evolution is described as:

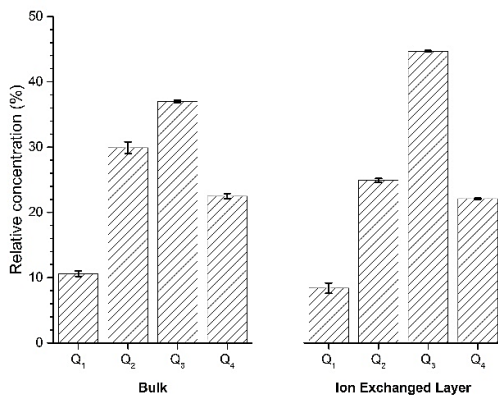
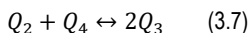


Figure III-42 Relative concentration of  $Q_n$  species in glass estimated from Raman spectra in Figure III-41

According to Figure III-42, the decrease in  $Q_2$  concentration and the increase of  $Q_3$  agree well with the proposed reaction for structural modifications ( Eq. 3.7); however,

the concentration of  $Q_4$  is almost constant and does not change. The of the detection of the peak corresponding  $Q_3'$  units during stuffing ions may be related to the apparent constant concentration of  $Q_4$ . Matson et al. reported a shoulder at  $1150\text{ cm}^{-1}$ , attributed to the formation of  $Q_3'$  units [145]. This unit is a  $Q_3$  with two different second neighbour environment [75]; such an environment is probably formed because of stuffing larger potassium ions in the glass structure.

Breaking and rearranging of the local bonds in the glass during electric field assisted ion exchange might produce a fully dense or relaxed glass with a structure similar to the as-melt glass. The lack of compressive stress on the surface of samples treated by EF-IE makes the ion exchange inefficient by the chemical strengthening point of view.

### 3.2.4 Mechanical performance

Figure III-43 shows the impressions of Vickers indentations on the surface of Raw glass, chemically strengthened and subjected to EF-IE. The indentations were produced using a maximum load of 19.62 N and the indentation time of 15s. The radial and median cracks are generated and well developed from the corners of indentation impression on the raw glass surface; some secondary cracks are also observed expanded from the Vickers' pyramid imprint (Figure III-43-a); furthermore, lateral cracks are also present beneath the glass surface and exhibiting by the birefringence of light.

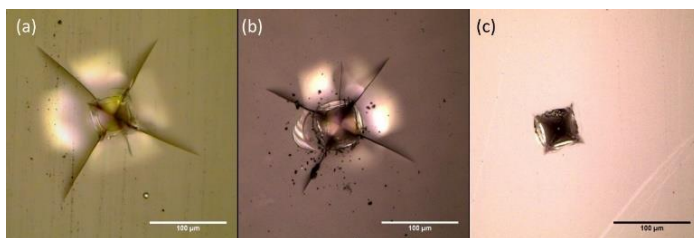


Figure III-43 Vickers indentations on glasses: (a) Raw tubes, (b) conventional ion exchanged and (c) ion-exchanged under E-filed ( $2000\text{ V cm}^{-1}$ )

The compressive stress generated on the glass surface by ion exchange on the glass surface precludes the propagation of cracks on the surface (Figure III-43-b). No cracks are observed on the surface of samples subjected to EF-IE; this is probably related to the generation of a strong compressive stress on the surface that prevents the nucleation of the cracks in the glass.

The optical methods cannot be employed for measuring the generated stress on the surface of samples subjected to EF-IE as no cracks are formed on the surface. The compressive stress on the surface can be measured using the load-displacement curves of Vickers indentation. Figure III-44 shows the load-displacement data of samples subjected to Vickers' indentations with the constant loading rate of  $16 \text{ mN s}^{-1}$ . The experimental data was fitted using Kick's law [155]. The displacement span between 1000 to 1400 nm is zoomed in Figure III-44-b.

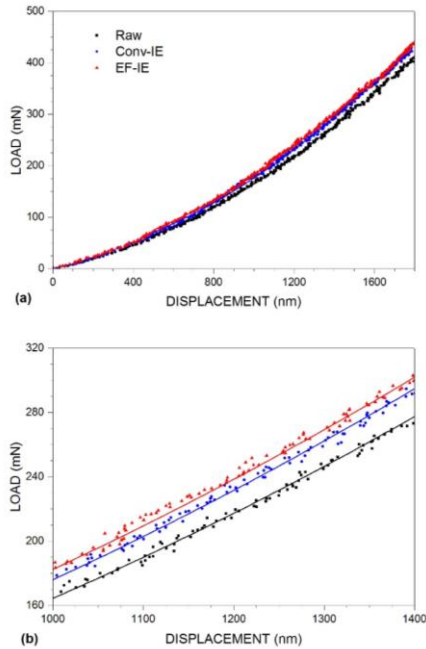


Figure III-44 Load-displacement curve produced from indentation of Raw glass, conventionally ion exchange at  $450^\circ\text{C}$  for 4 h and subjected to EF-IE ( $2000 \text{ V cm}^{-1}$ ).

The compressive stress (CS) on the surface acts as a hydrostatic pressure on the surface that prevents the penetration of invading indenter ( as discussed in section 2.3.2). The load required for certain penetration increases when the samples is treated by chemical strengthening according to Figure III-44-b; the surface compression generated by EF-IE is larger than conventional chemical strengthening. The CS on the

surface of glass after EF-IE is larger than the conventional ion exchange. The estimated compressive stresses are summarised in Table 14.

Table 14 Estimated compressive stress on the surface of tubes using the LOAD-DISPLACEMENT curves shown in Figure III-44; the numbers between parentheses present the errors in estimation

	Conv. Ion Exchange	EF-IE
Compressive Stress (MPa)	470 (120)	610 (100)

Figure III-45 shows the bending strength of glass tubes using Weibull distribution. The samples were treated by EF-IE with a field with the intensity of  $1000 \text{ V cm}^{-1}$  for 600 s in order to produce an exchanged layer as deep as the layer produced by chemical strengthening at  $450 \text{ }^\circ\text{C}$  for 4h. The strength of samples produced by subjecting to EF-IE through reversing the polarisation are also presented; the exchanged layer is produced on both sides of glass with the same depth.

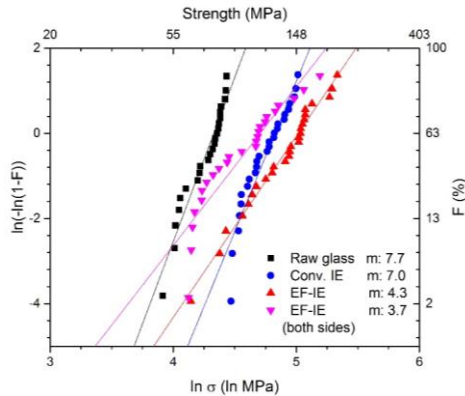


Figure III-45 Weibull distributions of glass tubes strength. Fitting lines used for the determination of Weibull modulus ( $m$ ) and specific characteristic strength (reported values) are shown ( $F$  = failure probability)

Although EF-IE ( $1000 \text{ V cm}^{-1}$  and 10 min) is as efficient as the conventional strengthening at  $450 \text{ }^\circ\text{C}$  for 4 h, the strength of samples became more scattered. The scattering can be related to the inhomogeneous distribution of the compressive stress across the glass. The generated compressive stress is larger than conventional strengthening (Figure III-44); furthermore, its depth is probably following the depth of exchange layer (Figure III-28). One may note that when a very deep ion exchange

layer is produced on outer surface of glass, the tensile stress generated in the inner surface can cause the failure of samples.

The samples treated by producing exchanged layers on both sides show more scattered strength than the single EF-IE samples. However, the characteristic strength of these samples is increased by EF-IE. The scattered strength is likely related to the manual treatment and variations of treatment condition. The chemical corrosion of samples, in particular by the salts anions, may account for the possible crack growth below the critical tensile stress [57]; understanding this phenomena requires more studies.

### **3.2.5 Summary and further studies**

Potassium exchange for sodium by electric field assisted ion exchange (EF-IE) generates strong compressive stress in the surface of borosilicate glasses. Applying an electric field decreases the required time for producing an exchanged layer that can cover the surface flaws of glass; therefore, EF-IE augments the glass strength. The E-field intensity plays a vital role in EF-IE by influencing the mobility of ions and the glass structure. Applying an E-field stronger than  $1000 \text{ V cm}^{-1}$  speeds up the potassium penetration into the glass and a deep compressive layer can be produced in the glass. However, the inhomogeneous distribution of stress in samples is an impediment to using EF-IE as a strengthening method.

By changing the E-field polarisation, the exchanged layer can be produced on the both sides of glass; when the polarisation is reversed a few sites in the exchanged layer are used for the penetration of sodium and, hence, most of the compressive stress generated by the stuffing of ions remains on the surface. Therefore, it is possible to use electric field assisted ion exchange for strengthening of flat glasses; however, implementing this technique requires more studies.



### 3.3 Chemical strengthening of flat borosilicate glass

This section investigates the influence of potassium for sodium exchange on the final mechanical performance of thin borosilicate glass. Furthermore, some heat treatments like annealing before the ion exchange process and heat treatments after ion exchange are examined with the aim of improving the final performance.

The concentration of alkali elements, which are involved in the exchange process, was estimated first by X-Ray Fluorescence analysis (XRF). X-ray beam emitted from a Mo cathode by the accelerating voltage of 40 kV was used for the X-ray fluorescence excitations; the fluorescence radiation of sample was collected with a solid state detector (Amptek X123). The X-ray spectrum was collected in a 20-min time span, and afterwards the concentration of elements was estimated using the spectrum fitting experimental data according to the method reported by Lutterotti, L. et al [156]. Figure III-46 shows the collected X-ray spectra in 1.5 to 3.75 keV window and the fitting spectrum; the estimated concentration of potassium and silicon are summarised in Table 15. It should be noted that the used setup can not detect the concentration of sodium in the samples. The potassium exchange for sodium is important in chemical strengthening; hence, the relative concentration of alkali elements, sodium and potassium, was estimated by EDS.

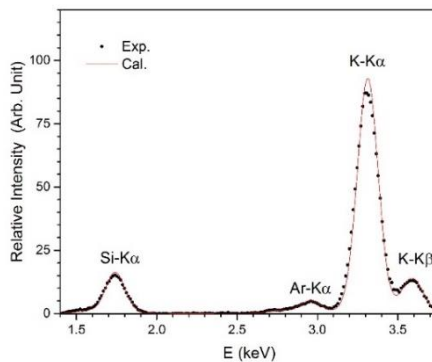


Figure III-46 XRF spectrum of the thin borosilicate glass, D263 Teco, in the spectrum within 1.5-3.7 keV window; Exp. : experimental data, Cal. Calculated

Table 15 Estimated concentration of potassium and silicon of thin glass estimated by fitting the XRF spectrum,

	Silicon	Potassium
Weight Ratio	0.393	0.464
Molar Ratio	0.057	0.095

### 3.3.1 Sodium-Potassium Ion Exchange

The surface chemical composition of thin glass was checked by EDS before and after immersing in the molten potassium nitrate bath at 375, 425 and 475°C for 4h. The relative molar concentration of sodium and potassium ( $Na/(Na+K)$  and  $K/(Na+K)$ ) are in Figure III-47. We see that sodium is replaced almost entirely with potassium on the surface of glass after immersing in the salt; however, the ratio varies slightly for the samples treated at different temperatures.

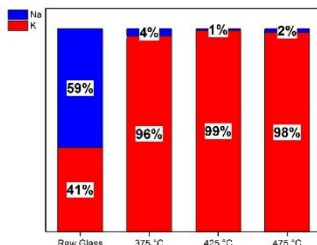


Figure III-47 Relative concentration of sodium and potassium, by considering the molar ratio, on the surface of thin borosilicate glass before and after immersing in molten potassium nitrate

The potassium concentration profiles near the surface of ion-exchanged samples, measured by EDS, are shown in Figure III-48. The chemical composition in the middle of each sample was considered as the baseline of concentration profiles; then, the noise of data was removed using a low pass filter, and afterwards the profiles were fitted using Eq. 1.12. The fitting lines are also shown in Figure III-48 to ease the comparison. The depth of layer extends to more than 40  $\mu\text{m}$  by subjecting to ion exchange at 475°C. The treatment at 425°C, which is a typical temperature for borosilicate glasses ( section 3.1.2 ), produces an exchanged layer thicker than typical flaws generated during processing [11, 13, 157, 158]. The inter-diffusion coefficient of K was estimated in samples via the concentration profiles; Figure III-49 shows the inter-diffusion coefficients in a linear coordination system ( logarithm of coefficient versus reciprocal temperature using Eq. 1.13). The activation energy of diffusion is estimated about 84  $\text{kJ mol}^{-1}$  by fitting the points with a linear function

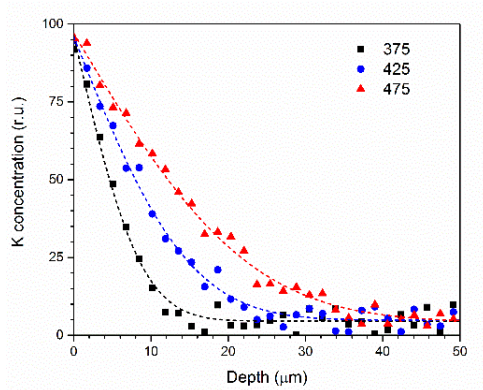


Figure III-48 Representative concentration profiles estimated from the measured line scans near the surface of thin borosilicate glass, subjected to ion exchange by immersing for 4 h in molten potassium nitrate

This value is slightly lower than the reported value for alkali borosilicate glasses (Figure III-35). The glass contains two alkali ions, sodium and potassium; therefore, the mixed alkali effect is probably responsible for the smaller activation energy for inter-diffusion of the ions [22, 52, 54, 137, 146].

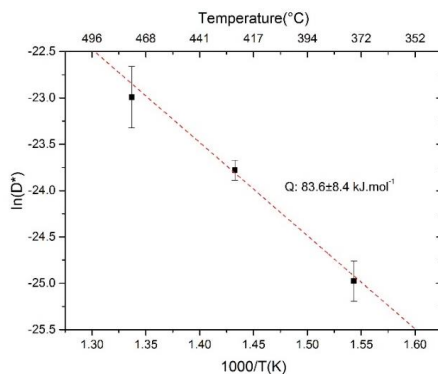


Figure III-49 Logarithm of the measured inter-diffusion coefficient,  $D$ , against the reciprocal temperature; the samples were immersed in molten potassium nitrate for 4 h.

Figure III-50 presents the surface compressive stress and its corresponding case depth, produced by subjecting to ion exchange for 4 h, as a function of the treatment temperature. The compressive stress, first, increases with increasing the temperature; then, it declines with the temperature increase. The stress generation in the glass is due to stuffing larger potassium ions into the smaller sites of sodium; the rate of ion exchange and, consequently, stuffing the ions increases when a higher temperature is used. The stress diminution is due to stress relaxation at high temperatures near  $T_g$ . Conversely, the case depth of stress extends continuously because of the increase of diffusion coefficient with temperature.

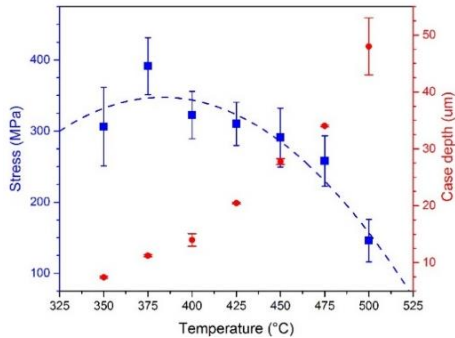


Figure III-50 Surface compressive stress and the corresponding case depth as function of the treatment temperature in the thin borosilicate glass

Figure III-51 shows the strength of samples using the Weibull distribution. Because of the thickness of samples, 200  $\mu\text{m}$ , the samples deformation during the ring-on-ring tests goes beyond the validity of linear elastic mechanics; therefore, the formulation is not applicable to measure the strength of samples. Using the failure load instead of the samples strength is, nonetheless, a reliable indicator of the strength of samples [7]. Moreover, we use the relative failure load to present the variations of strength in a clearer manner.

Potassium exchange for sodium augments the strength of samples. The glass becomes three times as strong the as-cut samples after Na/K ion exchange at 425°C for 4 h. We see that the strength of samples is smaller after being subjected to ion exchange at 475°C compared to the other treatment conditions. Figure III-50 revealed that the increase of case depth at 475°C is at the cost of compressive stress. One can conclude that the surface compression is not strong enough to “reinforce” the surface flaws even though it can cover most of the surface flaws.

Samples with the dimensions of  $150 \times 15 \times 0.2 \text{ mm}^3$  were also produced and subjected to chemical strengthening at  $425 \text{ }^\circ\text{C}$  for 4 h. These samples were tested by two-point bending configurations. The bending strength of samples was estimated around  $372 \pm 20 \text{ MPa}$ , which is substantially the same as the compressive stress present on the surface; whilst, raw samples broke during fixing between the fixture. Figure III-52 shows the fracture pattern of samples as cut and treated samples.

Ion exchange and, consequently, the presence of surface compression are responsible for the increase of the sample deflection before failure; as a result, the elastic energy becomes larger and crack branching occurs more during the failure [12, 159]. We see that the energy dissipation in the ion-exchanged sample produces a lot of bifurcated cracks, while branching rarely occurs in the as cut glass.

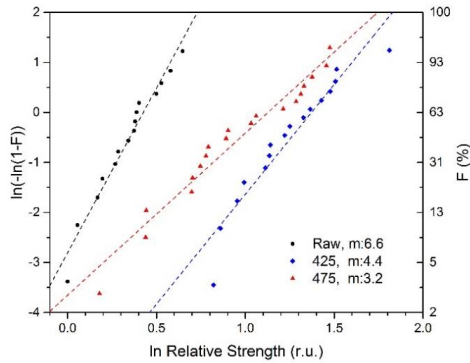


Figure III-51 Weibull distribution of the relative strength of as cut flat glass, and treated at  $425$  and  $475 \text{ }^\circ\text{C}$ .

The samples failure always started from the edge of the sample the cracks propagate across the glass. Figure III-53 shows the origin of crack propagation on the glass edge; the images were taken before the bending test.

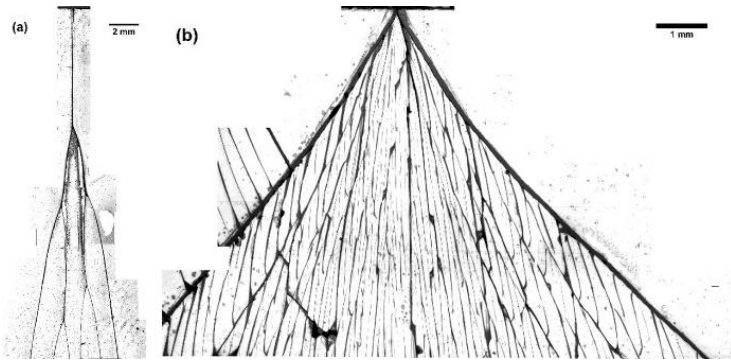


Figure III-52 Photographs of branching trees in (a) as-cut and (b) ion-exchanged glass at 425°C for 4h; Note the different magnification of images

Samples were produced by the scribe and bend technique; during scribing the glass, median cracks are formed on the surface and some “secondary median cracks” are also generated because of the fluctuations in the applied load of scribing. Although these cracks are “reinforced” by chemical strengthening, at a certain deformation the compressive stress at the crack tip is counterbalanced by the tensile stress due to deflection and the crack propagates. Therefore, the failure of all samples occur in a very narrow window of deformation, or stress. The samples were also subjected to dynamic fatigue tests under a bending load that varied between 0.7 to 0.9 of failure strain; interestingly, no failure in glass has been observed after 100000 cycles. This property is useful when the glass is going to be used in process such as roll-to-roll manufacturing.

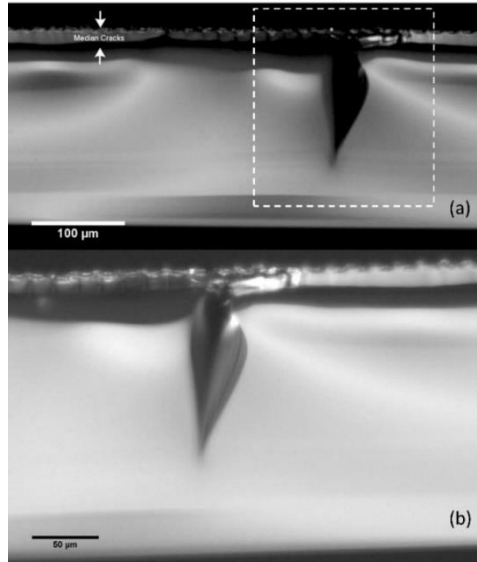


Figure III-53 Micrograph taken from thin borosilicate glass after cutting; median cracks form during the cutting process (a), in some locations some secondary the fluctuations of cutting load generates secondary median cracks.

The Vickers' indentation impressions produced on the raw glass and strengthened at 425°C for 4 h are shown in Figure III-54. Median/radial cracks are formed around the indentation imprint produced by 1.96 N on the as-cut glass (raw glass); by increasing the applied load, the cracks develop and expands in the sample. The lateral cracks are also formed beneath the surface and exhibit birefringence of light in the samples subjected to a load larger than 4.9 N.

We see that, the glass surface surrounding the Vickers' impression is crack free in the samples subjected to ion exchange. The presence of compressive stress in the surface is responsible for preventing the nucleation of median/radial and lateral cracks. However, we see that the shear faults are formed on the lateral faces of the imprint.

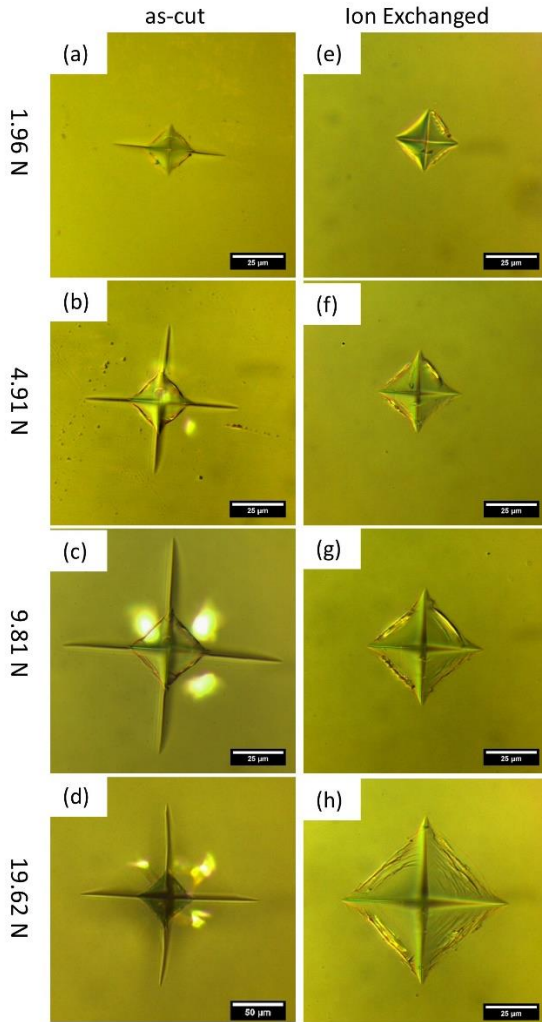


Figure III-54 Indentation imprints produced on as-cut and ion-exchanged glass; (a-d) as-cut sample; (e-h) ion-exchanged glass at 425°C for 4h; Indentations were produced by using load of (a and d): 1.96 N, (b & e): 4.91, (c & g): 9.81 and (d & h): 19.62 N; Note the different magnification of images

The invading indenter produces two types of stress on the surface: hydrostatic compression and shear stress [1, 97, 160-163]. The first one accounts for the densification of glass under load and the latter is responsible for the plastic deformation in the matter. By the penetration of a sharp indenter into the glass, the strain mismatch at the apex of invading pyramid produces the crack nucleus. The formation of shear faults changes the strain constraint; the produced faults are located in the compressive zone and, hence, the extension of such faults is not possible. Nonetheless, when the shear faults join, a median crack nucleus is generated from which the crack can extend. It is worthy to mention that because of the limited thickness of glass, the internal tensile stress is significant; therefore, stable crack growth occurs. We seldom observed such cracking in samples (it happened in less than one percent of indentations when using loads are larger than 29.43 N).

Stuffing of larger potassium ions into the smaller sodium sites causes dimensional swellings [164]; such dimensional changes may be adjusted by reduction of glass free volume [63, 73, 119]. One can expect that stuffing ions into a denser structure produces larger compressive stress and, therefore, results in more efficient chemical strengthening [165]. The glass structure and, hence, its free volume are influenced by the thermal history: annealing the glass before chemical strengthening changes the thermal history and might influence stress build up.

### **3.3.2 Effect of Annealing**

In this section, we investigate the influences of the annealing on the final strength of ion-exchanged glass. The Vickers' hardness of glass before and after annealing for 16 h at 425°C is shown in Figure III-55. Despite the significant overlap between the measured data ranges, there is an evident hardness increase after annealing if the mean values are considered. This, by and large, helps us compare the hardness variations. According to the Vickers' imprints produced by applying low loads, the hardness of glass is slightly increased after annealing, which is perhaps related to the variation of the elastic recovery of glass. The measured hardness of annealed glass is higher than the raw glass when it is measured by loads of 9.81 and 19.62 N. When the applied load is larger than 9.81 N, the produced cracks can be as long as the sample thickness; this probably changes the system compliance and influences the measurement (as shown in Figure III-56; the indentations were made by 9.81 N and 19.62 N).

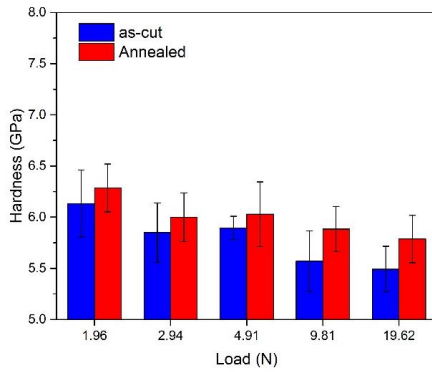


Figure III-55 Vickers' hardness measured on the surface of as-cut and annealed glass for 16 h at 425°C

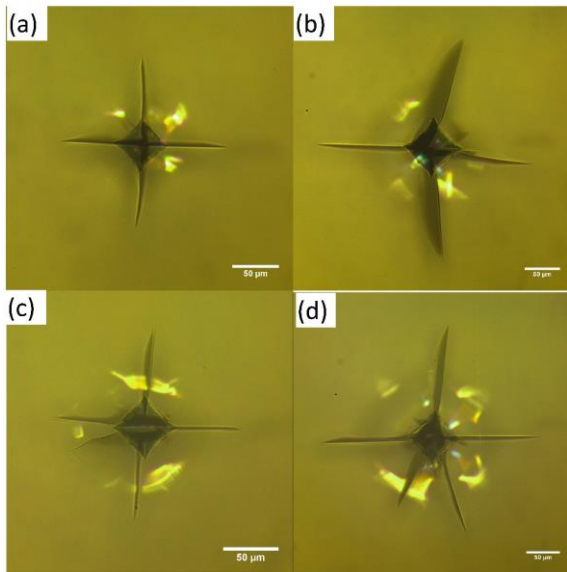


Figure III-56 Vickers impression on the surface of as-cut glass by using a load equal to (a) 9.81 N and (b) 19.62 N

Figure III-57 shows the length of cracks produced by the indentation as a function of applied load in a linear coordination using Eq. 3.1. The glass toughness is practically the same before and after annealing. It should be noted that the crack length corresponding the load of 19.62 N are excluded from the experimental data because of the crack length, as discussed before.

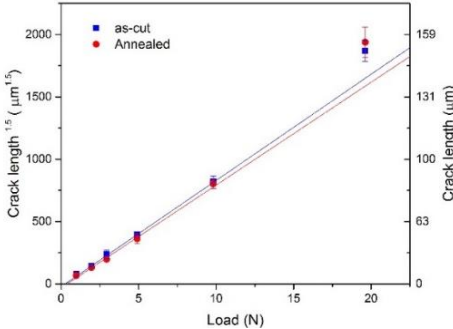


Figure III-57 Crack length as a function of the applied load in Vickers indentation on the surface of annealed and as cut glass.

Figure III-58 shows the heat flow and its derivative measured by DSC of as-cut and annealed glass. After the heat treatment for 16h at 425°C, the glass-transition temperature decreases slightly but significantly to a lower temperature.

It is mentioned before that the glass-transition temperature depends on the glass thermal history and the structure; therefore, the structural change is responsible for the glass-transition temperature decrease. If we assume that the glass has a positive thermal expansion coefficient<sup>4</sup>,  $7.2 \times 10^{-6} \text{ K}^{-1}$ , one can conclude that the volume of glass also decreases by subjecting to an elevated temperature below the transition temperature [70, 165].

The annealed samples were immersed in molten  $\text{KNO}_3$  at 425°C for 4 h. Table 16 summarises the compressive stress and the case depth in samples. The annealed

---

<sup>4</sup> The coefficient of thermal expansion is taken from the glass specification provided by Schott AG

samples show a slightly larger compressive stress on the surface compared to the raw glass subjected to ion exchange in the same conditions. The compressive stress increase can be explained by considering the analogy between the invasion of a sharp indenter to the surface and the penetration of a larger ions [1]. A sharp indenter strains glass against the surface and generates stress because of the elastic deformations of glass; then, the glass undergoes the plastic deformation after exceeding the yield strength. The stiffer glass network is probably responsible for the production of a larger compressive stress on the glass surface. The larger stress, produced by the denser glass structure, is confirming the reported results by Svenson et al. [165]. However, the dense structure of glass impedes the potassium penetration and, consequently, decreases the case depth.

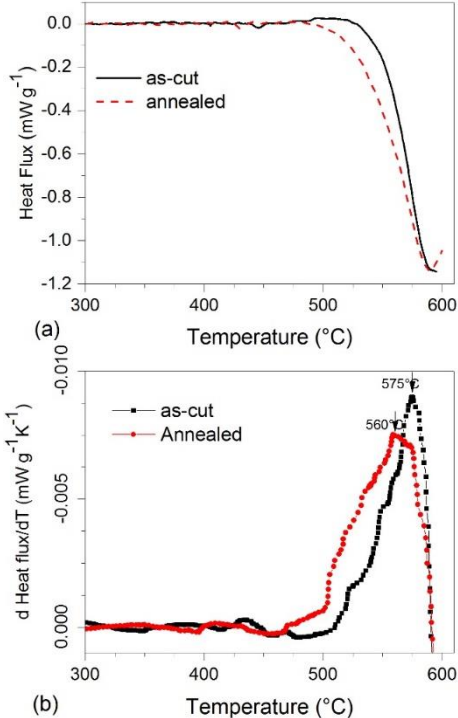


Figure III-58 Normalized heat flux and its derivative (from DSC analysis) against temperature for as-received and annealed glass for 16h at 425°C, (a) Heat flux curve, (b) the derivative of DSC curve.

Table 16 the compressive stress and the case depth produced on the surface of as-cut and annealed glass by ion exchange at 425°C for 4 h

	Compressive stress (MPa)	Case depth ( $\mu\text{m}$ )
<b>Ion Exchanged (IE)</b>	307(10)	20.5 (0.2)
<b>Annealed and Ion Exchanged</b>	331 (15)	16.9 (0.3)

Figure III-59 shows the hardness of glass after ion exchange in  $\text{KNO}_3$ . The glass hardness improves after ion exchange; we also see that the annealed glass shows a slightly larger hardness. As mentioned above, the increase of elastic modulus, which is a result of the denser structure, is probably responsible for the increase in elastic recovery and the hardness of glass.

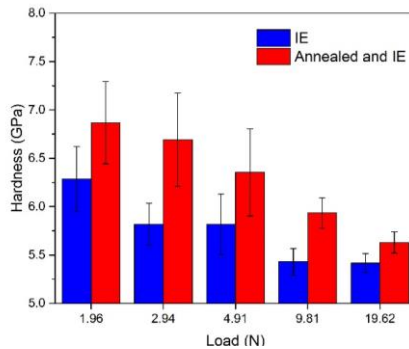


Figure III-59 Vickers' hardness measured on the surface of as-cut and annealed glass for 16 h at 425°C after subjecting to ion exchange in molten potassium nitrate.

The strength of annealed sample after the treatment at 425°C for 4 h is shown in Figure III-60 using Weibull distribution. The strength of both samples, ion exchange and annealed/ion-exchanged, is statistically identical (Kolmogorov-Smirnov test,  $P=0.63$ ). It is worth to mention that the annealed and IE samples is slightly more brittle than the IE glass. The annealing grows the hardness of glass while the toughness is practically constant; consequently, the brittleness (Hardness/toughness) increases. The larger brittleness makes the glass more prone to surface damages. From this perspective, the annealing is rather unhelpful for strengthening. One may note that the strength degradation of chemically strengthened glasses is rather more important than increasing the compressive stress build up on the surface [72]. The following part deals

with the relaxation of stress on the surface on the surface of the glass immersed in the molten potassium nitrate.

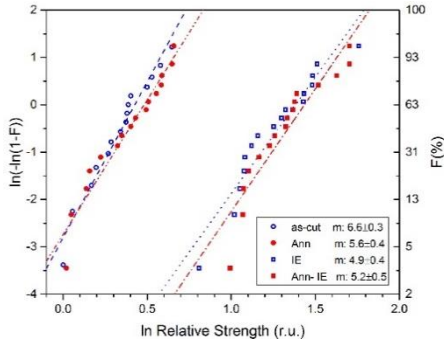


Figure III-60 Weibull distribution of the failure load for as-cut, Annealed (Ann), ion exchanged (IE) and annealed and ion-exchanged (Ann-IE) glass; the Weibull modulus (m) for each distribution is also shown.

### 3.3.3 Stress build up and relaxations

The produced compressive stress determines the final strength of ion-exchanged samples. Chemical strengthening is usually conducted by immersing glass in a molten salt bath at elevated temperatures below the glass-transition temperature; this also causes stress degradation because of the stress and structural relaxation [21, 66, 73].

The estimation of the compressive stress produced on the surface few minutes after the glass immersion in the salt bath is difficult. The experimental data is based on the birefringence of light in the glass; this usually occurs at a depth about 1-3  $\mu\text{m}$  beneath the surface [104, 105]; consequently, measuring the stress produced in the very first minutes of ion exchange is impossible. In this study, we use the stress relaxation trend in order to find the initial stress produced on the surface before the relaxations phenomena. Cut samples were immersed in a molten salt at a temperature between 400 to 450°C for a duration of 4-16 h; then, the compressive stress produced on the surface and its case depth were measured.

Figure III-61 shows the surface compressive stress measured by a stratorefractometer (section 2.3.2 ). The coordination is a linear coordination using the stretched exponential model (Eq. 1.29) :

$$\ln \sigma^R = \ln \sigma_0^R - \left(\frac{\tau}{t}\right)^Y \quad (3.8)$$

where  $\sigma^R$  and  $\sigma^{R_0}$  are the surface compressive stress and the zero time, or initial, compression, respectively;  $t$  and  $\tau$  being the time and the relaxation time, and  $\gamma$  is the stretching exponent [70, 77].

The stretched exponential model represents the stress relaxation (short-range relaxation) by  $\gamma = 3/5$ . Also, it represents the long-range structural relaxations in glass if  $\gamma = 3/7$  is used. The experimental data was fitted using both numbers to check the variations of the dominant relaxation process by changing the ion exchange temperature.

Figure III-61-a shows the experimental data and the fitting curves based on the stress relaxation on glass,  $\gamma = 3/5$ . Table 17 summarises the estimated parameters. The “zero-time stress” increases slightly by increasing the temperature. The generation of stress at zero time is dominantly governed by the stuffing of larger potassium ions into the glass; therefore, the zero-time stress increase is related to the increase in the amount of exchanged potassium in the glass surface; we reported before that the potassium exchange for sodium increases slightly with temperature and, consequently, the stuffing of ions improves a little bit (Figure III-47 and Figure III-50). However, the zero-time stress of samples treated at 450°C, which is significantly larger than the others, is more likely related to the generated error during the estimation because of the validity limit of the model. Nevertheless, by excluding the data corresponding samples treated at 450°C, one can assume that the “Zero-time Stress” in this glass equal to 330 MPa.

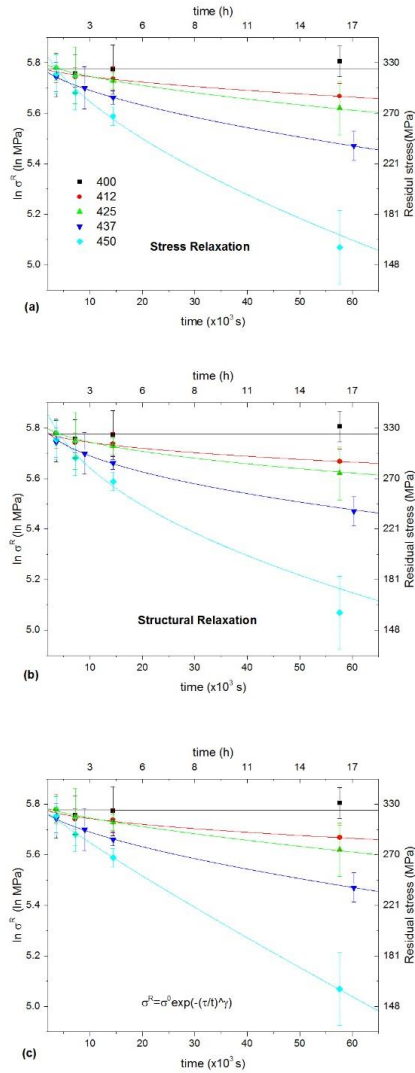


Figure III-61 Compressive stress generated on the surface of glass versus the treatment time; the experimental data was fitted by (a) stress relaxation model ( $\gamma= 3/5$ ), (b): structural relaxation ( $\gamma= 3/7$ ) and (c) by considering the “zero-time stress” equal to 330 MPa.

The relaxation time of samples treated at 400°C is 20 orders of magnitude longer than the rest of samples. At such temperature, the glass structure is stiff, and the structural modifications occur over a very long time; therefore, the influence of stress relaxation is hidden by the stress build-up.

Table 17 Zero time and relaxation time constant estimate by fitting the experimental data using  $\gamma=3/5$

Ion exchange temp. (°C)	Zero time stress (MPa)	$\tau$ (s)
400	323	$3.76 \times 10^{26}$
412	326	$1.99 \times 10^6$
425	335	$8.56 \times 10^5$
437	332	$3.75 \times 10^5$
450	376	$8.16 \times 10^4$

Figure III-61-b presents the surface stress data fitted by assuming the stress loss is due to the structural relaxations,  $\gamma = 3/7$ . The zero-time stress is slightly larger than the case of stress relaxation model with the relaxation times  $\tau$  of  $7.3 \times 10^4$  to  $5.4 \times 10^6$  s. The relaxation time due to the structural modifications is longer than the stress relaxation; therefore, one can conclude that the stress degradation on the surface is governed by the stress relaxation and the structural modifications have a minor role at lower temperatures, as expected.

The experimental data is also fitted with Eq. 3.8 and assuming the zero-time stress is the same for all temperatures, 330 MPa. Figure III-61-c shows the experimental data, and the fitting curves generated based on constant initial stress. The lines accommodate all points, especially, the data corresponding to 450 °C. Table 18 provides the stretching exponent corresponding to the fitted data presented in Figure III-61-c.

The exponent factor corresponding the samples treated at 400°C is zero, which represents stress build-up at such temperature as the dominant phenomenon. Though glass relaxation occurs at any temperature, the stress loss due to the relaxation is so slow, and in practice it is not possible to characterise ( Table 17). Increasing the temperature activates the relaxation mechanism and the stretching exponent becomes similar to the value attributed to the long-range relaxation,  $\gamma=0.43$ . At higher temperatures,  $\gamma$  becomes larger. Cation Induced Relaxation of Network (CIRON) may account for the long-range modification of glass at low temperatures [53, 54]. The structural relaxation occurs by breaking and forming new bridging oxygens to make

space for larger potassium ions diffusing into the glass [1]. This may occur by long-range changes in structure rather than changing the bonding angle of silicon-oxygen tetrahedra. By increasing the temperature, the Si-O network becomes less stiff which allows the bending of structural elements (Si-O tetrahedral units).

The stretching exponent of samples treated at 450°C is close to the upper limit of  $\gamma=1$ ; this representing a simple exponential decay of stress in glass due to the viscoelastic behaviour in which stress degradation is faster than stress build up because of stuffing potassium in glass.

Table 18 Stretched exponent of relaxation model,  $\gamma$ , and the corresponding standard error of fitting curves shown in Figure III-61-c

Temperature (°C)	Stretching exponent	
	$\gamma$	SE
400	0.0	0.1
412	0.5	0.1
425	0.7	0.2
437	0.6	0.1
450	0.9	0.0

A good fit to the viscoelastic properties of glass against temperature is obtained by using Vogel–Fulcher expression[70]:

$$\ln A = A_0 - \frac{B}{T-T_0} \quad (3.9)$$

where A is the property depending on temperature;  $A_0$ , B and  $T_0$  are constant, respectively. T is the absolute temperature. Figure III-62 shows the relaxation time as a function of reciprocal temperature. Considering the narrow temperature window of ion exchange process,  $T_0$  is considered zero to ease the measurements; furthermore, the temperature was normalised by the glass-transition temperature. The glass viscosity was measured using beam bending techniques, modified to fit the samples dimensions (Section 2.3 ). Figure III-63 shows the glass viscosity as a function of the normal reciprocal temperature ( $T_g/T$ ). If we consider the analogy between the relaxation time and viscosity behaviour, it is interesting to note the difference between the slope of the linear fits to the viscosity and relaxation data. Despite the rudimentary

means of measurement and approximation, the relaxation time is more dependent on the temperature than the viscosity. Although Burger's model has been reported to be successfully applied to creep and stress relaxation [71], using such models for the relaxation of ion-exchanged glasses, especially during the process, requires meticulous care.

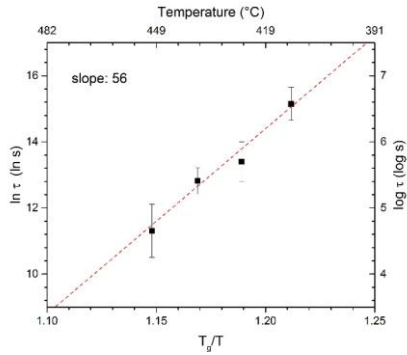


Figure III-62 Relaxation time as a function reciprocal normalised temperature using Vogel-Fulcher model

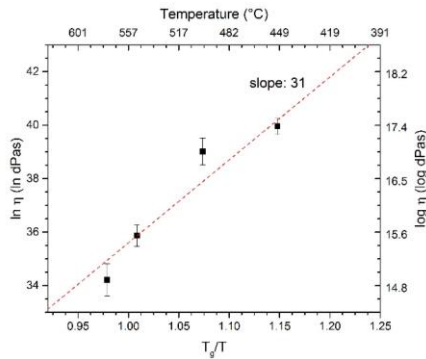


Figure III-63 Glass viscosity as a function reciprocal normalised temperature using Vogel-Fulcher model; Note: the second vertical scales are marked from the primary axis to ease the conversion to engineering scales.

It is of industrial interest to consider the degradation of the strengthened glass when it is subjected to elevated temperatures during application in techniques like roll-to-roll processes. Figure III-64-a shows the compressive stress of ion-exchanged samples at 425°C for 4h, and afterwards kept at 350°C for several minutes. The compressive stress declines very fast, and the relaxation follows simple exponential decay; moreover, the case depth of stress increases. The improvement of case depth is due to the diffusion of potassium inward the glass from the surface; consequently, the concentration of stuffed ions on the surface decreases and the surface compression declines.

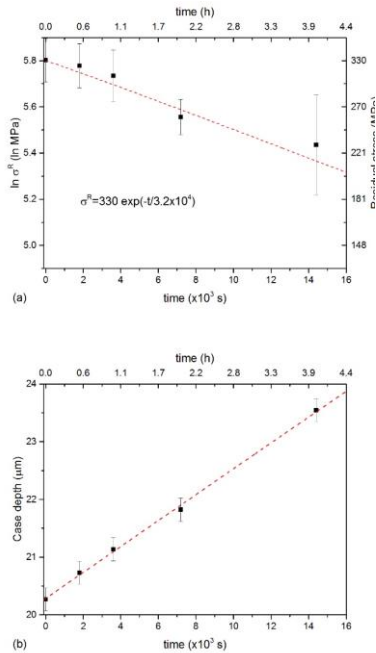


Figure III-64 (a) compressive stress on the surface of ion-exchanged glass at 425°C for 4h and kept at 350°C against time; (b) the corresponding case depth in samples

One last thing about the stress generation and relaxation on the surface of the thin glass is about the case depth of surface compression and the treatment time. Figure III-65 shows the case depth/the glass thickness of samples reported in Figure III-61 against the square root of time. As expected from Eq. 1.13 the case depth depends linearly on the square root of the time of treatment. As a technical point, it is worth to

note that the samples treated either by 400°C-16 h treatment or by 425°C-4 h treatment show a very similar compressive stress on the surface; one may expect that the final mechanical performance is also the same. Performing an ion exchange at a lower temperature for a longer time might be useful to avoid the effect of impurities like calcium on strengthening (as discussed in section 3.1.3 ).

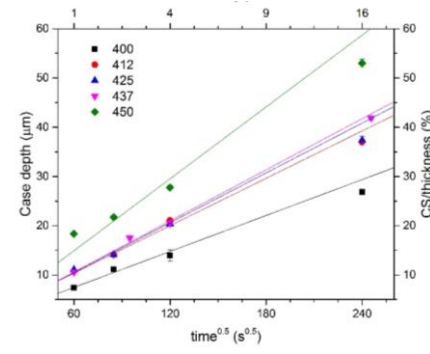


Figure III-65 case depth of compressive stress produced by ion exchange on the surface of thin borosilicate glass as a function of treatment time.

### 3.3.4 Influence of post-ion exchange heat treatment

Though chemical strengthening augments the mechanical resistance of glass, the strength becomes scattered and less reliable (Figure III-51). Several efforts have been made aimed to improve the reliability and decreasing the flaw sensibility of chemically strengthened glasses. Some of these methods are devoted to move the maximum of compressive stress from the surface inward the glass and making the contact damaging tolerable [4, 166-169]. However, the implementation of engineered stress in thin glass is difficult, especially when the thickness becomes less than 300 µm and the glass contains surface flaws [170, 171].

Stress relaxation can be exploited to improve the glass strength as well as its reliability [172-174]. Figure III-66 shows the compressive stress of thin glass treated at 500°C by immersing in the molten potassium nitrate. The annealing was carried out in the molten salt to prevent the decrease of surface compression because of the changes of surface composition. This method, also, improves the heating rate of glass surface.

The surface stress declines with subjecting to the heat treatment at 500°C; the relaxation time, in this case, is two orders of magnitude smaller than the samples subjected to the long ion exchange at 400-450°C.

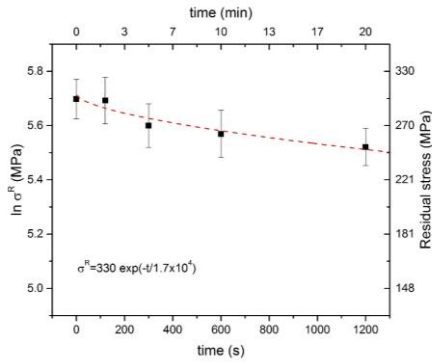


Figure III-66 Surface compress of samples ion exchanged at 425°C for 4h and heat-treated at 500°C

Figure III-67 shows the case depth of samples annealed at 500°C as a function of annealing time; as expected, the case depth of annealed glass is slightly deeper than the strengthened sample at 425°C by single-step ion exchange. The case depth increase is a linear function of square root of time, which is the typical behaviour of a diffusion-governed process like ion exchange.

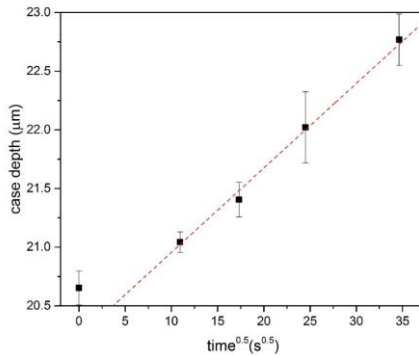


Figure III-67 case depth of compressive stress in samples heat-treated at 500°C

Figure III-68 compares potassium concentration profiles measured near the surface of heat treated samples. Because of the short treatment, the depth of layer in samples is almost the same and is similar to the depth of ion-exchanged samples at 425°C for 4h ( Figure III-48). However, the shape of potassium concentration profiles changes after annealing for 20 min. A layer with a constant concentration of potassium is formed beneath the surface, this is related to the fast penetration of potassium into the glass.

The relaxation rate at the surface increases with increasing the temperature; besides, the relaxation is faster at the surface of glass. One may note that the heat treatments at 500°C are probably responsible for the decline of compressive stress near the surface and, consequently, the formation of a maximum in stress profile at a certain distance from the glass surface. The hardness of sample measured by 0.98 N load is presented in Figure III-69. The heat treatment is clearly responsible for the decrease in hardness of glass which is, perhaps, related to the change in the local structure of glass and, consequently, the elastic recovery during unloading. The annealed glass is subjected to high temperatures and, therefore, its structure becomes similar to the structure of an as-melt glass with equivalent composition (the relaxed structure, CEAM glass). The hardness of silicate glasses decreases with increasing the atomic number of alkali ions; consequently, the hardness of ion-exchanged samples decreases when the surface layer is stress-free [175].

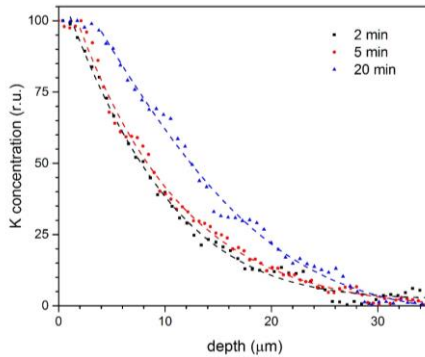


Figure III-68 Potassium concentration profiles measured near the surface of thin glass ion exchanged at 425°C for 4h and afterwards heat-treated at 500°C

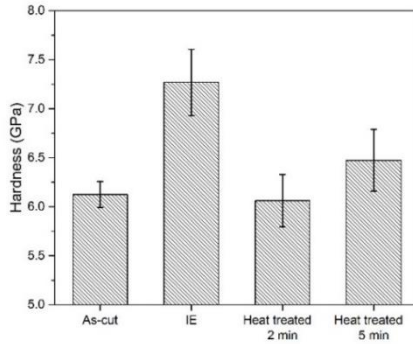


Figure III-69 Vickers' hardness of samples heat-treated at 500°C after subjecting to ion exchange at 425°C for 4h; the indentations were performed by using load =0.98 N, dwelling time= 15 s.

The bending strength of samples treated by ion exchange and heat treatment is presented in Figure III-70 using Weibull plots. The strength of ion-exchanged glass decreases by heat treatment at 500 °C for 2, 5 and 20 min.

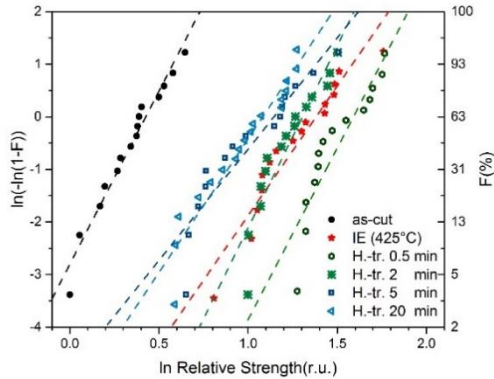


Figure III-70 Bending strength of thin glass ion exchanged (425°C-4h) and annealed at 500°C

The failure load corresponding the failure probability of 63 % is considered as the characteristic strength, CS, of samples. The ratio of the characteristic strength of treated samples to the ion raw glass,  $CS_{treated}/CS_{Raw}$ , is used in order to assess the

influence of the treatment time on the final strength of samples. Table 19 summarises the characteristic strength ratios and Weibull modulus.

The samples treated for 5 and 20 min shows similar strength and Weibull modulus, which is also expected from the concentration profiles reported in Figure III-68. Exposing to the elevated temperature, near the glass-transition temperature, causes stress relaxation which deteriorates the glass strength.

Table 19 Weibull modulus and Relative characteristic strength of heat-treated and ion-exchanged glass

	Weibull modulus		Relative characteristic Strength	
	Value	SD	Value	SD
<b>Raw Glass</b>	6.6	0.3	1.0	0.0
<b>IE at 425°C , 4h</b>	4.9	0.4	2.6	0.4
<b>IE and Ann. 30s</b>	6.5	0.8	3.2	1.1
<b>IE and Ann. 2 min</b>	6.9	0.7	2.4	0.5
<b>IE and Ann. 5 min</b>	4.2	0.5	2.1	0.4
<b>IE and Ann. 20 min</b>	5.1	0.4	1.9	0.2

The heat treatment for 2 min increases the Weibull modulus; however, the characteristic strength is not compromised. The limited relaxation on the glass surface may account for the improvement of the Weibull modulus by generating a maximum stress beneath the glass surface which is in agreement with the mentioned behaviour elsewhere [21].

The samples immersed for 0.5 min (30 s) in the molten potassium nitrate at 500°C show a relatively larger characteristic strength and Weibull modulus. The samples were directly immersed in the molten salt from room temperature; therefore, the salt solidified and melted in very few seconds after the immersion. As the treatment temperature is close to the glass-transition temperature, the surface of glass experiences the structural relaxations and the glass structure becomes more similar to the CEAM structure. However, due to the limited time, the relaxed layer is limited to few microns. A schematic draw of the relaxed layer formed on the surface of ion-exchanged glass is illustrated by Figure III-71.

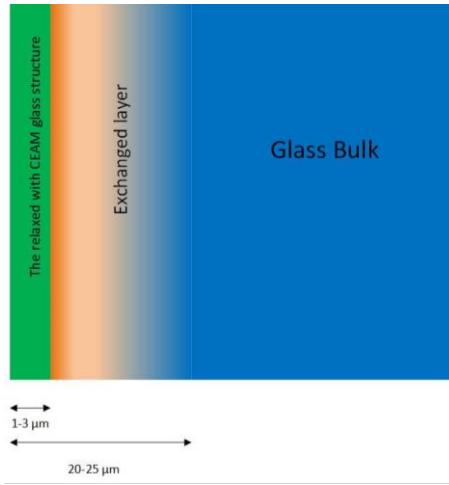


Figure III-71 Schematic of the formation of relaxed glass with CEAM structure on the surface of ion exchanged samples

The molar volume of CEAM glass is larger than the raw glass or ion exchanged [17, 63, 73]. Therefore, the very first layers of glass undergo the compression by stress build up due to the volume and thermal expansion mismatch between the layers; this can reinforce some of surface cracks and improve the mechanical resistance. We can estimate the compressive stress on the surface by considering the analogy to stress build up in enamels. The biaxial compressive stress,  $\sigma$ , in the surface layer due to the volume mismatch is given by:

$$\sigma = \frac{E}{1-\nu} \left( \frac{1}{3} \cdot \frac{\Delta V}{V_0} \right) \quad (3.10)$$

where  $E$  and  $\nu$  are elastic modulus and Poisson ratio, respectively.  $V_0$  is the molar volume of ion-exchanged glass, and  $\Delta V$  being the molar volume difference of ion exchange with CEAM structure and as ion exchange glass [63]. The compressive stress is estimated about 700 MPa which is twice as large as the surface compression produced by ion exchange. This method can improve the mechanical performance of thin glasses; however, implementing designed stressed profiles is not straightforward and requires more studies. One last point about the influence of the relaxation is that the short treatment can relax the stress in the vicinity of the crack tip and make the crack less influential.

### **3.3.5 Summary**

Ion exchange was conducted in order to improve the mechanical performance of thin borosilicate glass; it augments the glass strength and improves the damage resistance. The produced compression the surface by potassium exchange for sodium prevents the formation of median/radial cracks surrounding the Vickers indentations.

Although annealing prior to ion exchange densifies the glass and increases the surface compressive stress, it has no evident influence on the final bending strength. Conversely, heat treatment at 500 for 30 s improves the strength; this is probably related to a limited structural relaxation near the surface of glass. Such procedure can be exploited to improve the strength of thin ion-exchangeable glasses; however, it requires more studies.



## **Chapter IV. Conclusions**

This thesis investigated the potassium for sodium ion exchange in soda-borosilicate and alkali borosilicate glasses, especially those used in pharmaceutical packaging or thin flexible products, with the aim of improving the mechanical performance. It demonstrated that potassium/sodium exchange is a practical means of improving the strength of alkali borosilicate glass. This chapter summarises the key findings of this study, explains the key implications and comes up with suggestions for further studies.

### **4.1 Na/K exchange in soda borosilicate glass**

We first examined the feasibility of performing Na/K ion exchange in order to increase the strength of soda borosilicate glass. Afterwards, the influences of the treatment temperature, the glass composition, salts impurities and contaminations on the surface residual stress, the case depth of compression and the bending strength have been studied.

Potassium for sodium ion-exchange on the surface is responsible for the production of surface compression of  $350\pm 50$  MPa, which makes the glass twice as strong as untreated samples. It was found that the changes in the calcium oxide amount of glass affect the final case depth of exchanged layer; however, the impact of surface flaws is more dominant than the parameters like treatment temperature and sodium poisoning of salt. Conversely, a few amounts of calcium in the salt bath forestalls ion exchange and chemical strengthening. Calcium has an overwhelming influence on ion exchange due to the preferential absorption to the surface from the thermodynamics point of view.

### **4.2 Electric field assisted ion exchange of borosilicate glass**

Test tubes made from soda borosilicate glass were subjected to electric field assisted ion exchange in molten potassium nitrate, and the influences of the electric field intensity and its polarisation on the formation of concentration profiles near the glass surface were investigated.

Applying electric fields speeds up the Na/K ion exchange and produces thick chemical concentration profiles near the surface of the glass with a shape similar to a step

function. Electric field intensity plays a crucial role in the exchange of ions and the formation of concentration profiles. It determines the depth of ion-exchanged layer by affecting the structural modifications. Micro-Raman studies showed that the amount structural units of glass,  $Q_n$  species, are modified in a manner facilitating the movement of alkali ions, sodium and potassium, in the glass.

The energy favoured condition of electric current through the movement of charge carriers with the same diameter is probably responsible for the formation of potassium concentration profiles in the both sides of glasses subjected to the electric field assisted ion exchange by inverting the E-field polarisation or applying an AC E-field.

The compressive stress generated on the surface of soda borosilicate glass by electric field assisted ion exchange is significantly larger than the conventional ion exchange. The surface compression prevents the formation of median/radial cracks as well as lateral cracks during Vickers' indentations. Moreover, due to the geometry of studied samples, the inhomogeneous stress distribution of compressive stress can be neglected. It was found that the generated compressive stress by electric field assisted ion exchange augments the bending strength of glass if it is compared with the conventional ion exchange process regardless of the scattered strength of samples. The electric field assisted ion exchange is, surely, a practical step towards improving the mechanical performance of the borosilicate glass used in pharmaceutical packaging.

### **4.3 Chemical strengthening of thin alkali borosilicate glass**

Na-K ion exchange and chemical strengthening of alkali borosilicate glass were studied by checking the effect temperature on the replacement of sodium on the surface with potassium and the formation of compressive stress. Then, the enhancement of mechanical performance was considered by checking the bending strength and the fracture mechanics during Vickers' indentations. Afterwards, the stress and structural relaxations in glass have been studied and employed as a post-treatment step in order to increase the bending strength of ion-exchanged samples.

By conducting Na-K ion exchange at 425°C for 4h, a compressive stress of  $330 \pm 20$  MPa is generated on the surface; the surface compression has a depth about 20  $\mu\text{m}$  which can reinforce the surface flaws and increase the strength to three times as large as the untreated samples. The limited ion exchange at lower temperatures and stress

relaxation at higher temperatures account for the lack or the degradation of compressive stress on the surface and the consequent strength decline.

Samples treated by ion exchange show significantly high damage resistance to the formation of radial/median or lateral cracks during Vickers' indentation as a measure of the material vulnerability to damage: no cracks have been observed in the treated samples.

It was found that the densification of glass by annealing for 16 h at 425°C prior the ion exchange results in a small but apparent increase in the generated stress in the glass surface by ion exchange; however, no meaningful increase of bending strength was observed. The minute improvement of final strength in samples annealed before ion exchange made such treatments useless from the industrial standpoint.

The structural relaxation of glass is responsible for the surface compression degradation at elevated temperature and the relaxation in the glass surface occurs two orders of magnitude faster than the bulk glass, as expected. The expansion of ion-exchanged glasses by relaxation towards the structure of the compositionally equivalent as melt glass (CEAM) during a rapid heating and cooling can be used to make the surface residual stress larger. We demonstrated that the immersion of this glass for 30 s in a molten potassium nitrate at 500°C increases bending strength by 40 %.

#### **4.4 Implications and future research**

Sodium-potassium ion exchange is an appropriate and practical method for improving the bending strengthening of borosilicate glass used in pharmaceutical packaging because of the significant amount of soda in such products. The process can be easily implemented for the packaging products regarding their shape; furthermore, because of the minor influence of sodium poisoning on chemical strengthening, the salts used for chemical strengthening of soda lime silicate glasses can be exploited. Conversely, the calcium contamination is critical as it affects the chemical strengthening.

The chemically strengthened glass contains heavier alkali ions on the surface; therefore, the chemical durability of glass such as hydraulic resistance and possible reactions with the medicine is an issue which should be undergone scrutiny before using this treatment for applications like auto-injectors.

Despite the strong compressive stress produced by electric field assisted ion exchange on the surface of the borosilicate glass, which improves the damage resistance of glass, handling and cutting the final product requires meticulous care because of the imbalanced stress. Nevertheless, electric field assisted ion exchange strengthening is a promising approach to augment the strength of glass, especially the articles in packaging with a cylindrical shape.

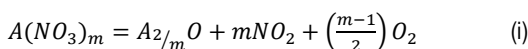
The governing mechanism for mass transfer changes when an E-field is applied. It seems that when an ion-exchanged layer contains two alkali ions, there is the split of current flow depending on the invading ions into the layer. Therefore, using AC E-fields is a good strategy aimed at producing balanced stress profiles in glass; however, understanding the glass corrosion in a nitrate salt under E-field is a must for implementing such a strengthening process.

Thin borosilicate glasses can be subjected to the very fast heating up and cooling down cycles; this makes it possible to exploit the glass structural relaxation at high temperature for enhancing the final mechanical performance of thin glasses treated by chemical strengthening. Still, several points such as the mechanism of relaxation, the distribution of the residual stress on the surface and damage and impact resistance of glass should be studied.

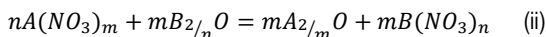
## Appendix I: Thermodynamics of molten salt

The exchange of sodium and potassium between the glass and the molten salt can be considered as a reaction in which the cations are swapped between the anion units such as oxide ( $O_2^-$ ) and nitrate ( $NO_3^-$ ). The decomposition of an alkali nitrate or alkali earth nitrate, yields alkali or alkali earth, cation attached to an oxide species, which is required for the exchange process. Despite the naïve assumptions of this paradigm, it can be employed to estimate whether slats cations remain in it or have a tendency towards exchange.

The reaction of a nitrate salt composed of " $A^{m+}$ " ions can be written as:



therefore, the reaction corresponding to the exchange of two cations,  $A^{m+}$  and  $B^{n+}$ , like sodium and calcium, can be considered as following:



Gibbs free energy of reaction (ii) can be calculated and considered as a measure for the replacement of cation in the salt and, consequently, ion exchange between the salt and glass. It should be noted that some of the nitrate salts, like calcium nitrate, decomposes at elevated temperatures, which must be considered for the estimation of the free energy of reactions. Nonetheless, most of the salts used in chemical strengthening are stable at the treatment temperature. In the following tables, the thermodynamic data of the decomposition of salts used in the research is summarised [176].

Table 20 Thermodynamic data of the decomposition of calcium nitrate

$Ca(NO_3)_2 = CaO + 2N_2O(g) + 1/2 O_2$			
T(K)	$\Delta H^\circ$ (kJ)	$\Delta S^\circ$ (J/K)	$\Delta G^\circ$ (kJ)
298.15	369.49	427.39	242.068
400.00	367.07	420.26	198.881
500.00	363.57	412.71	157.216
600.00	358.94	404.30	116.361
700.00	353.15	395.40	76.372
800.00	346.16	386.08	37.295
900.00	337.95	376.43	-0.833
1000.00	328.50	366.48	-37.918

Table 21 Thermodynamic data of the decomposition of caesium nitrate

$2\text{CsNO}_3 = \text{Cs}_2\text{O} + 2\text{N}_2\text{O}(\text{g}) + 1/2 \text{O}_2$			
T(K)	$\Delta\text{H}^\circ$ (kJ)	$\Delta\text{S}^\circ$ (J/K)	$\Delta\text{G}^\circ$ (kJ)
298.15	731.91	422.03	606.08
400.00	728.65	412.70	563.57
500.00	714.94	381.37	524.25
600.00	708.68	369.95	486.71
700.00	674.77	319.68	450.99
800.00	668.05	310.69	419.49
900.00	661.97	303.53	388.80
1000.00	656.50	297.76	358.74

Table 22 Thermodynamic data of the decomposition of potassium nitrate

$2\text{KNO}_3 = \text{K}_2\text{O} + 2\text{N}_2\text{O}(\text{g}) + 1/2 \text{O}_2$			
T(K)	$\Delta\text{H}^\circ$ (kJ)	$\Delta\text{S}^\circ$ (J/K)	$\Delta\text{G}^\circ$ (kJ)
298.15	693.95	418.52	569.17
400.00	690.38	408.31	527.06
500.00	674.22	369.54	489.45
600.00	669.04	360.07	453.00
700.00	644.73	320.58	420.32
800.00	640.19	314.52	388.58
900.00	636.17	309.77	357.37
1000.00	632.16	306.02	326.59

Table 23 Thermodynamic data of the decomposition of sodium nitrate

$2\text{NaNO}_3 = \text{Na}_2\text{O} + 2\text{N}_2\text{O}(\text{g}) + 1/2 \text{O}_2$			
T(K)	$\Delta\text{H}^\circ$ (kJ)	$\Delta\text{S}^\circ$ (J/K)	$\Delta\text{G}^\circ$ (kJ)
298.15	584.17	425.02	457.45
400.00	579.77	412.55	414.75
500.00	572.25	395.90	374.30
600.00	531.89	324.81	337.00
700.00	520.46	307.27	305.37
800.00	509.68	292.87	275.38
900.00	499.45	280.82	246.72
1000.00	489.72	270.56	219.16

# **Appendix II: Electric field assisted ion exchange in soda lime silicate glass**

**Part of this chapter has been published in:**

Ali Talimian, Gino Mariotto, Vincenzo M. Sglavo,

Electric Field Assisted Ion Exchange Strengthening of Borosilicate and Soda Lime Silicate Glass,

Int. J. App. Glass Sci. 2017; 00:1-10.

\*\*\*\*\*

The intention of this chapter is to demonstrate the feasibility of electric field assisted ion exchange on soda lime silicate glass. Potassium for sodium and caesium for sodium ion-exchange, the formation of chemical concentration profiles and stress build up by ion exchange are studied here.

## **I Introduction**

Soda lime silicate glass plays a vital role in the engineering applications, so several works are dedicated to the improvement of the mechanical strength of glass. Although many efforts have been made to study ion exchange with the aim of improving the mechanical performance of glass, chemically strengthened soda lime silicate glass is less commercialised and used in limited applications such as architectural designs or furniture, in practice. The limited case depth of glass and, therefore, damage vulnerability of the treated articles are the main drawback of ion exchange strengthening of soda lime silicate glass [1, 3, 7, 17, 20].

We demonstrated that by electric field assisted ion exchange strengthening, potassium concentration profiles with a large depth of layer can be produced in borosilicate glass (section 3.2 ). In this study, we investigate the influence of electric field assisted ion exchange for producing such profiles in soda lime silicate glass.

## II Material and method

Soda lime silicate (SLS, AR-Glas) glass tubes used in pharmaceutical packaging with an outer diameter of 9.8 mm and the wall thickness of 1 mm, bought from SCHOTT AG, were used in this part. The chemical composition and the glass-transition temperature of glass, measured according to the procedures given in section 2.3, are summarised in Table 24.

Table 24 Chemical composition and transition temperature of the glass tubes used in this work

	Chemical composition (wt%)								T <sub>g</sub> (°C)
	SiO <sub>2</sub>	B <sub>2</sub> O <sub>3</sub>	Al <sub>2</sub> O <sub>3</sub>	CaO	MgO	BaO	Na <sub>2</sub> O	K <sub>2</sub> O	
Soda lime silicate	69.0	1.0	4.0	5.0	3.0	2.0	13.0	3.0	525.0°C

The tubes were ultrasonically washed with water and acetone, and afterwards air dried at 105°C overnight. These test tubes had no rimmed end; therefore, tubes first grasped by alligator clips; then, they were immersed in the molten salt. Ion exchanges were conducted by the same procedure to the mentioned one in section 2.2.2. The E-fields were applied for 300s. Some samples were prepared by immersing in molten caesium nitrate salt ([Na]< 0.001 wt.% and T<sub>m</sub>=398.9 °C) at 465±15 °C. In order to avoid the thermal shock, the test tubes were kept over the salt bath for 20 min before and after ion exchange. Samples were characterised regarding the mechanical properties and the chemical composition as mentioned in section 2.3.

## III Results and discussion

### III.a K/Na exchange

The current density as a function of time for tubes subjected to E-field ion exchange in molten potassium nitrate is shown in Figure 0-1. The variation of current density is virtually similar to the borosilicate samples presented before in section 3.2.1. However, when a 1000 V.cm<sup>-1</sup> E-field is applied, the current density is equal to the applied current density limit (8 mA cm<sup>-2</sup>) for almost 60 s; then, it declines continuously with time. Interestingly, the current density passing through the samples is equal to the current density limit when the maximum applied field is 2000 V cm<sup>-1</sup>. The higher current density in soda lime silicate glass is related to the larger concentration of sodium, which is the charge carrier in glass (13 wt.% of Na<sub>2</sub>O vs. 7 wt.% in borosilicate).

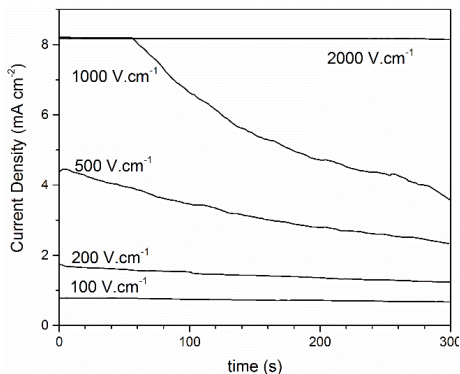


Figure 0-1 Current density against time in samples immersed in molten potassium nitrate and subjected to E-field varying between 100 to 3000  $\text{V cm}^{-1}$ . A current density limit equal to 8  $\text{mA cm}^{-2}$  is applied.

Figure 0-2 shows the potassium concentration profiles produced by E-field assisted ion exchange in soda lime silicate tubes. The concentration profiles are almost similar to borosilicate samples. It should be noted that the depth of exchanged layer is slightly smaller which is due to the limited time of ion exchange (300 s vs. 600 s). Nevertheless, the thickness of layers produced by applying  $1000 \text{ V cm}^{-1}$  is substantially similar to the depth of layer produced by conventional ion exchange at  $450^\circ\text{C}$  for 4h. There is a discrepancy between the actual depth of ion-exchanged layer in samples treated by applying  $2000 \text{ V cm}^{-1}$  measured by EDS line scans and the estimated values from the current density curve. Considering the fact that the glass used in this study consist both sodium and potassium, the penetration of potassium through the potassium site with a similar mechanism to the proposed on in Figure III-33 for the mass transfer might account for such a discrepancy in the depth of exchanged layer.

Figure 0-3 shows the diffusion coefficients of potassium estimated from the concentration profiles by fitting with Eq.1.21. As expected from the concentration of the alkali ions, sodium and potassium, the mobility and, consequently, the diffusion coefficient is large in soda lime silicate glass than the borosilicate test tubes.

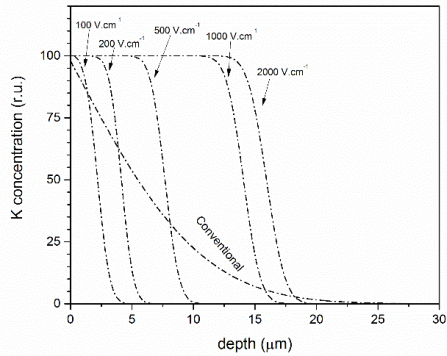


Figure 0-2 Relative potassium concentration profiles for tubes subjected to electric-field assisted ion exchange (EF-IE) at 400°C (Figure 0-1), and conventional ion exchange at 450°C for 4h

Moreover, by applying a certain E-field, the diffusion coefficient increases to a higher value. The threshold for the diffusion coefficient jump is clearly smaller in the case of soda-lime silicate glass, which is probably related to the different glass composition and structure.

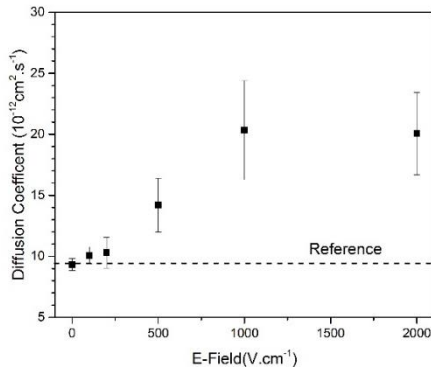


Figure 0-3 Apparent diffusion coefficient of potassium in the glass against the applied E-field

Figure 0-4 shows micro-Raman spectra collected on the soda lime silicate test tubes in the region between 200 and 1800  $\text{cm}^{-1}$ . The spectra involve three main regions containing peaks corresponding to silicon-oxygen bonds. The broad peak from 200 to 600  $\text{cm}^{-1}$  is mainly attributed to the bending/stretching of the Si-O-Si bond [145]; there

are three peaks at approximately 480, 570 and 630  $\text{cm}^{-1}$  assigned to the bending of  $Q_4$ ,  $Q_3$  and  $Q_2$  units, respectively [144, 145, 148]. The successive peak, located at 800  $\text{cm}^{-1}$ , is attributed to silicon vibrations in its tetrahedral cage with oxygen [75, 144, 148]. The last group of peaks appears between 850 and 1350  $\text{cm}^{-1}$  and is attributed to the scattering associated with vibrational stretching modes of  $Q_1$ ,  $Q_2$ ,  $Q_3$ , and  $Q_4$  species in silicate glasses [144, 146, 147, 150].

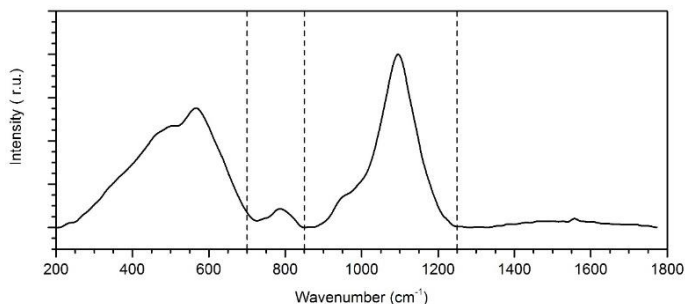


Figure 0-4 Micro-Raman spectrum collected from the raw soda lime silicate glass before EF-IE

Figure 0-5 shows the 850-1250  $\text{cm}^{-1}$  Raman band of the spectra measured on the samples treated under an electric field of 2000  $\text{V cm}^{-1}$ ; the spectra were recorded from the exchanged layer near the surface, and from the glass bulk which is far from the layer undergone ion exchange. The peak intensities were used as representative of the concentration of species in the glass and the amount of  $Q_n$  species was estimated according to the procedure described in section 3.2.3 ; the relative concentrations of species are summarised in Table 25.

The amount of  $Q_3$  species in ion-exchanged layer increases by around 10% and the concentration of  $Q_2$  and  $Q_4$  decreases by 5%. This change can be related to the structural modifications during the movement of ions, known as Cation Induced Relaxation of Network (CIRON), and hosting large potassium ions in sodium positions [53, 150]. This phenomenon is quite the same as the observed one in the case of borosilicate glasses.

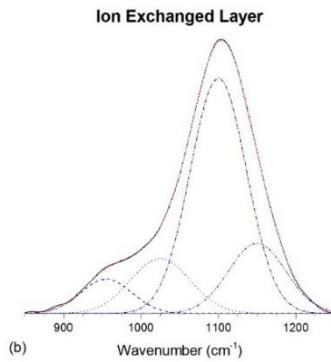
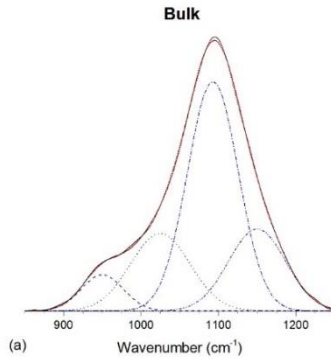


Figure 0-5 Micro-Raman spectra in the region of 850 to 1250  $\text{cm}^{-1}$  taken from the glass bulk and edge (EF-IE): Soda lime silicate glass; (a) bulk, (b) ion-exchanged layer

Table 25 Relative concentration of Q<sub>n</sub> species in glass estimated from Raman spectra in Figure 0-5; numbers between parentheses show the random error cumulated upon fitting

<b>Soda Borosilicate</b>		
	<b>Bulk</b>	<b>Edge</b>
<b>Q<sub>1</sub></b>	10.6(0.4)	8.4(0.8)
<b>Q<sub>2</sub></b>	29.9(0.9)	24.9(0.3)
<b>Q<sub>3</sub></b>	37.0(0.2)	44.6(0.1)
<b>Q<sub>4</sub></b>	22.5(0.4)	22.1(0.0)

### III.b Cs/Na exchange

The current density against time for the soda lime silicate samples subjected to EF-IE in molten caesium nitride are presented in Figure 0-6. The current density corresponding the samples subjected to the electric fields of 100 and 200  $\text{V cm}^{-1}$  is not reported because of the small values and the significant corresponding error. Interestingly, the current density curves are, overall, similar to the curves regarding the potassium exchange for sodium in glass. It should be mentioned that the penetration of caesium into the borosilicate samples are very limited and, in fact, no exchange happens with the same process; therefore, the corresponding data has is not reported.

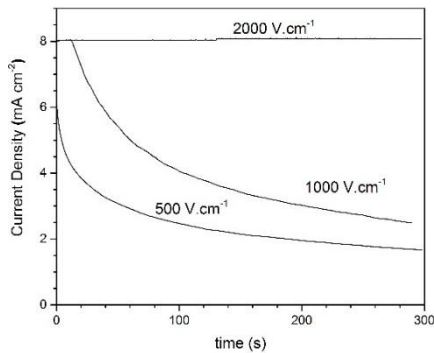


Figure 0-6 Current density against time in samples immersed in molten caesium nitrate and subjected to E-field varying between 100 to 3000  $\text{V cm}^{-1}$ . A current density limit equal to 8  $\text{mA cm}^{-2}$  is applied.

Figure 0-7 shows the X-ray spectrum collected by EDS analysis from the inner and outer surfaces of glass tubes treated by applying E-field of 500  $\text{V cm}^{-1}$ . Sodium and potassium are replaced with caesium in the surface. The measurements were conducted with an acceleration voltage of 20 kV and excitation of Cs-K $\alpha$  was not possible; therefore, the estimation of the concentration of elements was accompanied by a significant error and in practice impracticable. Nonetheless, the EDS analyses clearly show the exchange of potassium and sodium on the surface with caesium. One may note that the peaks attributed to calcium and barium are located near the adsorption edge of caesium [86, 89]; hence, the IE sample shows no significant peaks on corresponding those elements.

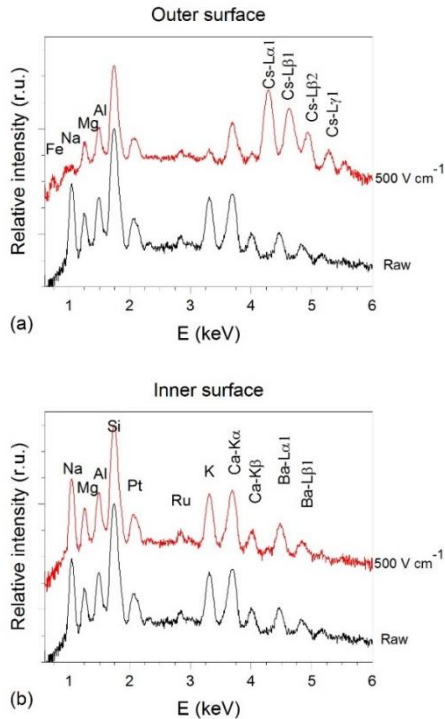


Figure 0-7 EDS spectra recorded on the outer and the inner surface of soda lime silicate glass tubes subjected to EF-IE in caesium nitrate containing. The spectrum corresponding the raw glass is shown for comparison; (a) outer surface, (b) inner surface

Caesium and potassium concentration profiles measured near the outer surface of tubes subjected to EF-IE are shown in Figure 0-8. Caesium concentration profiles resemble a shape similar to the profiles collected from the Na/K ion exchanges samples (Figure 0-2). The depth of exchanged layer is larger than the depth of layer in potassium exchanged layer; it is probably due to the higher temperature of treatment. One interesting point about these samples is that potassium is piled up in the end caesium rich layer. Potassium is less mobile compared to sodium and, therefore, the drift velocity of potassium ions under an electric field is smaller than sodium. When the glass is subjected to an E-field, the potassium layer must be moved for the penetration of caesium. Therefore, the formation of potassium and its movement inward the glass governs the ion exchange process; this is, perhaps,

responsible for the identical current density behaviour of caesium to potassium. However, further studies are required to understand how the potassium ions influence the penetration of caesium into the glass.

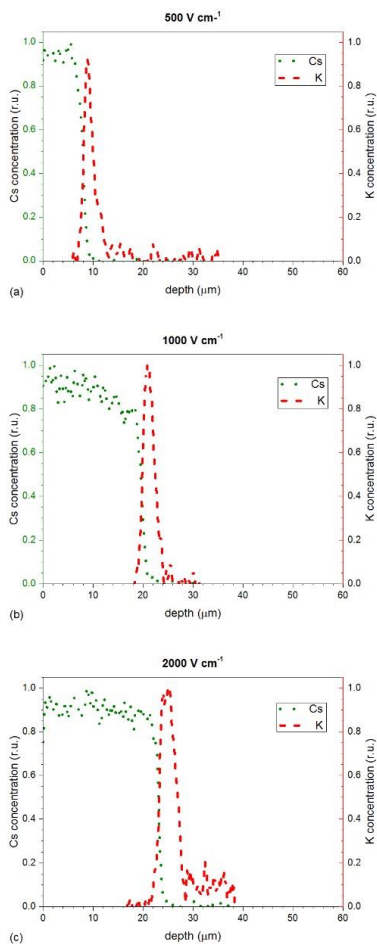


Figure 0-8 Relative caesium and potassium concentration profiles for tubes subjected to electric-field assisted ion exchange (EF-IE) in caesium nitrate at  $465^\circ\text{C}$ ; (a) E-field =  $500 \text{ V cm}^{-1}$ , (b) E-field= $1000 \text{ V cm}^{-1}$  and , (c) E-field= $2000 \text{ V cm}^{-1}$

### III.c Mechanical performance

Figure 0-9 shows typical micrographs of indentation imprints produced by Vickers's diamond with load of 19.62 N on raw soda lime silicate, ion exchanged at 450°C for 4h in potassium nitrate by conventional process, and subjected to EF-IE in potassium nitrate and caesium nitrate. The raw glass exhibits the radial/median cracks and lateral cracks which appeared from the light birefringence surrounding the impression. The conventional ion exchange is responsible for the limited extension of radial/median; furthermore, the produced compressive stress on the surface prevents the formation of lateral cracks. We see that no cracks are formed in the samples treated by EF-IE; this reveals the presence of a strong compressive stress on the surface which is produced by EF-IE.

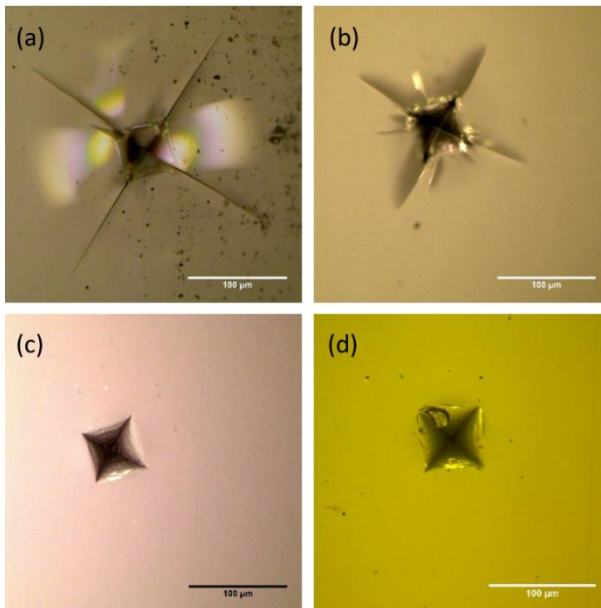


Figure 0-9 Vickers indentations, (19.61 N) on the soda lime silicate glass tubes: (a) Raw tubes, (b) conventional ion exchange; EF-IF under 2000 V. cm<sup>-1</sup> in (c) potassium nitrate and (d) caesium nitrate

The compressive stress on the surface of samples are estimated from the LOAD-DISPLACEMENT curves recorded during the indentation of samples with a maximum

load of 500 mN. The compressive stress in the samples at a depth of 1-2  $\mu\text{m}$  from the surface is shown in Figure 0-10.

Potassium for sodium ion-exchange conducted by conventional ion exchange produces a compressive stress about 500 MPa in samples; conversely, when EF-IE is carried out, the compressive stress improves to about 800 MPa. The limited time of ion exchange and the lower temperature compared to the conventional ion exchange prevents the stress loss because of relaxation and, therefore, the residual compressive on the surface of EF-IE samples is larger than the conventional ion exchange [73].

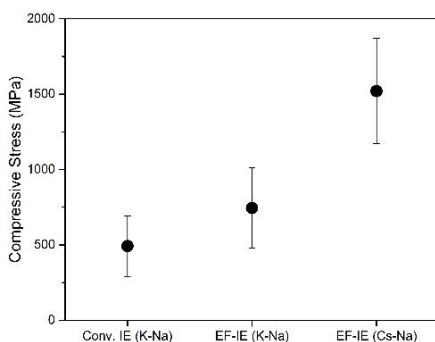


Figure 0-10 Estimated compressive stress on the surface of tubes using the LOAD-DISPLACEMENT curves of Vickers' indentation

Stuffing the larger caesium ions in the glass produces a higher compressive stress on the surface, about 1.5 GPa, compared to potassium-sodium exchange. The compressive stress generated in samples is significantly less than the estimated stress from Eq. 1.28. The discrepancy between the predicted stress and the practical value is related to the problems in measuring LNDC of glass. It is worth to mention that when the silicate glass network undergoes compression (such as compressive stress build up due to the stuffing of ions), at a certain pressure, the glass densifies and no more stress is generated. The elastic limit for soda lime silicate glass at room temperature is reported about 7 GPa [150, 177]; we expect that the elevated temperature at which the EF-IE is carried out decreases the densification threshold and stuffing of caesium caused densification of the silicate structure.

Figure 0-11 shows the bending strength of test tubes treated by ion exchange. Conventional ion exchange augments the strength of samples. To our astonishment, the strength of samples is not improved by electric field assisted ion exchange despite the enormous compressive stress on the surface. The surface of test tubes contains large flaws that can hinder the influence of the presence of compressive stress on the surface.

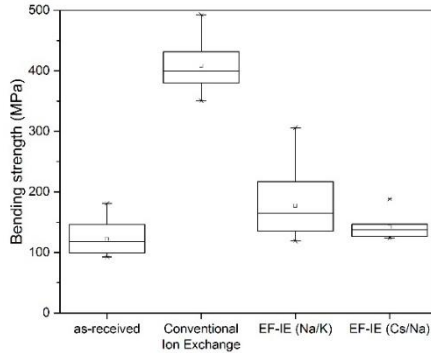


Figure 0-11 Bending strength soda lime silicate glass tubes subjected to ion exchange treatments in different conditions; mean value, 25th and 75th percentiles, maximum and minimum values are shown.

Figure 0-12 shows a typical fracture origin in test tubes treated by electric field assisted ion exchange (Cs/Na exchange). The fracture started from a surface defect that extends to about 100  $\mu\text{m}$  which is considerably deeper than the depth of exchanged layer produced by EF-IE; therefore, the defect front is located in the tensile stress zone. If we assume that the stress profile follows the chemical concentration profiles, we can roughly estimate the balancing tensile stress of samples. By considering the surface compression and its depth about 1.5 GPa and 50  $\mu\text{m}$ , respectively; the balancing tensile stress distributed across the sample (1000  $\mu\text{m}$ ) is about 70 MPa which is significantly larger than the stress reported for the conventional ion exchange. More studies are needed to investigate the influence of the large and inhomogeneous compressive stress produced by caesium exchange for sodium in soda lime silicate glass.

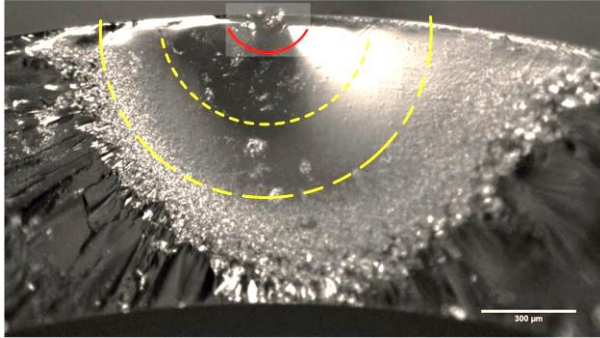


Figure 0-12 Typical fracture origin in treated samples with EF-IE; the surface flows are contaminated by a large substrate

#### IV Conclusions

Electric field assisted ion exchange, EF-IE, accelerates the Na/K exchange in soda-lime silicate glass. It produces step-like profiles with a case depth comparable with a conventional ion exchange at 450°C for 4h. The structural evolution of soda lime silicate glass during EF-IE can be described by the theory of cation induced relaxation of network, CIRON.

Electric field assisted ion exchange is also an effective technique for caesium exchange for sodium. Stuffing caesium in alkali sites of soda lime silicate glass generates a titanic compression stress compared to the conventional ion exchange strengthening.



## References

- [1] Varshneya, A.K., *Chemical Strengthening of Glass: Lessons Learned and Yet To Be Learned*. Int. J. Appl. Glass. Sci., **2010**. 1(2): p. 131-142.
- [2] Karlsson, S., B. Jonson, C. Stalhandske, *The technology of chemical glass strengthening - a review*. Glass Technology-European Journal of Glass Science and Technology Part A, **2010**. 51(2): p. 41-54.
- [3] Gy, R., *Ion exchange for glass strengthening*. Materials Science and Engineering: B, **2008**. 149(2): p. 159-165.
- [4] Green, D.J., *Recent Developments in Chemically Strengthened Glasses*. in: 64th Conference on Glass Problems: Ceramic Engineering and Science Proceedings, John Wiley & Sons, Inc., **2008**, p. 253-266.
- [5] Vincenzo, M.S., L. Luca, J.G. David, *Flaw-Insensitive Ion-Exchanged Glass: I, Theoretical Aspects*. J. Am. Ceram. Soc., **2004**. 84: p.
- [6] Bousbaa, C., A. Madjoubi, M. Hamidouche, N. Bouaouadja, *Effect of annealing and chemical strengthening on soda lime glass erosion wear by sand blasting*. J. Eur. Ceram. Soc., **2003**. 23(2): p. 331-343.
- [7] Varshneya, A.K., *Fundamentals of Inorganic Glasses*. Society of Glass Technology, **2006**.
- [8] Green, D.J., *An Introduction to the Mechanical Properties of Ceramics*. Cambridge University Press, **1998**.
- [9] Wachtman, J.B., W.R. Cannon, M.J. Matthewson, *Mechanical Properties of Ceramics*. John Wiley & Sons, Hoboken, New Jersey, United States, **2009**.
- [10] Sglavo, V.M., *Testing of Ceramics and Glasses by Indentation Techniques*. in: Ceramics – Processing, Reliability, Tribology and Wear, Wiley-VCH Verlag GmbH & Co. KGaA, **2006**, p. 365-377.
- [11] Bradt, R.C., R.E. Tressler, *Fractography of Glass*. Springer US, **2013**.
- [12] Freiman, S., J.J. Mecholsky, *The Fracture of Brittle Materials: Testing and Analysis*. Wiley, **2012**.

- [13] Bradt, R.C., *The fractography and crack patterns of broken glass*. Journal of failure analysis and prevention, **2011**.): p.
- [14] Kurkjian, C.R., P.K. Gupta, R.K. Brow, *The Strength of Silicate Glasses: What Do We Know, What Do We Need to Know?* Int. J. Appl. Glass. Sci., **2010**. 1(1): p. 27-37.
- [15] Kurkjian, C., *Mechanical Strength of Glasses-Studies Then and Now*. Glass Researcher, **2002**. 11: p. 1-6.
- [16] Shelby, J.E., *Introduction to Glass Science and Technology*. Royal Society of Chemistry, **2005**.
- [17] Varshneya, A.K., *The physics of chemical strengthening of glass: Room for a new view*. J. Non-Cryst. Solids, **2010**. 356(44-49): p. 2289-2294.
- [18] Kingery, W.D., *Introduction to Ceramics*. John Wiley & Sons, Incorporated, **2013**.
- [19] Karlsson, S., *Modification of Float Glass Surfaces by Ion Exchnage*. in: School of School of Engineering, Linnaeus University Kallered, pp. 176.
- [20] Varshneya, A.K., P.K. Kreski, *The chemistry of chemical strengthening of glass*. in: Ceram. Trans., **2012**, pp. 107-114.
- [21] Tyagi, V., A. Varshneya, *Measurement of progressive stress buildup during ion exchange in alkali aluminosilicate glass*. J. Non-Cryst. Solids, **1998**. 238(3): p. 186-192.
- [22] Varshneya, A.K., M.E. Milberg, *Ion Exchange in Sodium Borosilicate Glasses*. J. Am. Ceram. Soc., **1974**. 57(4): p. 165-169.
- [23] Doyle, P., *Recent developments in the production of stronger glass containers*. Packaging Technology and Science, **1988**. 1(1): p. 47-53.
- [24] Puche-Roig, A., V.P. Martin, S. Murcia-Mascaros, R.I. Puchades, *Float glass colouring by ion exchange*. J. Cult. Herit., **2008**. 9: p. E129-E133.
- [25] Mazzoldi, P., S. Carturan, A. Quaranta, C. Sada, V.M. Sglavo, *Ion exchange process: History, evolution and applications*. Rivista Del Nuovo Cimento, **2013**. 36(9): p. 397-460.
- [26] Mochel, E., *Alkali aluminosilicate glass article having an ion-exchanged surface layer*. in, Google Patents, **1974**.

- [27] Rinehart, D.W., *Chemical strengthening of glass*. in, Google Patents, **1977**.
- [28] Watanabe, M., *Chemical method of strengthening glass articles subjected to abrasion resistance treatment*. in, Google Patents, **1977**.
- [29] E, K.R., S.A. E, *Strengthening glass by multiple alkali ion exchange*. in, Google Patents, **1969**.
- [30] J, H., I. T, O. N, *Double ion exchange method for strengthening glass articles*. in, Google Patents, **1974**.
- [31] Varshneya, A.K., I.M. Spinelli, *High-strength, large-case-depth chemically strengthened lithium aluminosilicate glass*. Am. Ceram. Soc. Bull., **2009**. 88(5): p. 27-33.
- [32] Doremus, R.H., *Glass science*. John Wiley & Sons, Hoboken, New Jersey, United States, **1994**.
- [33] Robert, H.D., *Mechanism of electrical polarization of silica glass*. Appl. Phys. Lett., **2005**. 87: p.
- [34] Mehrer, H., *Diffusion in Solids: Fundamentals, Methods, Materials, Diffusion-Controlled Processes*. Springer Berlin Heidelberg, **2007**.
- [35] Shewmon, P., *Diffusion in Solids*. Wiley, **1991**.
- [36] Bird, R.B., W.E. Stewart, E.N. Lightfoot, *Transport Phenomena*. Wiley, **2007**.
- [37] Gaskell, D.R., *An Introduction to Transport Phenomena in Materials Engineering*. Macmillan Publishing Company, **1992**.
- [38] Xinwei, W., D. Rüdiger, *Sodium tracer diffusion in a sodium aluminosilicate glass*. J. Non-Cryst. Solids, **2011**. 357: p.
- [39] Xinwei, W., K.V. Arun, D. Rüdiger, *Sodium tracer diffusion in glasses of the type  $(Na_2O)_{0.2}(B_2O_3)_y(SiO_2)_{0.8-y}$* . J. Non-Cryst. Solids, **2011**. 357: p.
- [40] Hattori, Y., T. Wakasugi, H. Shiomi, J. Nishii, K. Kadono, *Li<sup>+</sup> for Na<sup>+</sup> ion-exchange-induced phase separation in borosilicate glass*. J. Mater. Res., **2012**. 27(07): p. 999-1005.

- [41] Tervonen, A., B. R. West, S. Honkanen, *Ion-exchanged glass waveguide technology: a review*. Optical Engineering, **2011**. 50(7): p. 71107.
- [42] Qing, D., K. Itoh, M. Murabayashi, *Fabrication of Spot Size Converters for Optical Chemical Sensors by Distributed-Field-Assisted Ion-Exchange*. Optical Review, **1996**): p.
- [43] Ramaswamy, R.V., R. Srivastava, *Ion-exchanged glass waveguides: a review*. J. Lightwave Technol., **1988**. 6: p.
- [44] Findakly, T., *Glass waveguides by ion exchange: a review*. Optical engineering, **1985**): p.
- [45] Araujo, R., *Thermodynamics of ion exchange*. J. Non-Cryst. Solids, **2004**. 349: p. 230-233.
- [46] Fu, A.I., J.C. Mauro, *Mutual diffusivity, network dilation, and salt bath poisoning effects in ion-exchanged glass*. J. Non-Cryst. Solids, **2013**. 363: p. 199-204.
- [47] Garfinkel, H.M., *Ion-exchange equilibriums between glass and molten salts*. The Journal of Physical Chemistry, **1968**. 72(12): p. 4175-4181.
- [48] Araujo, R.J., S. Likitvanichkul, Y. Thibault, D.C. Allan, *Ion exchange equilibria between glass and molten salts*. J. Non-Cryst. Solids, **2003**. 318(3): p. 262-267.
- [49] Araujo, R., *Interdiffusion in a one-dimensional interacting system*. J. Non-Cryst. Solids, **1993**. 152(1): p. 70-74.
- [50] Martin E, N., M. Ellen L, G. Harmon M, O. Joseph S, *Strengthening by Ion Exchange*. J. Am. Ceram. Soc., **1964**. 47: p.
- [51] Jost, W., *Diffusion in solids, liquids, gases*. Academic Press, **1960**.
- [52] Doremus, R.H., *Mixed-Alkali Effect and Interdiffusion of Na and K Ions in Glass*. J. Am. Ceram. Soc., **1974**. 57(11): p. 478-480.
- [53] Ingram, M.D., M.H. Wu, A. Coats, E.I. Kamitsos, C.P.E. Varsamis, N. Garcia, M. Sola, *Evidence from infrared spectroscopy of structural relaxation during field assisted and chemically driven ion exchange in soda lime silica glasses*. Phys. Chem. Glasses, **2005**. 46(2): p. 84-89.

- [54] Ingram, M.D., J.E. Davidson, A.M. Coats, E.I. Kamitsos, J.A. Kapoutsis, *Origins of anomalous mixed-alkali effects in ion-exchanged glasses*. Glass Sci. Technol., **2000**. 73(4): p. 89-104.
- [55] Lupascu, A., A. Kevorkian, T. Boudet, F.o. Saint-Andre', D. Persegol, M. Levy, *Modeling ion exchange in glass with concentration-dependent diffusion coefficients and mobilities*. Optical Engineering, **1996**. 35(6): p. 1603-1610.
- [56] Abou-EI-Leil, M., A.R. Cooper, *Analysis of Field-Assisted Binary Ion Exchange*. J. Am. Ceram. Soc., **1979**. 62(7-8): p. 390-395.
- [57] Abou-EI-Leil, M., A.R. Cooper, *Fracture of Soda-Lime Glass Tubes by Field-Assisted Ion Exchange*. J. Am. Ceram. Soc., **1978**. 61(3-4): p. 131-136.
- [58] Hao, Y., B. Zheng, H. Wang, W. Zheng, J. Yang, X. Jiang, Q. Zhou, M. Wang, *Experiments and analysis on Joule heating effect in field-assisted ion diffusion*. Optical Engineering, **2012**. 51(1): p. 014601-014601-014601-014606.
- [59] Richard, C.V., G. George, *Migration of Sodium Ions through Quartz Plates in an Electric Field. I*. The Journal of Chemical Physics, **1950**. 18: p.
- [60] Lipovskii, A.A., V.G. Melehin, V.D. Petrikov, *Electric-field-induced bleaching of ion-exchanged glasses containing copper nanoparticles*. Technical Physics Letters, **2006**. 32(3): p. 275-277.
- [61] Morten, M.S., Z. Qiuju, C.M. John, P. Marcel, M. Steen, Y. Yuanzheng, *Sodium diffusion in boroaluminosilicate glasses*. J. Non-Cryst. Solids, **2011**. 357: p.
- [62] Junwu, S., J.G. David, *Prediction of stress profiles in ion exchanged glasses*. J. Non-Cryst. Solids, **2004**. 344: p.
- [63] Varshneya, A.K., G.A. Olson, P.K. Kreski, P.K. Gupta, *Buildup and relaxation of stress in chemically strengthened glass*. J. Non-Cryst. Solids, **2015**. 427: p. 91-97.
- [64] Cooper, A.R., D.A. Krohn, *Strengthening of Glass Fibers: 11, Ion Exchange \**. J. Am. Ceram. Soc., **1969**. 52(12): p. 665-669.
- [65] Garfinkel, H.M., C.B. King, *Ion Concentration and Stress in a Chemically Tempered Glass*. J. Am. Ceram. Soc., **1970**. 53(12): p. 686-691.
- [66] Sane, A.Y., A.R. Cooper, *Stress Buildup and Relaxation during Ion-Exchange Strengthening of Glass*. J. Am. Ceram. Soc., **1987**. 70(2): p. 86-89.

- [67] Tandia, A., K.D. Vargheese, J.C. Mauro, *Elasticity of ion stuffing in chemically strengthened glass*. J. Non-Cryst. Solids, **2012**. 358(12-13): p. 1569-1574.
- [68] Kreski, P.K., A.K. Varshneya, A.N. Cormack, *Investigation of ion-exchange 'stuffed' glass structures by molecular dynamics simulation*. J. Non-Cryst. Solids, **2012**. 358(24): p. 3539-3545.
- [69] Varshneya, A., *Influence of strain energy on kinetics of ion exchange in glass*. J. Am. Ceram. Soc., **1975**. 58(3-4): p. 106-109.
- [70] Gutzow, I.S., O.V. Mazurin, J.W.P. Schmelzer, S.V. Todorova, B.B. Petroff, A.I. Priven, *Glasses and the Glass Transition*. Wiley, **2011**.
- [71] Shen, J., D.J. Green, R.E. Tressler, D.L. Shelleman, *Stress relaxation of a soda lime silicate glass below the glass transition temperature*. J. Non-Cryst. Solids, **2003**. 324(3): p. 277-288.
- [72] Seaman, J.H., P.J. Lezzi, T.A. Blanchet, M. Tomozawa, *Degradation of ion-exchange strengthened glasses due to surface stress relaxation*. J. Non-Cryst. Solids, **2014**. 403: p. 113-123.
- [73] Varshneya, A.K., *Mechanical model to simulate buildup and relaxation of stress during glass chemical strengthening*. J. Non-Cryst. Solids, **2016**. 433: p. 28-30.
- [74] Sglavo, V.M., A. Quaranta, V. Allodi, G. Mariotto, *Analysis of the surface structure of soda lime silicate glass after chemical strengthening in different KNO<sub>3</sub> salt baths*. J. Non-Cryst. Solids, **2014**. 401: p. 105-109.
- [75] Calahoo, C., J.W. Zwanziger, I.S. Butler, *Mechanical–Structural Investigation of Ion-Exchanged Lithium Silicate Glass using Micro-Raman Spectroscopy*. The Journal of Physical Chemistry C, **2016**. 120(13): p. 7213-7232.
- [76] Mauro, J.C., R.J. Loucks, *Forbidden glasses and the failure of fictive temperature*. J. Non-Cryst. Solids, **2009**. 355(10-12): p. 676680.
- [77] Potuzak, M., R.C. Welch, J.C. Mauro, *Topological origin of stretched exponential relaxation in glass*. The Journal of Chemical Physics, **2011**. 135(21): p. 214502.
- [78] Lu, X., E.M. Arruda, W.W. Schultz, *The effect of processing parameters on glass fiber birefringence development and relaxation*. Journal of Non-Newtonian Fluid Mechanics, **1999**. 86(1-2): p. 89-104.

- [79] Phillips, J.C., *Stretched exponential relaxation in molecular and electronic glasses*. Rep. Prog. Phys., **1996**. 59(9): p. 1133.
- [80] Sglavo, V.M., *Chemical Strengthening of Soda Lime Silicate Float Glass: Effect of Small Differences in the KNO<sub>3</sub> Bath*. Int. J. Appl. Glass. Sci., **2015**. 6(1): p. 72-82.
- [81] Talimian, A., V.M. Sglavo, *Ion-exchange strengthening of borosilicate glass: Influence of salt impurities and treatment temperature*. J. Non-Cryst. Solids, **2017**. 456: p. 12-21.
- [82] Talimian, A., V.M. Sglavo, *Electric Field-Assisted Ion Exchange of Borosilicate Glass Tubes*. in: A. Kilislioglu (Ed.) *Ion Exchange - Studies and Applications*, InTech, **2015**.
- [83] Aaldenberg, E.M., P.J. Lezzi, J.H. Seaman, T.A. Blanchet, M. Tomozawa, *Ion-Exchanged Lithium Aluminosilicate Glass: Strength and Dynamic Fatigue*. J. Am. Ceram. Soc., **2016**. 99(8): p. 2645-2654.
- [84] Morris, D.J., S.B. Myers, R.F. Cook, *Indentation crack initiation in ion-exchanged aluminosilicate glass*. J. Mater. Sci., **2004**. 39(7): p. 2399-2410.
- [85] Sane, A.Y., A.R. Cooper, *Anomalous Stress Profiles in Ion-Exchanged Glass*. J. Am. Ceram. Soc., **1978**. 61(7-8): p. 359-362.
- [86] Goldstein, J., D.E. Newbury, P. Echlin, D.C. Joy, C. Fiori, E. Lifshin, *Scanning Electron Microscopy and X-Ray Microanalysis: A Text for Biologists, Materials Scientists, and Geologists*. Springer US, **2013**.
- [87] Joy, D.C., *Monte Carlo Modeling for Electron Microscopy and Microanalysis*. Oxford University Press, **1995**.
- [88] Dapor, M., *Electron-Beam Interactions with Solids: Application of the Monte Carlo Method to Electron Scattering Problems*. Springer Berlin Heidelberg, **2003**.
- [89] Goldstein, J., *Scanning Electron Microscopy and X-ray Microanalysis: Third Edition*. Springer US, **2003**.
- [90] Lu, J., S.f.E. Mechanics, *Handbook of Measurement of Residual Stresses*. Fairmont Press, **1996**.
- [91] Marshall, D.B., B.R. Lawn, *Residual stress effects in sharp contact cracking*. J. Mater. Sci., **1979**. 14(8): p. 2001-2012.

- [92] Marshall, D.B., B.R. Lawn, *An Indentation Technique for Measuring Stresses in Tempered Glass Surfaces*. J. Am. Ceram. Soc., **1977**. 60(1-2): p. 86-87.
- [93] Vincenzo, M.S., B. Marco, P. Andrea, *Procedure for residual stress profile determination by curvature measurements*. Mech. Mater., **2005**. 37: p.
- [94] Valente, T., C. Bartuli, M. Sebastiani, A. Loreto, *Implementation and development of the incremental hole drilling method for the measurement of residual stress in thermal spray coatings*. J. Therm. Spray Technol., **2005**. 14(4): p. 462-470.
- [95] Zeng, K., D. Rowcliffe, *Experimental Measurement of Residual Stress Field around Sharp Indentation in Glass*. J. Am. Ceram. Soc., **1994**. 77(2): p. 524-530.
- [96] Scannell, G., L. Huang, T. Rouxel, *Elastic properties and indentation cracking behavior of Na<sub>2</sub>O-TiO<sub>2</sub>-SiO<sub>2</sub> glasses*. J. Non-Cryst. Solids, **2015**. 429: p. 129-142.
- [97] Cook, R.F., G.M. Pharr, *Direct Observation and Analysis of Indentation Cracking in Glasses and Ceramics*. J. Am. Ceram. Soc., **1990**. 73(4): p. 787-817.
- [98] Chiang, S.S., D.B. Marshall, A.G. Evans, *The response of solids to elastic/plastic indentation. I. Stresses and residual stresses*. J. Appl. Phys., **1982**. 53(1): p. 298-311.
- [99] Chiang, S., D. Marshall, A. Evans, *The response of solids to elastic plastic indentation. 2. Fracture initiation*. J. Appl. Phys., **1982**. 53(1): p. 312-317.
- [100] Martienssen, W., H. Warlimont, *Springer Handbook of Condensed Matter and Materials Data*. Springer, **2006**.
- [101] Lawn, B.R., E.R. Fuller, *Measurement of thin-layer surface stresses by indentation fracture*. J. Mater. Sci., **1984**. 19(12): p. 4061-4067.
- [102] Suresh, S., A.E. Giannakopoulos, *A new method for estimating residual stresses by instrumented sharp indentation*. Acta Mater., **1998**. 46(16): p. 5755-5767.
- [103] Oliver, W.C., G.M. Pharr, *Measurement of hardness and elastic modulus by instrumented indentation: Advances in understanding and refinements to methodology*. J. Mater. Res., **2004**. 19(1): p. 3-20.
- [104] Aben, H., C. Guillemet, *Photoelasticity of Glass*. Springer Berlin Heidelberg, **2012**.
- [105] Aben, H., J. Anton, A. Errapart, *Modern Photoelasticity for Residual Stress Measurement in Glass*. Strain, **2008**. 44: p.

- [106] ASTM, *Standard Test Method for Non-Destructive Photoelastic Measurement of Edge and Surface Stresses in Annealed, Heat-Strengthened, and Fully Tempered Flat Glass*. in: ASTM C1279-13, West Conshohocken, PA, **2013**.
- [107] Gulati, S.T., J. Westbrook, S. Carley, H. Vepakomma, T. Ono, *45.2: Two point bending of thin glass substrate*. in: *45.2: Two point bending of thin glass substrate*, Wiley Online Library, **2011**, pp. 652-654.
- [108] Glaesemann, G., *The Strength of Thin Fusion Drawn Glass Sheets*. in: 11th ESG conference, **2012**.
- [109] Quaranta, A., A. Rahman, G. Mariotto, C. Maurizio, E. Trave, F. Gonella, E. Cattaruzza, E. Gibaudo, J.E. Broquin, *Spectroscopic Investigation of Structural Rearrangements in Silver Ion-Exchanged Silicate Glasses*. *The Journal of Physical Chemistry C*, **2012**. 116(5): p. 3757-3764.
- [110] Zhang, Z.-M., S. Chen, Y.-Z. Liang, Z.-X. Liu, Q.-M. Zhang, L.-X. Ding, F. Ye, H. Zhou, *An intelligent background-correction algorithm for highly fluorescent samples in Raman spectroscopy*. *J. Raman Spectrosc.*, **2010**. 41(6): p. 659-669.
- [111] Lawn, B., *Fracture of Brittle Solids*. Cambridge University Press, **1993**.
- [112] Anstis, G.R., P. Chantikul, B.R. Lawn, D.B. Marshall, *A Critical Evaluation of Indentation Techniques for Measuring Fracture Toughness: I, Direct Crack Measurements*. *J. Am. Ceram. Soc.*, **1981**. 64(9): p. 533-538.
- [113] Krohn, D.A., D.P.H. Hasselman, *Relation of Flaw Size to Mirror in the Fracture of Glass*. *J. Am. Ceram. Soc.*, **1971**. 54(8): p. 411-411.
- [114] Sinton, C.W., W.C. LaCourse, M.J. O'Connell, *Variations in K<sup>+</sup>-Na<sup>+</sup> ion exchange depth in commercial and experimental float glass compositions*. *Mater. Res. Bull.*, **1999**. 34(14): p. 2351-2359.
- [115] Tomozawa, M., D.-L. Kim, A. Agarwal, K.M. Davis, *Water diffusion and surface structural relaxation of silica glasses*. *J. Non-Cryst. Solids*, **2001**. 288(1-3): p. 73-80.
- [116] Mauro, J.C., C.M. Truesdale, K. Adib, A.M. Whittier, A.W. Martin, *Chemical Strengthening of Alkali-Free Glass via Pressure Vessel Ion Exchange*. *Int. J. Appl. Glass. Sci.*, **2016**. 7(4): p. 446-451.

- [117] Sglavo, V.M., A. Talimian, N. Ocsko, *Influence of salt bath calcium contamination on soda lime silicate glass chemical strengthening*. J. Non-Cryst. Solids, **2017**. 458: p. 121-128.
- [118] Xiangchen, Z., H. Ouli, X. Cengzuo, Z. Yinghuan, *The effect of impurity ions in molten salt KNO<sub>3</sub> on ion-exchange and strengthening of glass*. J. Non-Cryst. Solids, **1986**. 80(1-3): p. 313-318.
- [119] Jannotti, P., G. Subhash, P. Ifju, P.K. Kreski, A.K. Varshneya, *Photoelastic Measurement of High Stress Profiles in Ion-Exchanged Glass*. Int. J. Appl. Glass. Sci., **2011**. 2(4): p. 275-281.
- [120] Dal Maschio, R., V.M. Sglavo, G.D. Sorarù, *Fracture mechanics determination of stress profiles in Na<sup>+</sup> · K ion-exchanged glass optical waveguides*. Materials Science and Engineering: A, **1989**. 119: p. L9-L12.
- [121] Kolitsch, A., E. Richter, *Untersuchungen zur Ionenbeweglichkeit in einem Natrium-Kalium-Alumosilikatglass: Zur Einfluss Geringer Kationischer Verunreinigung in KNO<sub>3</sub> auf den K<sup>+</sup>/Na<sup>+</sup> Ionenaustasch*. Silikattechnik, **1980**. 31(8): p. 247-249.
- [122] Kolitsch, A., E. Richter, W. Hinz, *The influence of small cationic contaminations upon alkaline self diffusion between molten salt and glass*. Silikattechnik, **1981**. 32(10): p. 311-312.
- [123] Gaskell, D.R., *Introduction to the Thermodynamics of Materials, Fifth Edition*. Taylor & Francis, **2008**.
- [124] Kirchheim, R., *On the mobility of alkaline earth ions in mixed alkali alkaline earth silicate glasses*. J. Non-Cryst. Solids, **2003**. 328(1–3): p. 157-163.
- [125] Hatano, M., S. Kanasugi, M. Konishi, *Temperature Dependencies of Inter-diffusion Coefficient and Mass-transfer Coefficient of Chemical Strengthening* in: ICG Annual Meeting 2015, Bangkok, **2015**.
- [126] Talimian, A., G. Mariotto, V.M. Sglavo, *Electric field-assisted ion exchange strengthening of borosilicate and soda lime silicate glass*. Int. J. Appl. Glass. Sci., **2017**. 00): p. 1-10.
- [127] Shaisha, E.E., A.R. Cooper, *Residual Stress in Singly and Doubly Ion-Exchanged Glass*. J. Am. Ceram. Soc., **1981**. 64(1): p. 34-36.

- [128] Gonella, F., P. Canton, E. Cattaruzza, A. Quaranta, C. Sada, A. Vomiero, *Field-assisted ion diffusion of transition metals for the synthesis of nanocomposite silicate glasses*. Materials Science and Engineering: C, **2006**. 26: p.
- [129] Cattaruzza, E., F. Gonella, S. Ali, C. Sada, A. Quaranta, *Silver and gold doping of SiO<sub>2</sub> glass by solid-state field-assisted diffusion*. J. Non-Cryst. Solids, **2009**. 355: p.
- [130] Quaranta, A., E. Cattaruzza, F. Gonella, G. Peruzzo, M. Giarola, G. Mariotto, *Field-assisted solid state doping of glasses for optical materials*. Opt. Mater., **2010**. 32(10): p. 1352-1355.
- [131] Ali, S., N. Ali, Y. Iqbal, A. Samreen, Q. Hayat, K. Hayat, M. Ajmal, M.J. Iqbal, *Structural modifications induced in silicate glass by field-aided solid-state diffusion of gold and chromium ions*. J. Non-Cryst. Solids, **2015**. 420: p. 38-42.
- [132] Ziemath, E.C., V.D. Araujo, C.A. Escanhoela, *Compositional and structural changes at the anodic surface of thermally poled soda-lime float glass*. J. Appl. Phys., **2008**. 104(5): p. 54912.
- [133] Mariappan, C., B. Roling, *Investigation of bioglass–electrode interfaces after thermal poling*. Solid State Ionics, **2008**. 179(19-20): p. 671-677.
- [134] Deparis, O., P.G. Kazansky, A. Podlipensky, A. Abdolvand, G. Seifert, H. Graener, *Evolution of poling-assisted bleaching of metal-doped nanocomposite glass with poling conditions*. Appl. Phys. Lett., **2005**. 86(26): p.
- [135] Calahoo, C., X.F. Zhang, J.W. Zwanziger, *Nanoindentation Study of the Surface of Ion-Exchanged Lithium Silicate Glass*. Journal of Physical Chemistry C, **2016**. 120(10): p. 5585-5598.
- [136] Gee, B., H. Eckert, *Cation Distribution in Mixed-Alkali Silicate Glasses. NMR Studies by <sup>23</sup>Na–{<sup>7</sup>Li} and <sup>23</sup>Na–{<sup>6</sup>Li} Spin Echo Double Resonance*. The Journal of Physical Chemistry, **1996**. 100(9): p. 3705-3712.
- [137] Roling, B., M. Ingram, *Mixed alkaline–earth effects in ion conducting glasses*. J. Non-Cryst. Solids, **2000**.): p.
- [138] Grandjean, A., M. Malki, C. Simonnet, *Effect of composition on ionic transport in SiO<sub>2</sub>-B<sub>2</sub>O<sub>3</sub>-Na<sub>2</sub>O glasses*. J. Non-Cryst. Solids, **2006**. 352(26-27): p. 2731-2736.

- [139] Kerridge, D.H., J. Cancela Rey, *Molten lithium nitrate-potassium nitrate eutectic: the reaction of compounds of titanium*. J. Inorg. Nucl. Chem., **1975**. 37(11): p. 2257-2260.
- [140] Harle, V., J.P. Deloume, L. Mosoni, B. Durand, M. Vrinat, M. Breyse, *Elaboration by reaction in molten nitrates and characterization of pure titanium oxide with large surface area*. Mater. Sci. Forum, **1994**. 152-5: p. 221-236.
- [141] Afanasiev, P., C. Geantet, *Synthesis of solid materials in molten nitrates*. Coord. Chem. Rev., **1998**. 178: p. 1725-1752.
- [142] Dong, H., *Surface Engineering of Light Alloys: Aluminium, Magnesium and Titanium Alloys*. Elsevier Science, **2010**.
- [143] Rahman, A., M. Giarola, E. Cattaruzza, F. Gonella, M. Mardegan, E. Trave, A. Quaranta, G. Mariotto, *Raman microspectroscopy investigation of Ag ion-exchanged glass layers*. J Nanosci Nanotechnol, **2012**. 12(11): p. 8573-8579.
- [144] McMillan, P., *Structural studies of silicate glasses and melts—applications and limitations of Raman spectroscopy*. Am. Mineral., **1984**. 69(7-8): p. 622-644.
- [145] Matson, D.W., S.K. Sharma, J.A. Philpotts, *The Structure of High-Silica Alkali-Silicate Glasses - a Raman-Spectroscopic Investigation*. J. Non-Cryst. Solids, **1983**. 58(2-3): p. 323-352.
- [146] Ollier, N., T. Charpentier, B. Boizot, G. Wallez, D. Ghaleb, *A Raman and MAS NMR study of mixed alkali Na–K and Na–Li aluminoborosilicate glasses*. J. Non-Cryst. Solids, **2004**. 341: p.
- [147] Gassman, P.L., J.S. McCloy, C.Z. Soderquist, M.J. Schweiger, *Raman analysis of perhenate and pertechnetate in alkali salts and borosilicate glasses*. J. Raman Spectrosc., **2014**. 45(1): p. 139-147.
- [148] Mcmillan, P., B. Piriou, *Raman-Spectroscopic Studies of Silicate and Related Glass Structure - a Review*. Bulletin De Mineralogie, **1983**. 106(1-2): p. 57-75.
- [149] Akagi, R., N. Ohtori, N. Umesaki, *Raman spectra of K<sub>2</sub>O–B<sub>2</sub>O<sub>3</sub> glasses and melts*. J. Non-Cryst. Solids, **2001**.): p.
- [150] Deschamps, T., C. Martinet, J.L. Bruneel, B. Champagnon, *Soda-lime silicate glass under hydrostatic pressure and indentation: a micro-Raman study*. J Phys Condens Matter, **2011**. 23(3): p. 035402.

- [151] Maniu, D., I. Ardelean, T. Iliescu, S. Cinta, O. Cozar, *Raman spectroscopic investigations of the oxide glass system  $(1-x)(3B_2O_3 \cdot K_2O) xMO$  ( $MO = V_2O_5$  or  $CuO$ )*. J. Mol. Struct., **1997**. 410: p. 291-294.
- [152] Meera, B.N., A.K. Sood, N. Chandrabhas, J. Ramakrishna, *Raman-Study of Lead Borate Glasses*. J. Non-Cryst. Solids, **1990**. 126(3): p. 224-230.
- [153] Iliescu, T., S. Simon, D. Maniu, I. Ardelean, *Raman-Spectroscopy of Oxide Glass System  $(1-X)[Yb_2O_3 \cdot Zl_2O]Xgd_2O_3$* . J. Mol. Struct., **1993**. 294: p. 201-203.
- [154] Larkin, P., *Infrared and Raman Spectroscopy: Principles and Spectral Interpretation*. Elsevier Science, **2011**.
- [155] Bigerelle, M., P.E. Mazeran, M. Rachik, *The first indenter-sample contact and the indentation size effect in nano-hardness measurement*. Materials Science & Engineering C-Biomimetic and Supramolecular Systems, **2007**. 27(5-8): p. 1448-1451.
- [156] Lutterotti, L., F. Dell'Amore, D.E. Angelucci, F. Carrer, S. Gialanella, *Combined X-ray diffraction and fluorescence analysis in the cultural heritage field*. Microchem. J., **2016**. 126: p. 423-430.
- [157] Quinn, G.D., B.T. Sparenberg, P. Koshy, L.K. Ives, S. Jahanmir, D.D. Arola, *Flexural Strength of Ceramic and Glass Rods*. J. Test. Eval., **2009**. 37(3): p. 222-244.
- [158] Ropp, R.C., *Handbook of Glass Fractography*. AuthorHouse, **2008**.
- [159] Rabinovitch, A., D. Bahat, *Differentiation of crack branching types in fractured glass*. Epl, **2011**. 95(1): p. 16003.
- [160] Sreeram, A.N., A.K. Varshneya, D.R. Swiler, *Microhardness and indentation toughness versus average coordination number in isostructural chalcogenide glass systems*. J. Non-Cryst. Solids, **1991**. 130(3): p. 225-235.
- [161] Lawn, B., R. Wilshaw, *Indentation fracture: principles and applications*. J. Mater. Sci., **1975**.): p.
- [162] Lawn, B.R., M.V. Swain, *Microfracture beneath point indentations in brittle solids*. J. Mater. Sci., **1975**. 10(1): p. 113-122.

- [163] Rouxel, T., *Driving force for indentation cracking in glass: composition, pressure and temperature dependence*. Philos Trans A Math Phys Eng Sci, **2015**. 373(2038): p. 20140140.
- [164] Miliou, A.N., R. Srivastava, R.V. Ramaswamy, *Modeling of the index change in K(+)-Na(+) ion-exchanged glass*. Appl. Opt., **1991**. 30(6): p. 674-681.
- [165] Svenson, M.N., L.M. Thirion, R.E. Youngman, J.C. Mauro, M. Bauchy, S.J. Rzoska, M. Bockowski, M.M. Smedskjaer, *Effects of Thermal and Pressure Histories on the Chemical Strengthening of Sodium Aluminosilicate Glass*. Frontiers in Materials, **2016**. 3: p.
- [166] Shen, J., D.J. Green, *Variable-Temperature Ion-Exchanged Engineered Stress Profile (ESP) Glasses*. J. Am. Ceram. Soc., **2003**. 86(11): p. 1979-1981.
- [167] Matthew, B.A., J.G. David, S.J. Glass, *Fracture behavior of engineered stress profile soda lime silicate glass*. J. Non-Cryst. Solids, **2003**. 321: p.
- [168] Green, D.J., *Critical parameters in the processing of engineered stress profile glasses*. J. Non-Cryst. Solids, **2003**. 316(1): p. 35-41.
- [169] Abrams, M.B., *Crack propagation and fracture in engineered stress profile glass*. Doctor's Thesis in Materials Science and Engineering, The Pennsylvania State University, PA, **2004**.): p.
- [170] Berthier da Cunha, T., J.P. Wu, O. Peitl, V.M. Fokin, E.D. Zanotto, L. Iannucci, A.R. Boccaccini, *Mechanical Properties and Impact Resistance of a New Transparent Glass-Ceramic*. Adv. Eng. Mater., **2007**. 9(3): p. 191-196.
- [171] Green, D.J., *Engineering residual stress profiles for increased mechanical reliability*. in: Key Eng. Mater., **2004**, pp. 1829-1834.
- [172] Lezzi, P.J., M. Tomozawa, *An Overview of the Strengthening of Glass Fibers by Surface Stress Relaxation*. Int. J. Appl. Glass. Sci., **2015**. 6(1): p. 34-44.
- [173] Lezzi, P.J., Q.R. Xiao, M. Tomozawa, T.A. Blanchet, *Strength increase of silica glass fibers by surface stress relaxation: A new mechanical strengthening method*. J. Non-Cryst. Solids, **2013**. 379): p. 95-106.
- [174] Lezzi, P.J., J.H. Seaman, M. Tomozawa, *Strengthening of E-glass fibers by surface stress relaxation*. J. Non-Cryst. Solids, **2014**.): p.

[175] Sehgal, J., S. Ito, *A new low-brittleness glass in the soda-lime-silica class family*. J. Am. Ceram. Soc., **1998**. 81(9): p. 2485-2488.

[176] Stern, K.H., *High Temperature Properties and Thermal Decomposition of Inorganic Salts with Oxyanions*. Taylor & Francis, **2000**.

[177] Deschamps, T., J. Margueritat, C. Martinet, A. Mermet, B. Champagnon, *Elastic moduli of permanently densified silica glasses*. Sci. Rep., **2014**. 4: p. 7193.



## Scientific Production

1. Ali Talimian, Vincenzo M. Sglavo, Can Annealing Improve the Chemical Strengthening of Thin Borosilicate Glass? , Journal of Non-Crystalline Solids, DOI:10.1016/j.jnoncrsol.2017.03.038
2. Ali Talimian, Gino Mariotto, Vincenzo M. Sglavo, Electric field-assisted ion exchange strengthening of borosilicate and soda lime silicate glass, Int J Appl Glass Sci. 2017; 00:1-10
3. Vincenzo M. Sglavo, Ali Talimian, Norbert Oskco, Chemical Strengthening of Soda Lime Silicate Glass in Calcium Contaminated Salt, Journal of Non-Crystalline Solids, 458 (2017) 121-128.
4. Ali Talimian and Vincenzo M. Sglavo, Ion Exchange Strengthening of Borosilicate Glass: influence of salt impurities and treating temperature, Journal of Non-Crystalline Solids, 456 (2017) 12-21.
5. Ali Talimian and Vincenzo M. Sglavo. Electric Field-Assisted Ion Exchange of Borosilicate Glass Tubes, Ion Exchange - Studies and Applications, Prof. Ayben Kilislioglu (Ed.), ISBN: 978-953-51-2164-0, InTech, DOI: 10.5772/60805.



## Participation to Congresses, Schools and Workshops

### Conferences:

1. Ali Talimian, Vincenzo M. Sglavo, Chemical Strengthening of Alkali Borosilicate Glass: A Study on Stress Generation and Relaxation, CersJ-GOMD joint symposium 2016, Kyoto, Japan
2. Norbert Ocsko, Ali Talimian, Vincenzo M. Sglavo, Influence of Calcium on Sodium-Potassium Ion Exchange Strengthening of Silicate Glasses, CersJ-GOMD joint symposium 2016, Kyoto, Japan
3. Ali Talimian, Vincenzo M. Sglavo, Sequential Electric Field Assisted Ion Exchange: Engineered Stress Profile Glasses, Glass and Optical Materials Division Mtg., American Ceramic Society, (GOMD-S1-119-2016)
4. Hamid Hassani, Norbert Ocsko, Ali Talimian, Vincenzo M. Sglavo, Effect of salt impurities on the chemical strengthening of float glass by ion-exchange, Glass and Optical Materials Division Mtg., American Ceramic Society, (GOMD-S1-119-2016)
5. Ali Talimian, Vincenzo M. Sglavo, Effect of Electric Field Intensity and Frequency on the Mechanical Properties of Glass Tubes Subjected to E-Field-Assisted Ion Exchange, ICG Annual Meeting 2015, 20th-23rd September, 2015, Thailand

### Schools:

- The Advanced School on Glasses and Glass-Ceramics (G&GC São Carlos), São Carlos, São Paulo, Brazil, August 1-9, 2015.
- Materials Characterisation by the Combined Analysis MAUD 2015, Trento Italy, October 19-23, 2015



## Acknowledgements

First, I would like to acknowledge my advisor, Prof. Vincenzo Sglavo. I feel privileged to have worked with him and without his hard work, dedication, supervision and direction this project would not have been possible I would also like to appreciate the help and critical comments of Prof. Gino Marritto and Prof. Paolo Scardi.

This project was made possible through the generous support from Schott AG. I warmly thank them for their support and contribution of supplying thin glass, D263 Teco®. I am also grateful for the help and support of organisations who helped me with the travel grants: FAPESP (The São Paulo Research Foundation), the Department of Materials Engineering of the Federal University of São Carlos (UFSCar) and the Glass and Optical Materials Division (GOMD) of the American Ceramic Society.

The sample analysis was conducted in several laboratories and I thank all those who helped me with the measurements. Dr. Mirco D'Incau for micro-hardness measurements and Dr. Marco Giarola for the structural analysis of samples.

Finally, the last three years in Trento are unquestionably unforgettable, despite all my sarcastic comments. Thank you to all my friends and colleagues.